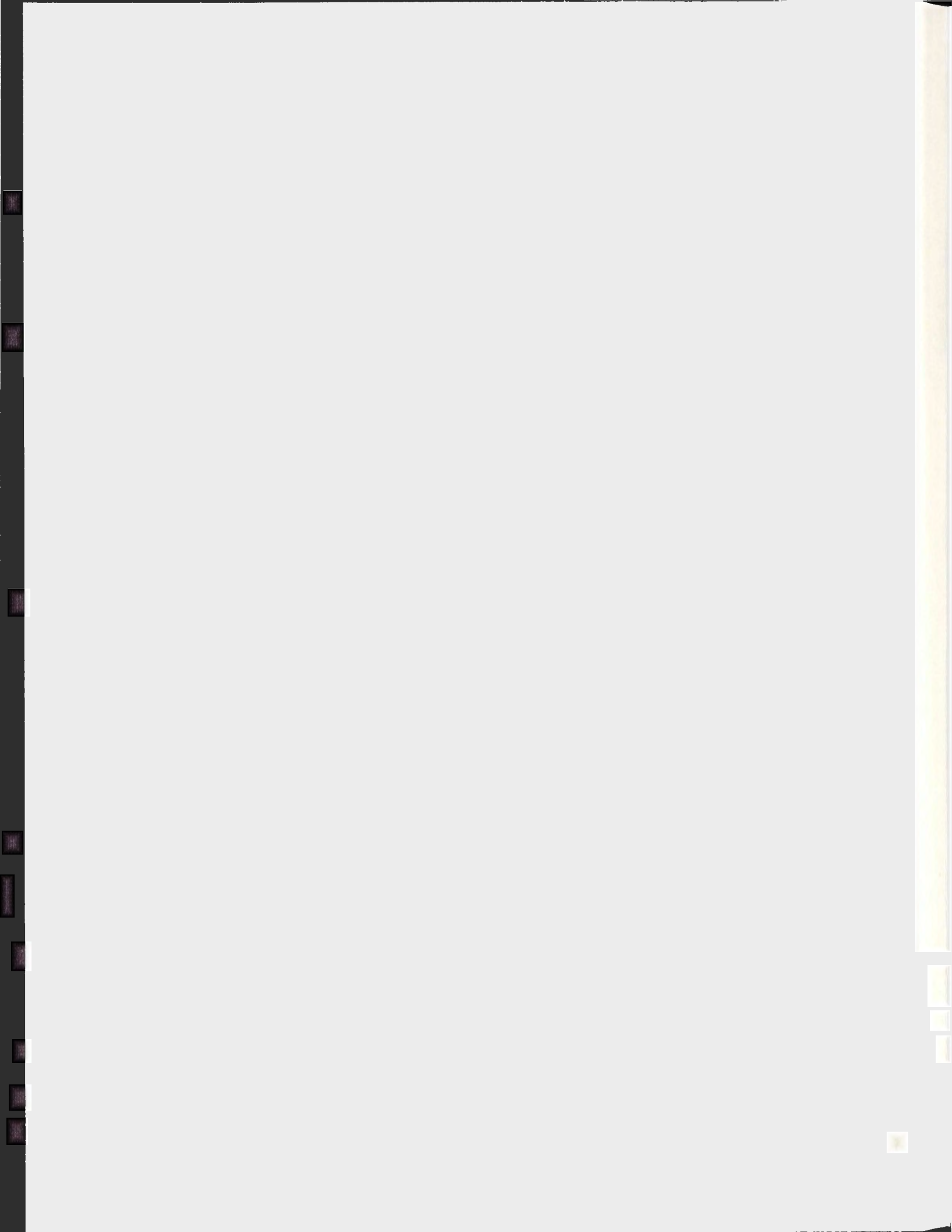


GAS-PHASE FRAGMENTATION STUDIES OF A SERIES
OF BIOTIN DERIVATIVES AND OF A CORE
OLIGOSACCHARIDE BY TANDEM MASS SPECTROMETRY

SALIM SIOUD



**Gas-Phase Fragmentation Studies of A Series of Biotin Derivatives
and of A Core Oligosaccharide by Tandem Mass Spectrometry**

by:

Salim Sioud

B.Sc. Chemistry, IUT Betune, University D'Artois, France, 2007

**A thesis submitted to the School of Graduate Studies in partial fulfillment
of the requirements for the degree of Master of Science.**

Department of Chemistry

Memorial University of Newfoundland and Labrador

April 10, 2010

ABSTRACT

The gas-phase fragmentation of a series of commercially available biotinyl reagents have been evaluated by electrospray ionization mass spectrometry (ESI-MS) and collision induced dissociation tandem mass spectrometry (CID-MS/MS) analyses using a QqTOF-MS/MS hybrid instrument. In general it has been observed that the CID-MS/MS fragmentation routes of the five precursor protonated molecules obtained from the biotin linkers *1-5* afforded a series of product ions formed essentially by similar routes. The genesis and structural identities of all the product ions obtained from the biotin linkers *1-5* have been assigned. All of the exact mass assignments of the protonated molecules and the product ions were verified by conducting separate CID-MS/MS analysis of the deuterium labeled precursor ions.

The ESI-QqTOF-MS structural elucidation of the core oligosaccharide of *Aeromonas hydrophila* (chemotype II) lipopolysaccharide has been investigated and it was demonstrated that it contained a 4-*O*-linked phosphorylated group Kdo residue which was glycosylated by the remaining outer core oligosaccharide through its O-5 position. After, releasing the core oligosaccharide from the native LPS with acid, the phosphorylated Kdo residue eliminated phosphoric acid to produce a core oligosaccharide containing a mixture of diastereomeric 4,8- and 4,7-anhydro- α -keto acids and an open olefinic Kdo residue. The characteristic glycone sequence was elucidated by CID-MS/MS of the protonated molecule of the native core oligosaccharide. In addition, the analysis of the Hakamori permethylated core oligosaccharide was carried out by ESI-QqTOF-MS and MALDI-TOF-MS analyses. The presence of more than nine isobaric isomers of this core was noticed. The

collision-induced dissociation analysis (CID-MS/MS) of the various protonated permethylated core oligosaccharide molecules showed a similar and diagnostic fragmentation pattern.

To confirm these obtained results, the permethylation of the core oligosaccharide SJ-48R has been performed with a different methylation method (Ciucanu & Kerek method). It was realized that the extra minor satellite signals obtained in the ESI-QqTOF-MS and MALDI-TOF-MS analyses were DMSO stable covalent addition products, which have occurred by a Michael addition on the 4,8-Kdo exocyclic double bond and on the C-3-C-4 double bond of the olefinic open-chain Kdo residue. To our knowledge, this is the first time that DMSO adducts have been observed in the gas phase, and they have never before been reported.

ACKNOWLEDGMENTS

I would like to express my deep gratitude to my supervisor Dr. Joseph Banoub, Adjunct Professor of Chemistry at Memorial Univeristy and Head, Special Projects at the Science Branch of the Department of Fisheries and Oceans, for welcoming me into his lab during these two years, for his advice, and for supervising the study.

I would also like to thank Professors Travis Fridgen and Yuming Zhao for their advice and for serving on my supervisory committee.

I would like to thank the Department of Fisheries and Oceans (DFO), St. John's for providing the resources which enabled me to perform my research studies. I would like to express special gratitude to Mr. Howard Hodder for his assistance and his help.

Thanks to the school of graduate studies and NSERC for the financial support throughout my degree program.

TABLE OF CONTENTS

ABSTRACT	ii
ACKNOWLEDGMENTS.....	iv
LIST OF FIGURES	ix
LIST OF SCHEMES.....	xiii
LIST OF TABLES.....	xvi
LIST OF ABBREVIATIONS	xviii
CHAPTER 1: INTRODUCTION.....	1
1.1. Mass spectrometry	2
1.2. Ionization techniques	4
1.2.1. Hard or direct ionization techniques	4
1.2.2. Soft or indirect ionization techniques	5
1.2.2.1. MALDI.....	6
1.2.2.2. Electrospray ionization (ESI).....	9
1.3. Mass analyzers.....	11
1.3.1. Quadrupole analyzer	12
1.3.2. Time of flight (TOF) analyzer	13
1.4. Gas-phase ion formation and fragmentation	16
1.4.1. Principle of tandem mass spectrometer operation	16
1.4.2. CID-MS/MS analysis using a hybrid quadrupole orthogonal time-of-flight mass spectrometer	19

1.4.3. Gas-Phase fragmentation of glycoconjugates during mass spectrometry analysis	21
1.5. LPS-non-derived conjugate as a vaccine candidate.....	23
1.5.1. Lipopolysaccharides: (LPSs).....	23
1.5.2. Lipopolysaccharide-protein conjugate vaccines.....	25
1.5.2.1. Biotin reagents: potential linkers for glycoconjugate performance	26
CHAPTER 2: MATERIALS AND METHODS	29
2.1. Biotin reagents.....	29
2.1.1. The origin and structure of the biotin reagents.....	29
2.1.2. Isotopic Labelling: hydrogen deuterium exchange of biotin reagents.....	29
2.1.3. ESI-QqTOF-MS of the biotin reagents	32
2.1.4. Low-energy collision CID-MS/MS and <i>quasi</i> -MS ³ analyses	33
2.2. The core oligosaccharide of <i>Aeromonas hydrophila</i> (chemotype II) lipopolysaccharide.....	34
2.2.1. Bacterial culture	34
2.2.2. Extraction and purification of the core oligosaccharide	34
2.2.3. Permethylation procedure for the core oligosaccharide.....	34
2.2.3.1. The Hakomori methylation method	34
2.2.3.2. The Ciucanu & Kerek methylation method.....	35
2.3. Electrospray quadrupole orthogonal time-of-flight mass spectrometry ..	37
2.4. Matrix-assisted laser desorption ionization mass spectrometry	38

CHAPTER 3: GAS-PHASE FRAGMENTATION STUDY OF A SERIES OF BIOTIN REAGENTS USING AN ELECTROSPRAY IONIZATION TANDEM MASS SPECTROMETRY QqTOF-HYBRID INSTRUMENT.....	39
3.1. Introduction	39
3.2. ESI-QqTOF-MS analysis of the biotin reagents 1-5	42
3.3. CID-MS/MS analysis of biotin reagents 1-5.....	43
3.3.1. CID-MS/MS of the $[M+H]^+$ ion at m/z 689.2854 selected from the psoralen-PEO-biotin linker 1 and <i>quasi-MS</i> ³ analysis of the precursor $[M+H$ -photoreactive psoralen group] ⁺ ion 1 <i>b</i> at m/z 487. 2507	43
3.3.2. CID-MS/MS of the $[M+H]^+$ precursor ion at m/z 492.2277 selected from the <i>p</i> -aminobenzoyl biocytin linker 2	49
3.3.3. CID-MS/MS of the $[M+H]^+$ ion at m/z 534.2630 selected from the photoactivatable biotin linker 3.....	53
3.3.4. CID-MS/MS of the protonated molecule $[M+H]^+$ ion at m/z 733.3634 selected from the PEO-biotin dimer linker 4 and <i>quasi-MS</i> ³ analysis of $[M+H$ -biotinyl group] ⁺ precursor ion 4 <i>b</i> at m/z 507.2832	57
3.3.5. CID-MS/MS of the protonated molecule $[M+H]^+$ at m/z 880.1853 obtained from the Sulfo SBED biotin linker 5.....	61
3.3.5.1. <i>Quasi-MS</i> ³ analysis of the $[M+2H-Na]^+$ ion at m/z 858.2060 and the $[$ biotinyl groupC ₆ H ₁₀ NO(photoactivatable aryl azide group) $]$ ⁺ ion 5 <i>f</i> at m/z 500.2018	61
3.4. Conclusion.....	67

CHAPTER 4: CONFIRMATION AND CHARACTERIZATION OF THE PRESENCE OF THE 4-O-PHOSPHORYLATED KDO REDUCING END GROUP OF THE LPS CORE OLIGOSACCHARIDE OF <i>AEROMONAS HYDROPHILA</i> (CHEMOTYPE II) USING TANDEM MASS SPECTROMETRY	69
4.1. Introduction	69
4.2. Analysis of the core oligosaccharide by ESI ((+)/(-))-QqTOF-MS and MALDI-QqTOF-MS	71
4.3. Electrospray ionization tandem mass spectrometry analysis of the permethylated core oligosaccharide	83
4.3.1. ESI-QqTOF-MS analysis of the permethylated native core oligosaccharide.....	83
4.3.2. A new interpretation of the ESI-QqTOF-MS analysis of the three minor satellite signals of the permethylated core oligosaccharide.....	89
4.4. ESI-CID-MS/MS analysis of the permethylated core oligosaccharide ...	95
4.4.1. ESI-CID-MS/MS analyses of the protonated precursor ions obtained from the permethylated core oligosaccharide	95
4.4.2. ESI-CID-MS/MS analyses of various DMSO adducts of the permethylated core oligosaccharide	104
4.5. Conclusion.....	110
GENERAL CONCLUSION.....	112
REFERENCES	114
APPENDIX A.....	132
APPENDIX B.....	140

LIST OF FIGURES

- Figure 1.1:** General schematic representation of a mass spectrometer.....P 3
- Figure 1.2:** Schematic representations showing the process of desorption/ionization of the analytes during Nitrogen UV laser beam irradiation and formation of the ionized species.....P 8
- Figure 1.3:** Schematic representation of an electrospray source (ES) in positive ion mode: Charges droplets are created due to the high voltage occurrence at the tip of the capillary. After desorption, they undergo Coulomb explosions, then turn into micro-droplets.....P 10
- Figure 1.4:** Schematic representation of the production of charged droplets during the ES ionization processP 11
- Figure 1.5:** Schematic representation of a quadrupole mass analyzer showing the oscillation of ions to reach the detector.P 13
- Figure 1.6:** Schematic representation of the reflecting time of flight (TOF) analyzer by considering two ions ($m_A > m_B$). The ion which has the lower mass will reach first the detector.....P 14
- Figure 1.7:** Schematic representation of the orthogonal injection system of the reflecting TOF mass spectrometerP 15
- Figure 1.8:** Schematic representation of the QSTAR hybrid Qq-TOF. It is also representative of a hybrid quadrupole orthogonal time-of-flight mass spectrometer.....P 18
- Figure 1.9:** During CID MS/MS analysis, a precursor ion is selected in the first mass analyzer (MS1) and is then dissociated in the collision cell with a stream of inert gas,

and finally the product ions are separated in the second analyzer (MS2).
.....P 20

Figure 1.10: Possible fragmentation pathways during CID-MS/MS of a glycoconjugate corresponding to maltose according to the Domon & Costello Nomenclature.P 22

Figure 1.11: Schematic representation of gram negative bacterial membrane and a lipopolysaccharide structureP 24

Figure 1.12: Biotin molecular formula. It is composed of a tetrahydroimidizalone ring fused to a tetrahydrothiophene ring substituted at the C-2 position with valeric acid.....P 27

Figure 2.1: The molecular structure of biotin linkers (*1-5*).....P 30-31

Figure 2.2: Structure of the core oligosaccharide of *Aeromonas hydrophila* (chemotype II) lipopolysaccharide.P 36

Figure 3.1: (a) ESI-QqTOF-MS (+) of the psoralen-PEO-biotin *1*.....P 46

Figure 3.1 (continued): (b) CID-MS/MS of the selected protonated precursor ion at m/z 689.2854 from psoralen PEO Biotin *1*; (c) *quasi*-MS³ of the selected ion *1b* at m/z 487.2507 from psoralen PEO Biotin *1*.....P 47

Figure 3.2: (a) ESI-QqTOF-MS (+) of the *p*-aminobenzoyl biocytin *2*; (b) CID-MS/MS of the selected protonated precursor ion *2a* at m/z 492.2277 from *p*-aminobenzoyl biocytin *2*.P 51

Figure 3.3: (a) ESI-QqTOF-MS (+) of the photoreactive biotin *3*; (b) CID-MS/MS of the selected protonated precursor ion *3a* at m/z 534.2630 from photoreactive biotin *3*.....P 55

Figure 3.4: (a) ESI-QqTOF-MS (+) of the PEO-biotin Dimer *4*.....P 58

Figure 3.4 (continued): (b) CID-MS/MS of the selected protonated precursor ion **4a** at m/z 733.3634 from PEO Biotin Dimer **4**; (c) *quasi*-MS³ of the selected ion **4b** at m/z 507.2832 from PEO Biotin Dimer **4**.....P 59

Figure 3.5: (a) ESI-QqTOF-MS (+) of the Sodiated Sulfo SBED **5**; (b) CID/MS/MS of selected protonated precursor ion **5a** at m/z 880.1853 from sodiated sulfo-SBED.....P 63

Figure 3.5 (continued): (c) *Quasi*-MS³ of the selected ion **5b** at m/z 858.2060 from sodiated sulfo-SBED **5**; (d) *quasi*-MS³ of the selected ion **5f** at m/z 500.2018 from sodiated sulfo-SBED **5**.....P 64

Figure 4.1: (a) ESI-MS (+) of the homogeneous mixture of the native core oligosaccharide with diastereomeric pairs; (b) ESI-MS (-) of the molecule characteristic of the native core oligosaccharide with diastereomeric pairs.....P 74

Figure 4.2: (a) ESI (+)-CID-MS/MS of the selected $[M + H]^+$ protonated molecular ion at m/z 1312.4467 from the native core oligosaccharide; (b) ESI (-)-CID-MS/MS of the selected $[M-H]^-$ deprotonated molecular ion at m/z 1310.9216 from the native core oligosaccharide.....P 77

Figure 4.3: ESI-MS (+) of the homogeneous mixture of the permethylated core oligosaccharideP 87

Figure 4.4: ESI-CID-MS/MS of the selected precursor ion at m/z 1676.8630 from the permethylated core oligosaccharid.....P 99

Figure 4.5: ESI-CID-MS/MS of the selected precursor ion at m/z 1690.8666 from the permethylated core oligosaccharideP 100

Figure 4.6: ESI-CID-MS/MS of the selected precursor ion at m/z 1704.8543 from the permethylated core oligosaccharideP 101

Figure 4.7: ESI-CID-MS/MS of the selected precursor ion at <i>m/z</i> 1718.8338 from the permethylated core oligosaccharide	P 102
Figure 4.8: ESI-CID-MS/MS of the selected precursor ion at <i>m/z</i> 1732.9415 from the permethylated core oligosaccharide.....	P 103
Figure 4.9: ESI-CID-MS/MS of the selected precursor ion at <i>m/z</i> 1764.8589 from the permethylated core oligosaccharide.....	P 106
Figure 4.10: ESI-CID-MS/MS of the selected precursor ion at <i>m/z</i> 1796.9027 from the permethylated core oligosaccharide.....	P 107
Figure 4.11: ESI-CID-MS/MS of the selected precursor ion at <i>m/z</i> 1810.9359 from the permethylated core oligosaccharide	P 108
Figure B.1: MALDI-MS (+) of the homogeneous mixture of the native core oligosaccharide.....	P 141
Figure B.2: MALDI-CID-MS/MS (+) of the selected precursor ion at <i>m/z</i> 1312.4514 from the homogeneous mixture of the native core oligosaccharide.	P 142
Figure B.3: MALDI-MS (+) of the homoogeneous mixture of the permethylated core oligosaccharide.....	P 143
Figure B.4: MALDI-CID-MS/MS of the selected precursor ion at <i>m/z</i> 1810.9656 from the permethylated core oligosaccharide.....	P 144
Figure B.5: MALDI-CID-MS/MS of the selected precursor ion at <i>m/z</i> 1796.9282 from the permethylated core oligosaccharide.....	P 145
Figure B.6: MALDI-CID-MS/MS of the selected precursor ion at <i>m/z</i> 1676.8969 from the permethylated core oligosaccharide.....	P 146

LIST OF SCHEMES

- Scheme 3.1:** The proposed fragmentation routes of the psoralen-PEO-biotin **1** obtained during the CID-MS/MS of the protonated precursor ion **1a** at m/z 689.2859 and the *quasi*-MS³ of the precursor ion **1b** at m/z 487.2587..... P 48
- Scheme 3.2:** The proposed fragmentation routes of the *p*-aminobenzoyl-biotin **2** obtained during CID-MS/MS of the protonated precursor ion **2a** at m/z 492.2278.....P 52
- Scheme 3.3:** The proposed fragmentation routes of the photoactivatable biotin **3** obtained during the CID-MS/MS of the protonated precursor ion **3a** at m/z 534.2561.....P 56
- Scheme 3.4:** The proposed fragmentation routes of PEO-biotin Dimer **4** obtained during the CID-MS/MS of the protonated precursor ion **4a** at m/z 733.3637 and the ion **4b** at m/z 507.2847.....P 60
- Scheme 3.5 (a):** The proposed fragmentation routes of the sodiated sulfo SBED **5** obtained during the CID-MS/MS of the protonated precursor ion **5a** at m/z 880.1818.....P 65
- Scheme 3.5 (b):** The proposed fragmentation routes of the sodiated sulfo-SBED **5** during the *quasi*-MS³ of the precursor ions: **5b** at m/z 858.2064 and **5f** at m/z 500.2018.....P 66
- Scheme 4.1:** Formation of the olefinic *D*-arabino-3-en-2-ulonic acid open chain **2A** after acetic acid treatment and possible structures of the diastereomeric forms of the 4,8-anhydro (**3A/3A'**)- and 4,7-anhydro (**4A/4A'**) derivatives of the enolizable α -keto-acid.....P 75

Scheme 4.2 (a): General fragmentation patterns of the protonated molecular ion $[M+H]^+$ at m/z 1312.4331 from the native core oligosaccharide of *Aeromonas hydrophila* (Chemotype II).....P 81

Scheme 4.2 (b): The proposed fragmentation routes of the $[M + H]^+$ protonated precursor ion at m/z 1312.4331 from the native core oligosaccharide of *Aeromonas hydrophila* (Chemotype II).....P 82

Scheme 4.3: The permethylated core oligosaccharide with eight protonated precursor ions: $[M_1+H]^+$, $[M_2+H]^+$, $[M_3+H]^+$, $[M_4+H]^+$, $[M_5+H]^+$, $[M_6 + H]^+$, $[M_7+H]^+$ and $[M_8+H]^+$ ions at m/z 1676.8630, 1690.8666, 1704.8543, 1718.8338, 1732.9415, 1764.8589, 1796.9027 and 1810.9359 respectively. The symbol R' represents the full and over-methylated molecules containing the 4,8-anhydro derivative of the enolizable α -keto acid terminal and the open olefinic Kdo residue.....P 88

Scheme 4.4 (a): Proposed mechanism of the formation of DMSO adducts of the permethylated core oligosaccharide: $[M_4+H+CH_3SOCH_3]^+$, $[M_5+H+CH_3SOCH_3]^+$ ions at m/z 1796.9027 and 1810.9359 respectively, resulting from the Michael addition reaction of the dimsyl anion on the C-2-C-3 double bond of the 4,8-anhydro Kdo-residue.....P 92

Scheme 4.4 (b): Proposed mechanism of the formation of DMSO adduct of the permethylated core oligosaccharide: $[M_6]^+$ ion at m/z 1764.8589, resulting from the Michael addition reaction of the dimsyl anion on the C-3-C-4 double bond of the open olefinic Kdo-residue.....P 93

Scheme 4.5: The proposed fragmentation routes of the permethylated protonated precursor ions: $[M_1+H]^+$, $[M_2+H]^+$, $[M_3+H]^+$, $[M_4+H]^+$, and $[M_5+H]^+$ ions at m/z 1676.8773, 1690.8530, 1704.9262, 1718.8914, and 1732.9166 respectively. The

symbol R' represents the various full- and over-methylated molecules composed of the 4,8-anhydro derivative of the enolizabe α -keto acid terminal residue.....P 98

Scheme 4.6: The proposed fragmentation routes of the DMSO adducts of the permethylated core oligosaccharide: $[M_6]^+$, $[M_4+H+CH_3SOCH_3]^+$, and $[M_5+H+CH_3SOCH_3]^+$ ions at m/z 1764.9647, 1796.9578, and 1810.8907 respectively. The symbol R'' represents the various DMSO adducts of the permethylated core oligosaccharide.....P 105

LIST OF TABLES

Table 4.1: List of characteristic fragment ions observed in ESI-QqTOF-CID-MS/MS analysis of the protonated molecule $[M+H]^+$ at m/z 1312.4467 of the core oligosaccharide of <i>Aeromonas hydrophila</i> Chemotype II.....	P 80
Table 4.2: Diagnostic protonated and sodiated molecular ions occurring from the ESI-QqTOF-MS of the permethylated homogenous mixture of the core oligosaccharide of <i>Aeromonas hydrophila</i> (Chemotype II).....	P 94
Table 4.3: List of similar fragment ions observed during ESI-QqTOF-CID-MS/MS analyses of the permethylated precursor ions: $[M_n + H]^+$ ($n = 1-5$) at m/z 1676.8773, 1690.8530, 1704.9262, 1718.8914, and 1732.9166 respectively of the permethylated core oligosaccharide of <i>Aeromonas hydrophila</i> (Chemotype II).....	P 97
Table A.1: Characteristic product ions observed in the CID-MS/MS of the $[M+H]^+$ ion at m/z 689.2859 and the <i>quasi</i> -MS ³ analysis of the $[M+H$ -photoreactive psoralen group] ⁺ ion at m/z 487.2587 from psoralen- PEO-Biotin <i>1</i>	P 133-134
Table A.2: Characteristic product ions observed in the CID-MS/MS of the $[M+H]^+$ ion at m/z 492.2278 from <i>p</i> -aminobenzoyl biocytin <i>2</i>	P 135
Table A.3: Characteristic product ions observed in the CID-MS/MS of the $[M+H]^+$ ion at m/z 534.2561 from the photoreactive Biotin <i>3</i>	P 136
Table A.4: Characteristic product ions observed in the CID-MS/MS of the $[M+H]^+$ ion at m/z 733.3637 and the <i>quasi</i> -MS ³ analysis of the $[M+H$ -biotinyl group] ⁺ ion at m/z 507.2847 from the PEO-Biotin Dimer <i>4</i>	P 137

Table A.5: Characteristic product ions observed in the CID-MS/MS of the $[M+H]^+$ ion at m/z 880.1818 and the *quasi*-MS³ analysis of the $[M+2H-Na]^+$ ion at m/z 858.2064 from the Sulfo-SBED 5.....P 138-139

LIST OF ABBREVIATIONS

AP: Atmospheric Pressure

BPEN: Biotin Polyethylene oxide-*N*-hydroxysuccinimide

Biotin-PEO-biotin: biotinyl-hexaethyleneglycol dimer

BeqQ-MS: A hybrid mass spectrometer of BEQQ geometry (B, magnetic sector; E, electric sector; Q, quadrupole mass filter)

CI: Chemical Ionisation

CID: Collision Induced Dissociation

Da : Dalton

DIOS: Desorption/ Ionization on Silicon

DMSO: dimethyl sulfoxide

DNA: Deoxyribonucleic acid

DP: Declustering Potential

EI: Electron Impact

ESI: Electrospray Ionization

DC: Current Potential

FAB: Fast Atom Bombardment

FP: Focusing Potential

FT-ICR: Fourier Transform Ion Cyclotron Resonance

FWHM: Full Width at Half Maximum

GC-MS: Gas Chromatography Mass Spectrometry

GlcNH₂: Glucosamine

Glc: Glucose

H/D: Hydrogen / Deuterium

Hep: *L-glycero-D-manno-heptose*

LC-MS: Liquid Chromatography-Mass Spectrometry

LPS: Lipopolysaccharide

LSIMS: Liquid Secondary Ion Mass Spectrometry

LIAD-MS: Laser-Induced Acoustic Desorption Mass Spectrometry

Kdo: α -3-deoxy-D-manno-oct-2-ulosonic acid

NHS: *N*-hydroxysuccinimide

MS/MS: Tandem Mass Spectrometry

m/z: mass to charge ratio

MALDI: Matrix Assisted Laser Desorption Ionization

PEG: Polyethylene Glycol

PEO: polyethylene oxide

RF: Radiofrequency

Sulfo-SBED: (sulfosuccinimidyl-2-[6-(biotinamido)-2-(*p*-azidobenzamido)-
hexanoamido] ethyl-1,3-dithiopropionate

TOF: Time of Flight

Qq-TOF: Quadrupole Orthogonal Time of Flight

QIT: Quadrupole Ion Trap

Qhq: Quadrupole Hexapole Quadrupole

CHAPTER 1: INTRODUCTION

Glycoconjugates are key regulated biomolecular structures which are present on the cell-surface of organisms. They are composed of several inter-glycosylated sugar units (glycoforms) covalently attached to either lipids or proteins. The major structural diversity of the glycoconjugates provides the ability to modulate protein function, to mediate molecular interactions, as well as to alter the physical properties and stability of protein.

Despite the continuing growth of glycobiology as a prominent field of research, the structural tools available to researchers are quite limited. This limited progress is due to the lack of molecular and chemical tools available to probe the roles of the molecular structures of the glycoconjugates. In addition, it is difficult to evaluate the activities of the enzymes responsible for processing the glycan part of the glycoconjugates. Indeed, the role of the glycan moiety of glycoconjugates is still poorly understood. In a variety of cases, the sugars, which may be responsible for antigenicity, do not appear as a simple decoration of lipid or protein bases. Glycoconjugates represent a variety of molecules which are present in living organisms, animals, plants, fungi and bacteria, and in which the proteins and the lipid moieties are involved in important biological activities. The covalent attachments are essential to regulate the variety of enzyme activities and the cell signal transmissions. The glycoconjugates are involved as important protective antigens.

Mass spectrometry is the tool of choice for the analysis of complex biomolecules and therefore it has been used for identification and characterization of different biotin reagents, oligosaccharides, and glycoconjugates.

The first part of the investigation reported in this thesis involved the study of biotin reagents using electrospray ionization tandem mass spectrometry carried out on quadrupole orthogonal time-of-flight hybrid instrument. The second part consisted of the characterization of the core oligosaccharide of *Aeromonas hydrophila* (chemotype II) lipopolysaccharide using ESI and MALDI tandem mass spectrometry.

1.1. Mass spectrometry

Mass spectrometry is an analytical method for determining the molecular mass of a chemical or biological compound. This technique holds an integral place in analytical chemistry due to its sensitivity, its low sample consumption and its relative rapidity of analysis.

Mass spectrometry determines the masses of molecules, whereby an electrical charge is placed on the molecule and the resulting ions are separated by their mass-to-charge ratio (m/z). There are numerous types of mass spectrometers, varying in the types of ionization source and mass analyzer configuration. The following sections overview the main techniques of mass spectrometry used in the context of this thesis.

The mass spectrometer is typically composed of three main parts: the ionization source, the analyzer and the detector (**Figure 1.1**). In the source, the molecule undergoes ionization under a reduced vacuum atmosphere and is heated to a certain temperature. It is in the ionization source that the fragment ions are also formed. In the analyzer, the molecular and fragment ions are essentially separated according to their mass-to-charge ratio (m/z). Finally, the detector collects the ions, quantifies their intensities and amplifies their signals. All of these procedures are conducted in a low pressure vacuum in order to minimize collision between ions and

molecules of gas. After the detector, a computer system processes the data and generates a mass spectrum, which specifies the variation of ion current observed according to the ratio (m/z). The ionization sources, the analyzers and the detectors can be associated in various configurations and accordingly can create a variety of mass spectrometers. However the proper choice of ionization source and analyzer type will depend on the nature of the sample (polarity variance) and on the data type desired (sensitivity, resolution and mass range).

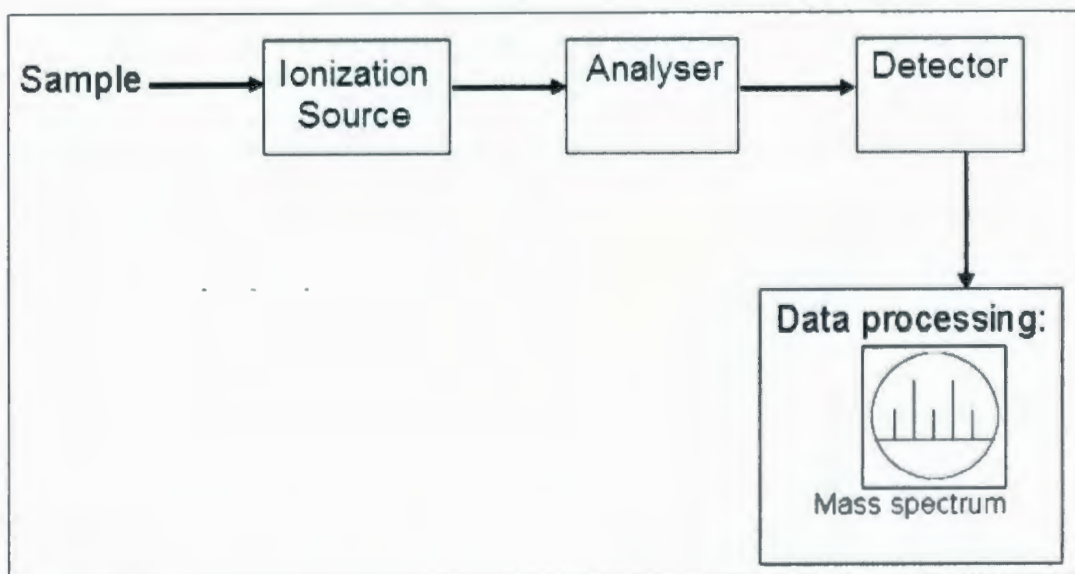


Figure 1.1: General schematic representation of a mass spectrometer

1.2. Ionization techniques

1.2.1. Hard or direct ionization techniques

Electron impact ionization (EI) and chemical ionization (CI) are both traditional techniques. They are called "hard" techniques for sample analysis because they use enough internal energy to cause substantial fragmentation of the analyte. Both techniques work under the same principle. During EI and under a high degree of vacuum a sample e.g. consisting on molecules "M" is evaporated by a thermal effect and is then bombarded by energetic electron beams:



The chemical ionization method (CI) in which the ionization occurs by interaction between the reactive ions and a reactive gas is a "softer" method than EI, although it is still considered to be a hard ionization technique. The protonation of the ion occurs by two steps: the first step is the electron impact ionization of the gas such as methane and the second is the protonation of the molecule M by a reactive gas, such as methane:



In addition, the EI/CI ionization sources are methods of choice when dealing with compounds having small molecular mass because they can also be coupled to a GC instrument and the sample can be introduced in the source in the gas phase.¹

1.2.2. Soft or indirect ionization techniques

These methods are called "soft" because they give the minimum internal energy to the analyte to induce fragmentation. Numerous soft ionization techniques, each with their own merits, have been developed:

- Fast atom bombardment (FAB).^{2,3}
- Liquid secondary mass spectrometry (LSIMS).⁴
- Matrix assisted laser desorption ionization (MALDI).^{5,6}
- Electrospray ionization (ESI).⁷

In the last century, the development of the new soft ionization techniques namely electrospray ionization (ESI) and matrix-assisted laser desorption ionization (MALDI), have made an important contribution to a variety of fields (biological, chemical, physical...etc). They have resulted in the award of the Nobel Prize in Chemistry (2002) to John Fenn for ESI and Koichi Tanaka for MALDI.^{8,9}

Soft ionization techniques such as fast atom bombardment (FAB) ionization, matrix-assisted laser desorption ionization (MALDI) and electrospray ionization (ESI) allow conventional single-stage direct MS analysis, and the characterization of complex biomolecular species. In addition to single-stage mass spectrometry, tandem mass spectrometry using collision-induced dissociation or CID-MS/MS has become a particularly important analytical method for structural characterization of biomolecules. The fragmentations of the precursor ions selected are primarily induced in a tandem mass spectrometer by collisions with neutral gas molecules using either low or high energies, which depend mainly on the type of the tandem mass

spectrometer used: QIT-MS/MS, QQQ-MS/MS, QhQ-MS/MS, QqTOF-MS/MS, FT-ICR-MS/MS, BEqQ-MS/MS, and MALDI-TOF-TOF-MS/MS.¹⁰⁻¹⁶

1.2.2.1. MALDI

MALDI is a soft ionization technique which is used extensively for the analysis of large biomolecules, mainly peptides and proteins. MALDI is well-suited for the direct analysis of biomolecules in tissues because of its high sensitivity, high tolerance for salts and other contaminants, and a wide mass range with little fragmentation. A variety of studies such as structural characterization of oligosaccharides and the characterization of vitellogenin protein (a fish biomarker) have been done using MALDI-Qq-TOF in tandem.^{17,18} However numerous investigations have also involved conventional MALDI instruments combined with other techniques. For example, the analysis of rough-type lipopolysaccharides by combined thin-layer chromatography and MALDI mass spectrometry and the detection of affinity of purified crosslinked peptides by MALDI-TOF MS combined with chemical crosslinking of proteins.^{19,20} Moreover MALDI has been used as an efficient tool for the study of DNA,²¹ glycoconjugates,²² and lipids.²³

1.2.2.1.1. Principles of MALDI

The matrix/sample mixture (with a large excess of matrix) is placed on a plate and, after evaporation of the solvent, the matrix will then co-crystallize with the analyte. The most commonly used laser type is the nitrogen laser (337 nm). Next, the proper choice of matrix is very important, with 2,5-dihydroxybenzoic acid (DHB),²⁴

sinapinic acid (SA) and α -cyano-4-hydroxycinnamic acid (CHCA) being the most commonly used matrices for the analysis of proteins and peptides.^{25, 26} The sample is dissolved in an appropriate matrix that has a strong absorption at the wavelength of the laser used. As such, the absorbed laser energy can lead to ionization of the analytes. The resulting ions are then desorbed by proton-transfer between the photoexcited matrix and the analyte (**Figure 1.2**). In fact, however, the exact MALDI ionization process is not very well known. According to the most common assumption, the MALDI ionization phenomenon is identified as a composition of three distinct processes:

- Excitation of molecules of the matrix by the laser photons.
- Emission of the target molecules (analytes) in the gas phase (desorption).²⁷
- Ionization of molecules in the gas phase.²⁸

During laser irradiation ($h\nu$), the molecules of matrix (MH) are excited according the following equation: $MH + h\nu \rightarrow [MH]^*$. Then the energy is transferred to the analyte. In addition, the molecules of matrix and of analytes are ejected into the gas phase. Finally, the ionization process seems to be occurring in gas phase according to two different phenomena:

- A proton-transfer mechanism resulting from acid/base reaction.²⁹
- A proton-transfer when the matrix ions collide with the target molecule (analyte) in the gas phase.

The MALDI ionization technique provides weakly charged ions (monocharged ions) which facilitates the interpretation of the MS results. MALDI has been improved by the application of new techniques operating under atmospheric pressure (AP).³⁰ This improvement has expanded the possibilities and applications of MALDI sources in developing new sources of Atmospheric Pressure (AP-MALDI) such as Desorption/ Ionization on Silicon (AP-DIOS) and Laser-Induced Acoustic Desorption Mass Spectrometry (LIAD-MS).^{31, 32} The advantage of these new sources is that they do not need matrices.

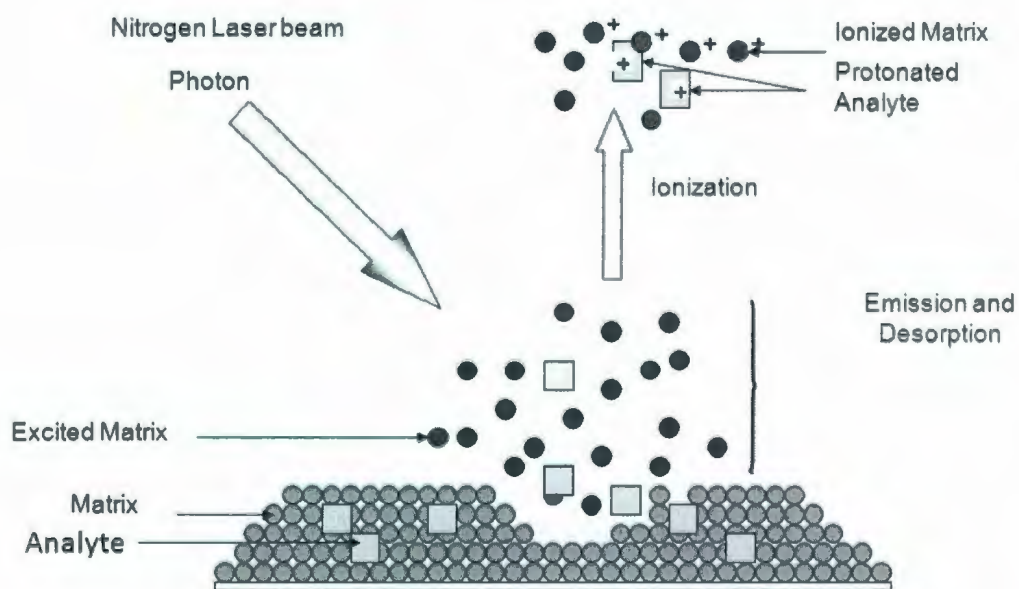


Figure 1.2: Schematic representations showing the process of desorption/ionization of the analytes during Nitrogen UV laser beam irradiation and formation of the ionized species.

1.2.2.2. Electrospray ionization (ESI)

Electrospray sources can produce ions in the gas phase from ions which exist in solution. In 1968, Dole's group described the phenomenon of ionization by ES to generate gas phase-charged ions from macromolecules in solution.³³

After coupling ESI to a quadrupole mass analyzer as well as devoting a great deal of effort toward optimization, the first mass spectrometer capable of analyzing proteins up to 40 kDa was developed.^{7,34} Electrospray ionization (ESI) is characterized by forming multicharged ions in a soft atmospheric ionization technique that can accommodate flow-rates up to 1000 mL /min and is increasingly becoming one of the most popular ionization techniques for LC-MS.³⁵ An electrical potential is applied to the spray nozzle, creating an ionized solution. Eventually the solvent evaporates and charge is applied to the sample molecule. The electrical potential can vary in polarity and creates negative ions, molecules that have lost a proton, or positive ions, molecules that have gained a proton. For example, ESI-QqTOF-MSMS instruments facilitate the structural determination of the individual species in a single analysis. The molecular ion of interest is selected by the first analyzer (MS1) and fragmented by collision induced dissociation (CID) in the collision chamber (MS2).

1.2.2.2.1. Principle of the electrospray source

During electrospray ionization mode, the sample is dissolved in a polar organic solvent, either acidic or basic, and is infused through a capillary, under atmospheric pressure into the source. 2-6 kV is applied at the extremity of the capillary to generate charged droplets, and the ions migrate with the aid of an

electrical field and are dried by warm nitrogen gas. The electrospray process can be assisted by a gas nebulizer. This leads to formation of a series of break-up droplets which are reduced continuously inside the source and resulting in the generation of ions in the gas phase.³⁶ Finally, at the end of the ionization process, single and multi-charged ions are formed (**Figure 1.3**).³³

The electrospray source can be considered as an electrolytic cell in which oxidation-reduction reactions occur between the capillary and the solvent. Indeed, this phenomenon is called an electrophoretic mechanism (**Figure 1.4**).

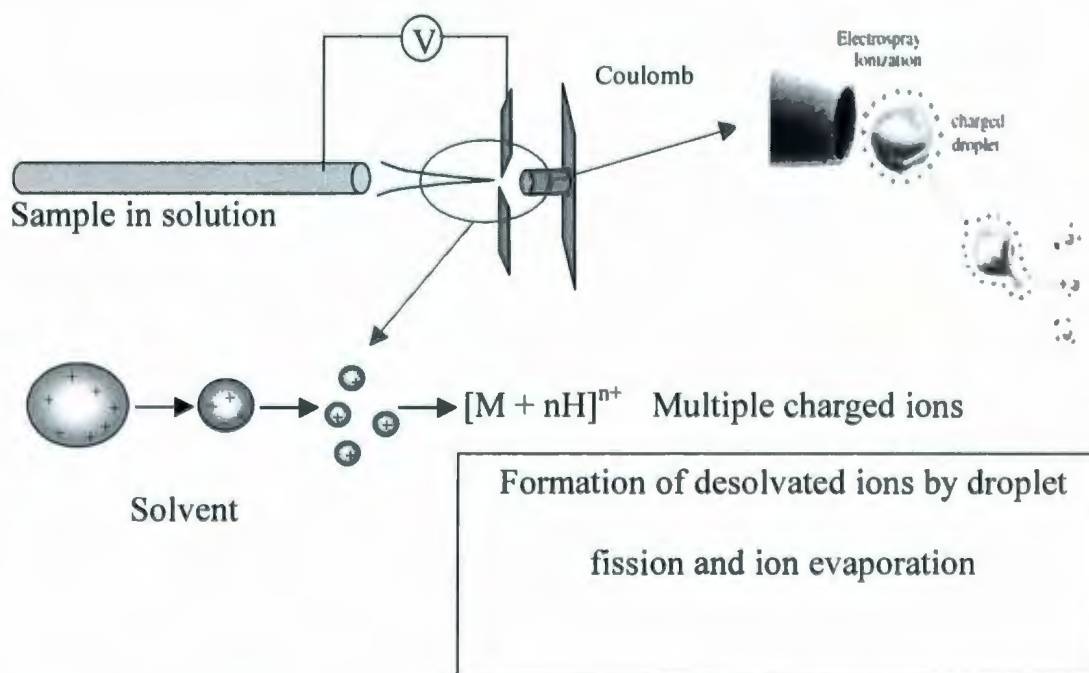


Figure 1.3: Schematic representation of an electrospray source (ES) in positive ion mode: Charged droplets are created due to the high voltage applied at the tip of the capillary. After desorption, they undergo Coulomb explosions, then turn into microdroplets and nanodroplets.

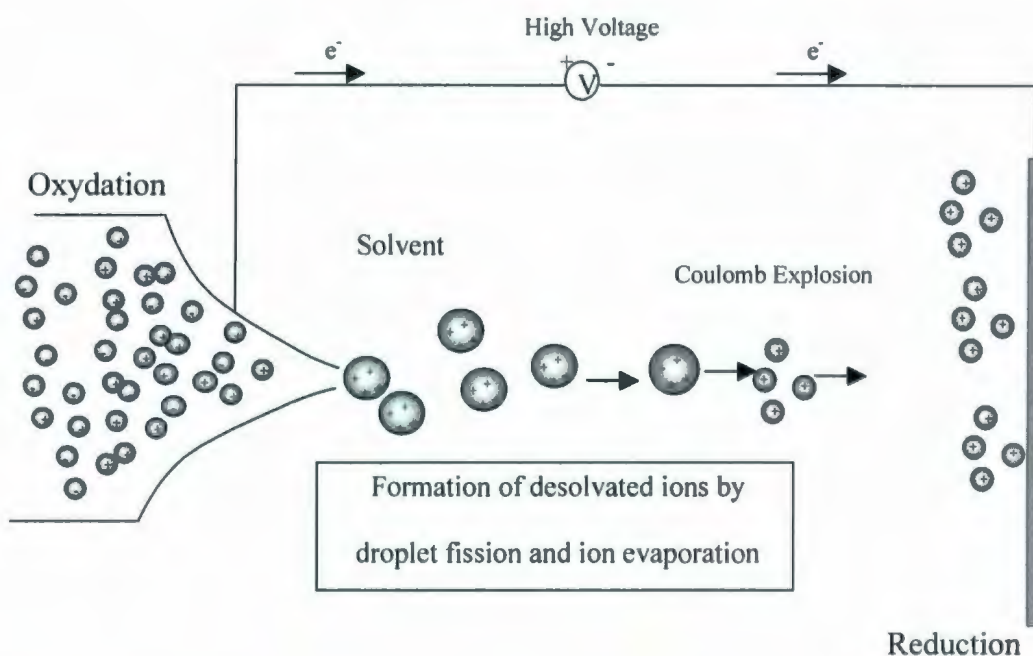


Figure 1.4: Schematic representation of the production of charged droplets during the ES ionization process according to Kebarle & Tang.³⁶ The ES source behaves as an electrolytic cell according to Blade *et al.*³⁷

1.3. Mass analyzers

The main functions of the mass analyzers are based on the separation of ions according to their mass-to-charge ratios (m/z). There are a wide variety of analyzers. The most common are known as scanning analysers, in which the isolation of ions is electrically-driven. Hence, a variety of devices are equipped with hybrid analyzers, which combine several types of analyzers utilizing the specific characteristics of each. However, the choices of mass analyzer will eventually depend on the mass range, the accuracy of the mass measurement and the capacity to distinguish ions having m/z values which are close to one another (resolution). In this section, the focus will be

mostly on quadrupole (Q), time of flight (TOF), and coupling quadrupole/time of flight (Q-TOF) analyzers, which are characteristic of hybrid mass instruments (the ability to do MS/MS).

1.3.1. Quadrupole analyzer

Quadrupole analyzers, also called mass filters, use the stability of the ion trajectories in the quadrupole chamber, based on the potential which is applied to separate the ions according to their mass-to-charge ratios (m/z) (Figure 1.5). The quadrupole analyser is composed of four parallel rods connected electrically.³⁸ The simultaneous application of a direct current potential (DC) and a radiofrequency potential (RF) causes the ions to oscillate between the cylinders. However, only one m/z value will possess the "right" trajectory and survive the path to reach the detector. The rest will collide with rods and will be ejected. The ions are pulsed in the quadrupole by the application of a total electric field according to the following equation: $\Phi_0 = \pm(U \pm V \cos \omega t)$, where Φ_0 is the voltage applied to the rods, ω is the frequency, U is the DC voltage and V is the RF voltage amplitude. The trajectory of the ions will obey the Mathieu equation (developed in 1866). The ions will be separated according to their mass-to-charge ratios (m/z). The advantages of using quadrupole mass analysers are their excellent transmission efficiency, their suitability for GC, LC, and CE applications, and they are low cost, easy to use and require little maintenance. However the major disadvantages are the limitations in terms of mass range (< 4000 Da) and the necessity of coupling more than two quadrupole analyzers to do MS/MS analysis.

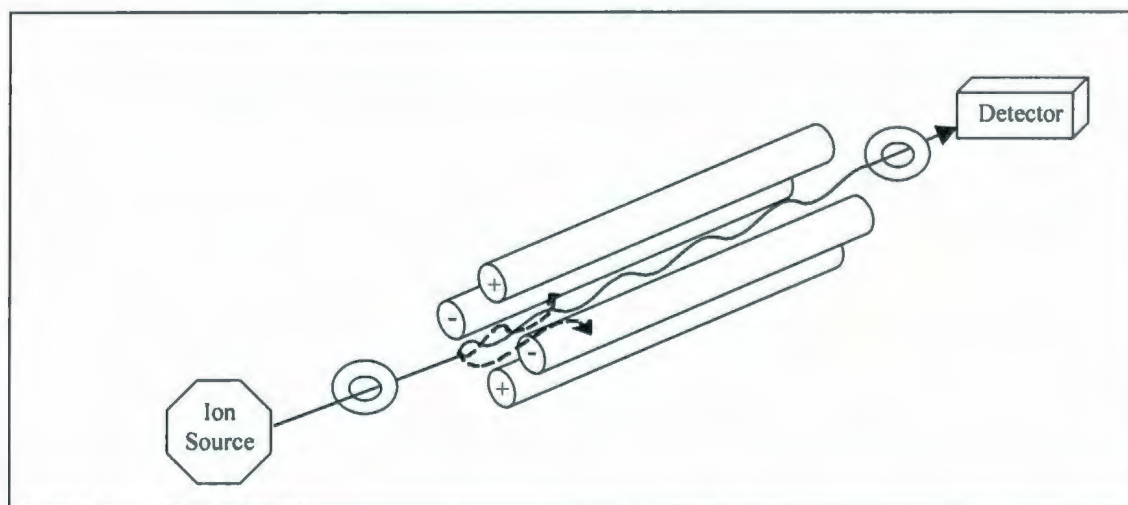


Figure 1.5: Schematic representation of a quadrupole mass analyzer showing the oscillation of ions to reach the detector.³⁹

1.3.2. Time of flight (TOF) analyzer

The TOF analyzer was first described by Stephens in 1946 and is the simplest analyzer type.⁴⁰ By the end of the 20th century, Brown and Lennon had focused and redeveloped this technique.⁴¹ The ions formed in the source are accelerated according to a voltage V_s and travel through the analyzer (d) to reach the detector without the aid of any other acceleration process. Indeed, when an ion leaves the source with a mass m and a total charge $q = Ze$, it will have a kinetic energy (E_c). Consequently, all the ions will reach the detector, contrary to other analyzer types such as the quadrupole. The correlation between the mass/charge ratio and the time of flight is expressed in the following equation: $E_c = 1/2mv^2 = qV_s$. However, the equation can be reduced to more simply illustrate the right correlation between m/z and the time of

flight (t_f): $m/z = K t_f^2$ where K is the calibration factor. Thus the calibration factor between t and m/z is a function of the experimental conditions.

The main advantage of this type of analyzer is the ability to analyze a very high mass range of molecules; however, the main drawback is its low resolution. Consequently, to overcome this drawback, an electrostatic ion mirror has been introduced (reflectron), increasing the resolution power and therefore accuracy in measuring the mass (Figure 1.6).⁴²

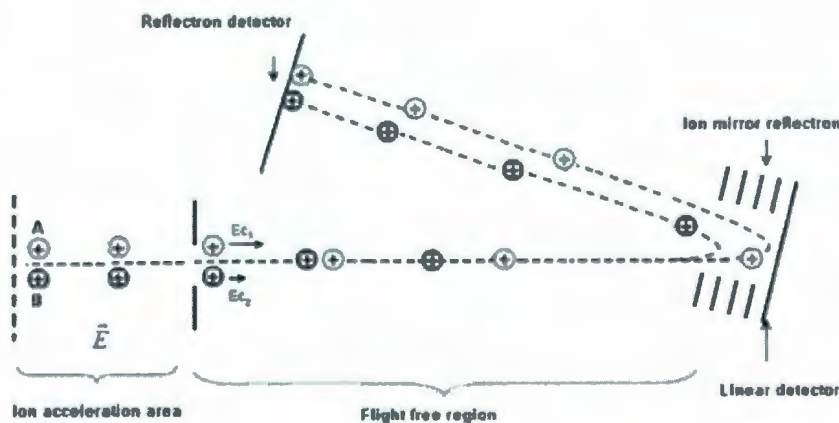


Figure 1.6: Schematic representation of the reflecting time of flight (TOF) analyzer by considering two ions with different masses ($m_A > m_B$). The ion which has the lower mass will reach first the detector.

Analyzers such as the time of flight are preferable and are the most adopted for pulsed ionization methods such as MALDI. The laser shot will determine the starting time for the time measurement, during which the ions reach the detector. Nevertheless, it is not suitable to combine ESI and TOF. However since the discovery of the orthogonal injection system, the properties of ESI and TOF combined together have shown great potential.⁴³ As shown in **Figure 1.7**, the ions are injected by undergoing both a continued and a pulsed ionization. The ions arrive continuously in the source within the Y axis. They are then accelerated and pulsed with a pusher within the Z axis which will accelerate the ions to reach the same level of energy and give the start of the measurement of flight time.⁴³

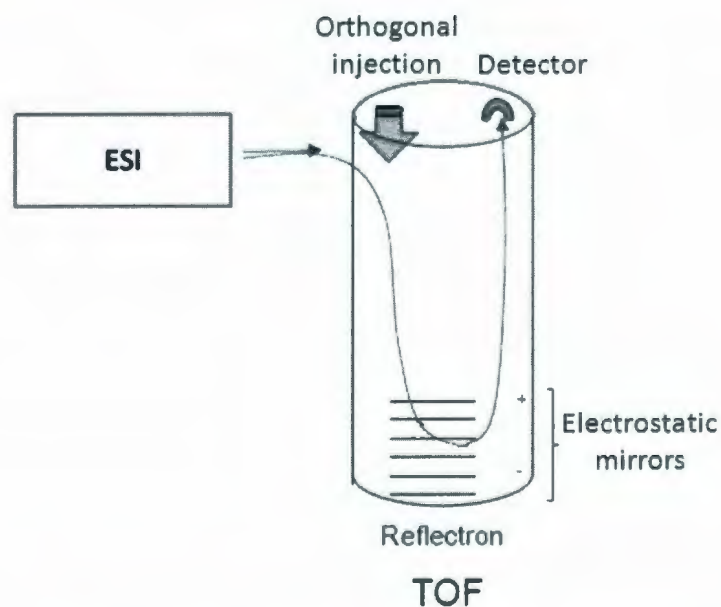


Figure 1.7: Schematic representation of the orthogonal injection system of the reflecting TOF mass spectrometer according to Verentchikov.*et al.*⁴³

1.4. Gas-phase ion formation and fragmentation

The formation of the ions and their fragmentation in the gas phase take place in the ionization source and the mass analyser. The fragmentation of ions can provide valuable information on molecular structure; the precursor ion will dissociate to give fragment ions. Some fragmentation processes occur by collision with a collision gas in the source (single-stage mass spectrometry). However, tandem mass spectrometers which contain multiple mass analyzers connected in a series allow an accurate selection of the precursor ion in the first analyzer and then the fragmentation process of this ion is performed by the second analyzer (collision cell) resulting in the formation of product ions. The structure and identities of these product ions are extremely useful in determining the molecular structural information of the selected precursor ion.

1.4.1. Principle of tandem mass spectrometer operation

The multistage analyses used in tandem mass spectrometry are performed in separate analyzers; there are usually three: the first one selects the precursor ion (MS1), the second in which the collision of the precursor ion with the collision gas occurs, followed by formation of the product ions (MS2); and the third, which analyzes and sorts the product ions (MS3). This kind of analysis is commonly used in triple quadrupole and hybrid analyzers (Q-TOF for example). The tandem mass spectrometer used in this thesis work is a hybrid instrument of ESI-QqTOF-MS and MALDI-QqTOF-MS. This type of instrument, which is shown in **Figure 1.8**, is composed of three quadrupole analyzers MS0, MS1 and MS2, and one reflectron time

of flight (TOF) analyzer which is connected in series. The function of the first quadrupole MS0 is an Rf focusing quadrupole only, while the second quadrupole MS1 acts as a selector of the precursor ions, the third quadrupole (MS2) plays the role of the collision cell, and the TOF analyzer separates the ions according to their m/z ratio. The advantage of using this hybrid instrument is shown by the extreme ease of switching the ion source from ESI to MALDI, the possibility of operating in a moderate resolution mode, and the ability to measure high mass ranges with high accuracy.

In this work, one type of device has been used for the analysis by switching ESI to MALDI with extreme ease, namely the QqTOF-tandem mass spectrometer (QSTAR XL) hybrid instrument.

QSTAR XL - Schematics

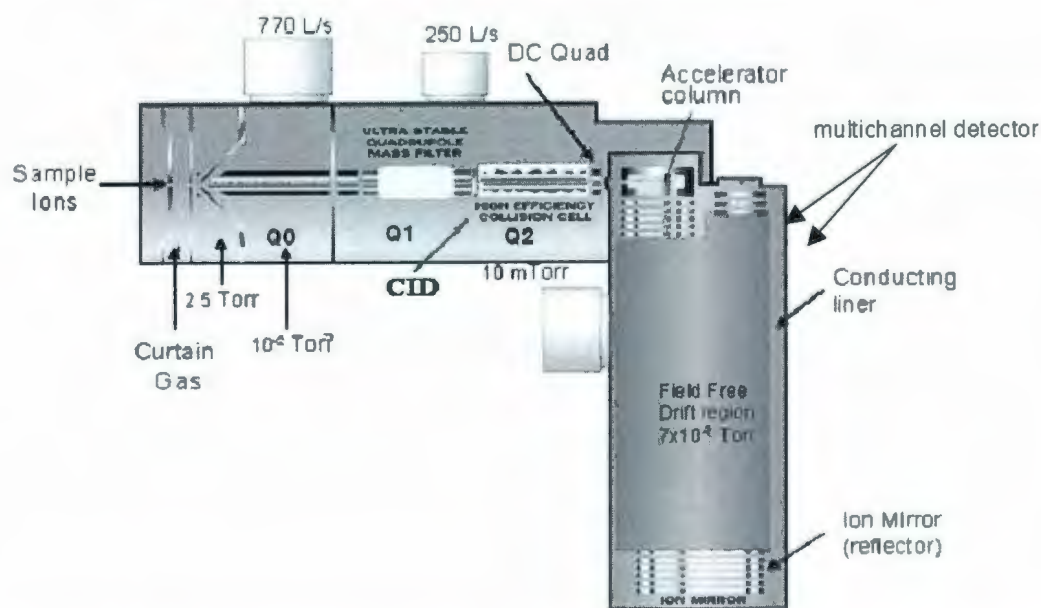


Figure 1.8: Schematic representation of the QSTAR hybrid Qq-TOF. It is also representative of a hybrid quadrupole orthogonal time-of-flight mass spectrometer (Provided by Applied Biosystems).

1.4.2. CID-MS/MS analysis using a hybrid quadrupole orthogonal time-of-flight mass spectrometer

The collision induced dissociation MS/MS (CID-MS/MS) analysis corresponds to the fragmentation of a selected ion which occurs in space within a mass analyzer. Moreover, during MS/MS analysis the selected precursor ion within the collision cell undergoes collision with a stream of inert gas (e.g. xenon, argon, nitrogen) (**Figure 1.9**). Hence, the fragmentation of the precursor ions is the result of the increase of the internal energy of the precursor ion followed by the dissociation of this ion by forming fragment ions (product ions). In this case, Collision-Induced-Dissociation (CID) occurs, which was first described by Jennings in 1968 and confirmed by McLafferty and his co-workers in 1973.^{44,45} The QSTAR hybrid QqTOF instrument is a good example of one which has low-energy CID analysis capability.

ESI-Qq-TOF-MS/MS: Tandem Mass Spectrometry

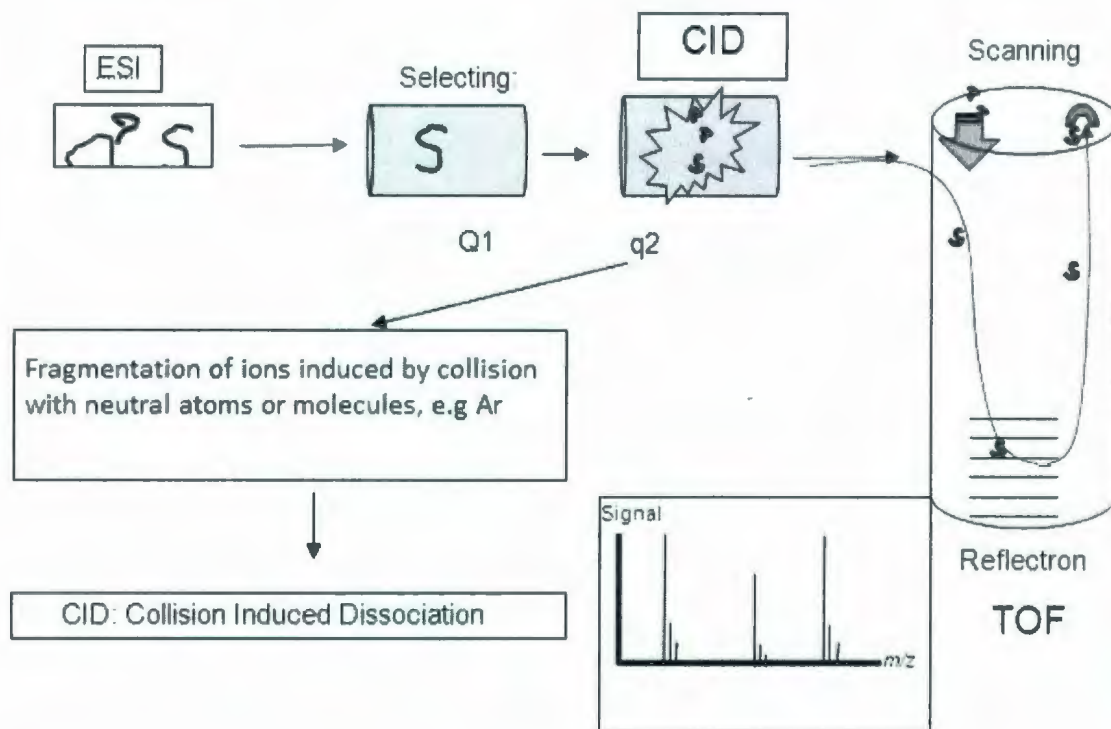
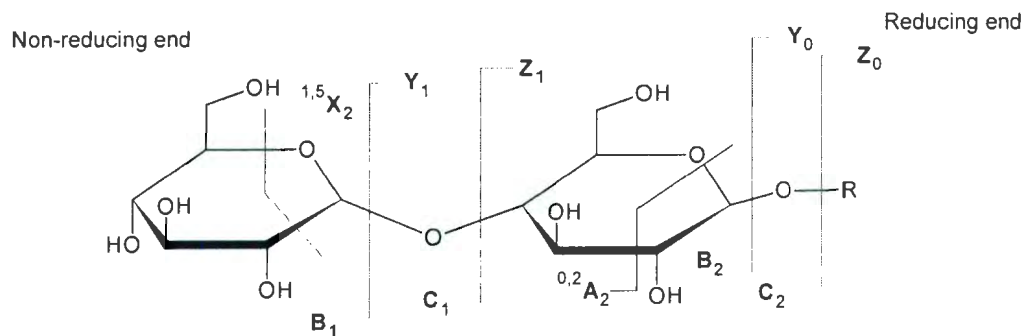


Figure 1.9: During CID MS/MS analysis a precursor ion is selected in the first mass analyzer (MS1) and is then dissociated in the collision cell with a stream of inert gas, the daughter ions are separated in the second analyzer (MS2).

1.4.3. Gas-Phase fragmentation of glycoconjugates during mass spectrometry analysis

The glycoconjugates consist of a large number of molecules formed from a covalent linkage between glycosyl chains (oligosaccharides or polysaccharides) and proteins, peptides and lipid aglycons. Recently, mass spectrometry was shown to be an excellent means for the structural elucidation and characterization of glycoconjugates.^{46a,46b,17,13a,13b}

The CID analysis of the protonated molecules of complex glycoconjugates was first described by Domon and Costello.^{46a,46b} They proposed a universal mechanism of fragmentation routes during FAB MS/MS analysis of complex glycoproteins. For example, **Figure 1.10** represents a simple illustration of the nomenclature of the fragmentation of a glycosyldisaccharide (maltose) portion during CID-MS/MS analysis. The product ions which are assigned as A, B, and C correspond to the fragments that occur from a non-reducing end of the oligosaccharide, and those which are labeled as X, Y, and Z correspond to the fragments that occur from a reducing end of the oligosaccharide (aglycon). Fragment ions which are assigned as A and X correspond to the fragments occurring from the cleavage across the glycosidic ring, and are coded by labeling each ring bond with a number that is assigned according to the sugar unit being fragmented and to the position of the breakage (**Figure 1.10**).



α -D-Glucopyranosyl-(1 \rightarrow 4)-D-Glucopyranose

Figure 1.10: Possible fragmentation pathways during CID-MS/MS of a glycoconjugate corresponding to maltose according to the Domon & Costello Nomenclature.^{46a,46b}

1.5. LPS-non-derived conjugate as a vaccine candidate

1.5.1. Lipopolysaccharides: (LPSs)

During the last decade, lipopolysaccharides (LPSs) have been studied in light of their being significant biological components of outer membranes in gram-negative bacterial cells. It was determined that LPSs are toxic, complex macromolecules and are found in the outer membranes of all gram-negative bacteria.⁴⁷ LPSs are known for causing endotoxic shock and pyrogenic activity. Also, LPSs can activate and compliment macrophages. However the endotoxic properties of LPSs reside largely in the lipid A components. LPSs are composed of two different parts: lipid A and a polysaccharide part beyond the outer membranes. It has been proven that the lipid A produces toxic properties and is responsible for the biological activities of endotoxins. Lipid A is generally composed of a glycosamine disaccharide containing both *N*- and *O*-linked fatty acids.⁴⁸ The polysaccharide fraction of the LPS consists of an internal core linked to lipid A, and an external core linked to a chain polysaccharide residue also called the *O*-specific chain. The latter is composed of repeating oligosaccharide units whose structure and composition are different for various genera and bacterial serotypes.⁴⁹ The outer core consists of hexoses (primarily glucose), galactose, and *N*-acetyl-glucosamine. However the inner core oligosaccharide is composed of specific residues characteristic of LPSs, such as L-glycero-D-manno-heptose (Hep) and 3-deoxy-D-manno-octulosonic acid (Kdo).⁵⁰ Kdo is a unique and specific 8-carbon sugar present in the LPSs of a wide variety of gram-negative bacteria. It has been demonstrated that it has important biological activities in LPSs.⁵¹

Different LPSs have been used in derived conjugates in numerous therapeutic studies as protective vaccines.⁴⁷⁻⁵⁴ The general schematic representation of lipopolysaccharide structure is presented in **Figure 1.11**.

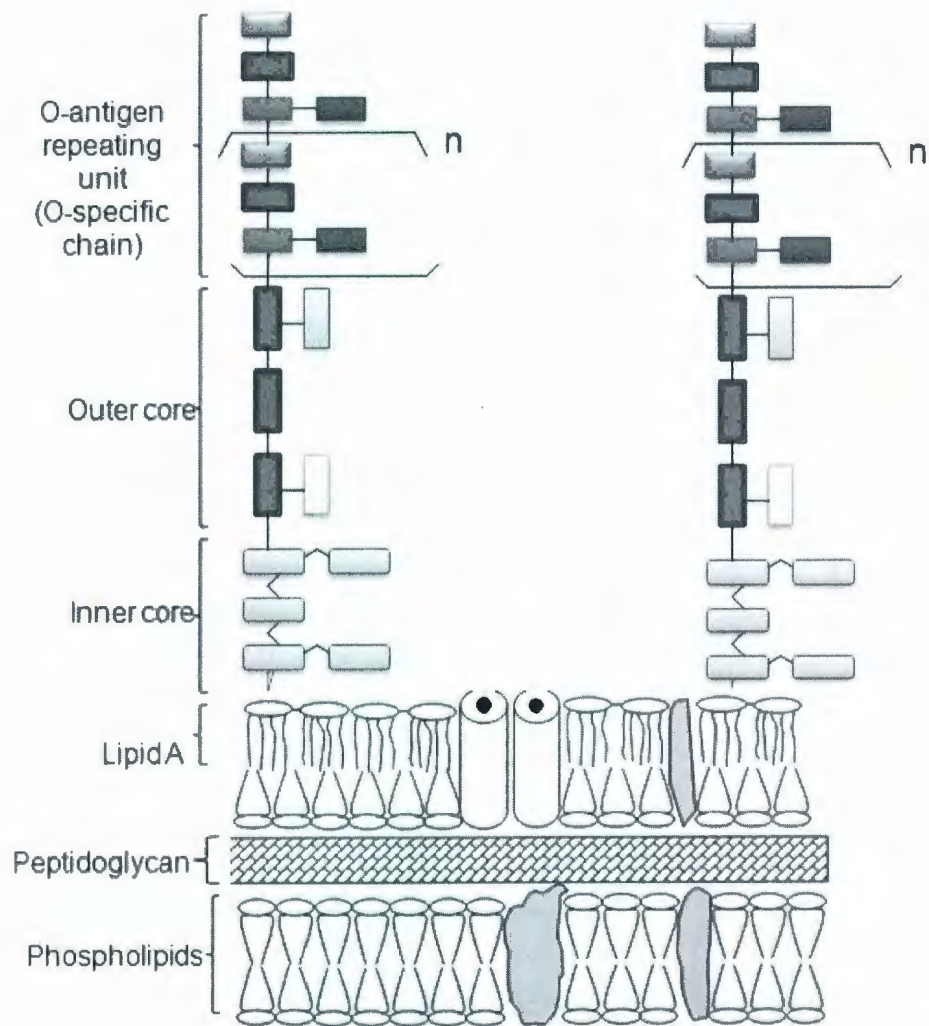


Figure 1.11: Schematic representation of gram negative bacterial membrane and a lipopolysaccharide structure.⁵⁵

1.5.2. Lipopolysaccharide-protein conjugate vaccines

In 1929 Avery and Goebel created a neoglycoprotein by attaching a polysaccharide to a protein carrier in order to enhance the immunogenicity of polysaccharide antigens.⁵⁶ The polysaccharide-protein conjugate vaccines are more efficient in inducing an immune response than polysaccharide vaccines which are made from purified polysaccharide antigens. Since then, numerous methods have been investigated for the synthesis of glycoconjugates which have been found to be very efficient and useful for vaccine development.⁵⁷⁻⁵⁹

The attachment between the LPS and the protein carrier could be either by a direct attachment, or through specific linkers. Using linkers or spacers to join the sugar residue and the protein carrier by a covalent bond is a very efficient method in terms of controlling the chemical process and molecular stability.⁶⁰ On the other hand, the choice of the carrier protein for conjugation is important. Bovine serum albumen (BSA) is a protein carrier most commonly used in the formulation of the LPS-protein conjugate vaccine. BSA is stable and could enhance the immune response due to its large size. Due to this fact it will be recognized by the immune system and will trigger an immunological reaction.⁶¹

LPS-protein and polysaccharide-protein conjugates have been investigated in a recent variety of articles which report the efficiency of the conjugate vaccines for protection against a variety of bacterial diseases.^{52,53,62} For example Joanna Kubler-Kielb *et al* have investigated sugar-protein conjugate vaccines for *Bordetella* species. They demonstrated new conjugation procedures to produce efficient vaccines by using mild acid hydrolysis and/or deamination of the inner core oligosaccharide of the

LPS for binding the protein carrier. Mass spectrometry investigations have been conducted using MALDI-TOF MS analysis in order to evaluate the yield of glycoconjugate reactions and to characterize the conjugates.⁵²

1.5.2.1. Biotin reagents: potential linkers for glycoconjugate performance

Biotin reagents are essentially composed of biotin molecules which can be derivatized to incorporate various reactive groups. The essential function of those reactive groups is to allow the attachment with other molecules within different functional groups such as primary amines, sulfhydryls, and carboxyl groups.

1.5.2.1.1. The Biotin molecule

Biotin is known as either vitamin H or as vitamin B7, and is a water-soluble B-complex vitamin, which has a nominal mass of 244 Da and an empirical formula of $C_{10}H_{16}N_2O_3S$.⁶⁵ Its valeric acid chain can be derivatized to incorporate different functional groups (**Figure 1.12**). Consequently, these varieties of biotin reagents offer a large choice for the biotinylation of a variety of molecules. The proper choice of this vitamin is useful and efficient for molecule biotinylation because, when attached to macromolecules, it does not affect their biological activity and their properties. Furthermore, the biotin molecule has a very high affinity with both Avidin and Streptavidin represented by the non-covalent interaction which is characterized by $K_a = 10 M^{-1}$.^{63,64} This complex binding allows the enhancement of the sensitivity in many assay procedures and is therefore a useful tool in designing nonradioactive purification and detection systems.^{14, 20}

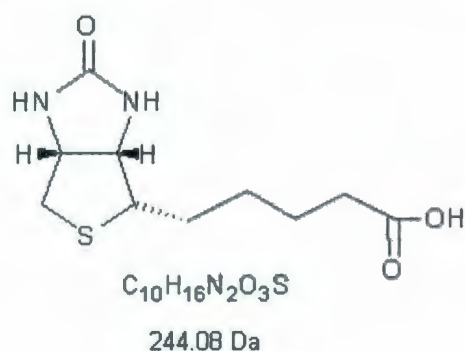


Figure 1.12: Biotin molecular formula. It is composed of a tetrahydroimidazole ring fused to a tetrahydrothiophene ring substituted at the C-2 position with valeric acid.⁶⁵

1.5.2.1.2. Biotin labelling

A variety of biotin reagents are commercially available and the proper choices of the appropriate biotin reagents are facilitated by selection according to their reactivity. Indeed, according to the functional groups of the biotin reagents to be conjugated, specific biotin reagents are available for binding specific molecules. Therefore, the biotin can label different molecules or macromolecules such as protein/peptide, polysaccharide/oligosaccharides, DNA/nucleic acid, etc.

There have been a multitude of reports dealing with the identification of intact protein-biotin complexes by matrix-assisted laser desorption/ionization mass spectrometry (MALDI-MS).^{66,67,68,69} Biotin plays an important role as one of the most efficient non-radioactive DNA labels which can be detected by MALDI-MS, using, for example, the biotin–protein–conjugated-streptavidin system.⁷⁰⁻⁷³

It has been observed that DNA sequencing using MS requires stringent purity of the analytes that are introduced into the mass spectrometer. Approaches for purifying DNA samples which rely on the strong interaction of biotin and the protein

streptavidin on solid surfaces such as magnetic beads have been widely used. Consequently, the MALDI-MS sequencing of oligonucleotides which generates Sanger-sequencing fragments using biotinylated dideoxynucleotides, followed by capture with streptavidin coated magnetic beads, has been extensively used.⁷⁴ In addition, there have been numerous reports on the electrospray ionization (ESI)-MS characterization of labeled oligonucleotides using biotin.⁷⁰⁻⁷⁴

CHAPTER 2: MATERIALS AND METHODS

2.1. Biotin reagents

2.1.1. The origin and structure of the biotin reagents

The five biotin linkers which are represented in **Figure 2.1** and used in this study were commercially-available products purchased from Pierce (Rockford, IL). The general structures are Psoralen-PEO-B (psoralen-polyethylene oxide-biotin) **1**, *p*-aminobenzoyl biocytin **2**, Photoactivatable biotin **3**, B-PEO-B dimer (biotinyl-hexaethyleneglycol dimer) **4**, and (sulfosuccinimidyl-2-[6-(biotinamido)-2-(*p*-azidobenzamido)-hexanoamido] ethyl-1, 3-dithiopropionate) known as Sulfo-SBED **5**.

2.1.2. Isotopic Labelling: hydrogen deuterium exchange of biotin reagents

In order to confirm the fragment ions obtained by ESI-CID-MS/MS analysis of each biotin reagent, the biotin linkers **1-5** were dissolved in 99% methanol- d_1 ($0.25 \mu\text{g } \mu\text{L}^{-1}$) and were kept under stirring at room temperature for about 2 hours to assess the full amide hydrogen exchange rate. Then the five deuterated biotin reagents were infused directly in the tandem mass spectrometer.

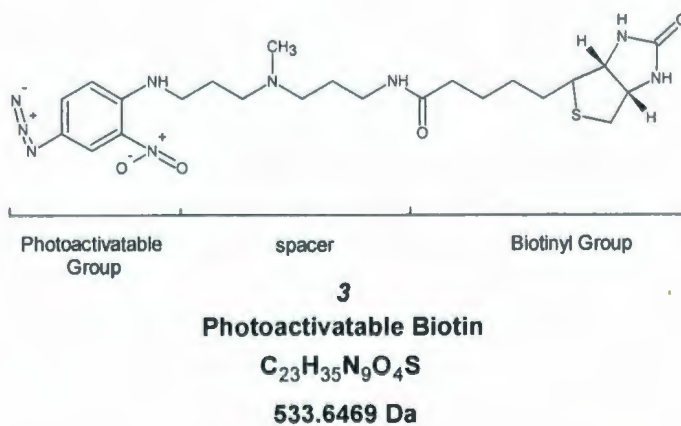
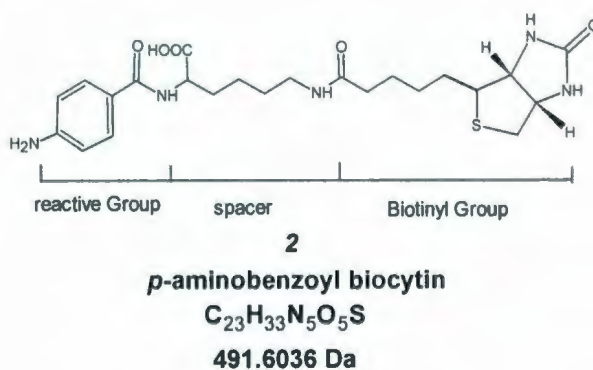
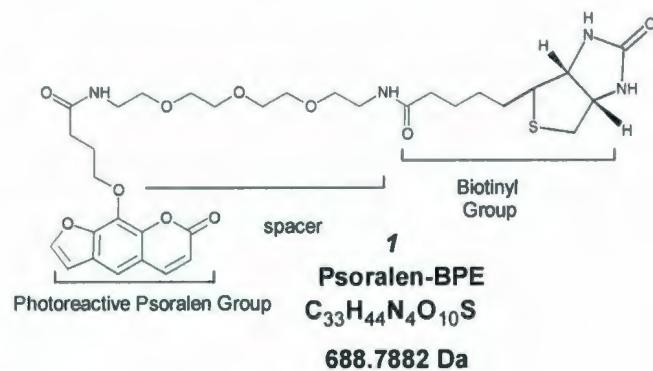
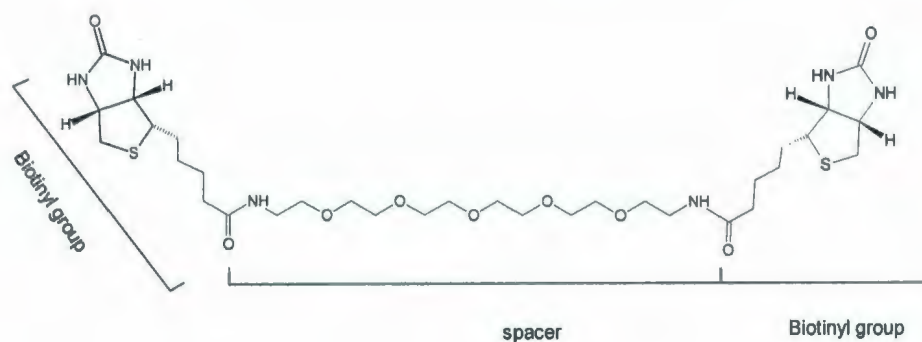


Figure 2.1: The molecular structure of biotin linkers (1-3).

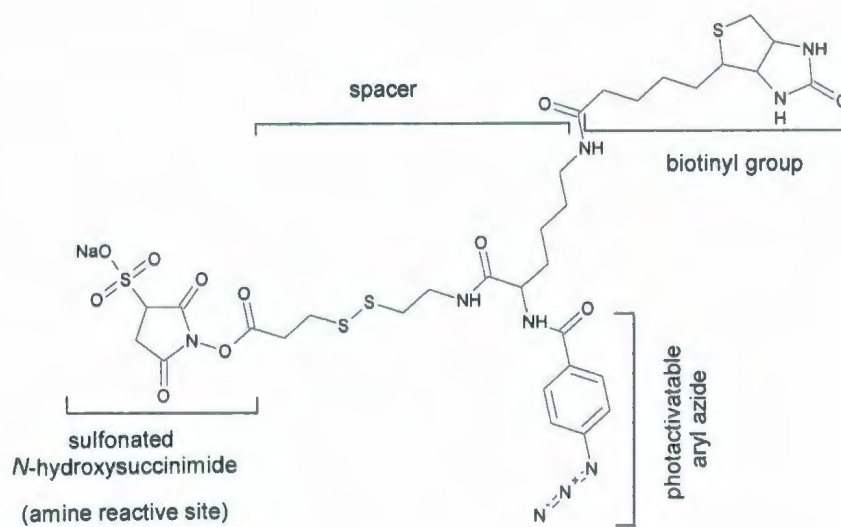


4

B-PEO-B
(biotinyl-hexaethyleneglycol)

$C_{32}H_{56}N_6O_9S_2$

732.9518 Da



5

Sulfo-SBED

$C_{32}H_{42}N_9NaO_{11}S_4$

879.9793 Da

Figure 2.1(continued): The molecular structure of biotin linkers (4-5).

2.1.3. ESI-QqTOF-MS of the biotin reagents

Electrospray ionization-mass spectra of all the biotin linkers were acquired in the positive ion mode using an Applied Biosystems API-QSTAR XL quadrupole orthogonal time of-flight (QqTOF)-MS/MS hybrid tandem mass spectrometer (Applied Biosystems International-MDS Sciex, Foster City, California, USA). This instrument is capable of analyzing a mass range of m/z 5 to 40,000, with a resolution of 10,000 FWHM in the positive ion mode. ESI was performed with the Turbo Ionspray source operated at 5.5 kV. The ESI-MS were recorded with a cone voltage setting (Declustering Potential 1) varying from 60 to 120 volts. All other instrument parameters were kept constant for the ESI-MS analysis (N_2 , Curtain Gas = 20 psi; ion source gas 1 = 20 psi; Air, ion source gas 2 = 0 psi; Declustering Potential 1 (DP1) = 50-120 V; Declustering Potential 2 (DP2) = 250 V, Focusing Potential = 10V and temperature = ambient). The biotin linkers were dissolved in 1:1 methanol/water or dichloromethane/methanol ($1.0 \text{ mg}\cdot\text{mL}^{-1}$). The sample solution was then infused directly, with an integrated Harvard syringe pump (Harvard Apparatus, Hollister, MA) at a rate of $5.0 \text{ }\mu\text{L}\cdot\text{min}^{-1}$. 0.1% formic acid was added to increase the formation of the protonated molecules in the mass spectrometer. The TOF analyzer was calibrated for high masses using a Pep-Tyf peptide which was dissolved in a 1:1 mixture of acetonitrile (ACN or CH_3CN): water (H_2O) and checking for the exact masses of the $[\text{M}+\text{H}]^+$ at m/z 1638.8485 and $[\text{M}+2\text{H}]^{2+}$ at m/z 819.9279. For low masses, the TOF analyzer was calibrated using penta-*O*-acetyl- β -D-galactopyranose and checking for the exact masses of the $[\text{M}+\text{H}-\text{AcOH}]^+$ ion ($\text{C}_{14}\text{H}_{19}\text{O}_9$) at m/z

331.1024 and octa-*O*-acetyl- β -D-lactopyranose and checking for the $[M+H-AcOH]^+$ ion ($C_{26}H_{33}O_{17}$) at m/z 617.1712.

2.1.4. Low-energy collision CID-MS/MS and *quasi-MS*³ analyses

The product ion scans were recorded with the same QqTOF-MS/MS hybrid instrument. In the product ion mode, the first quadrupole (Q1) selected the corresponding precursor ion. The precursor ion was fragmented into product ions by collision with nitrogen in the LINACTM quadrupole collision cell. Nitrogen collision gas was added to the enclosed chamber of the quadrupole (Q2) for collisional activation of the sample ions. The product ion scans were recorded with Collision Energy (CE) varying between 20 to 50 eV and the CID gas conditions were optimized to ensure that the precursor ion remained abundant. The product ions were scanned and sorted in the orthogonal mass resolving time-of-flight analyzer which measured the occurrence of particular product ions, previously formed in the Q2.

A series of second-generation ESI-CID-MS/MS experiments on the diagnostic product ions were conducted to confirm the various established fragmentation routes. These second generation MS/MS experiments (also called *quasi-MS*³) were initiated by CID in the atmospheric pressure/vacuum interface.^{75,76}

2.2. The core oligosaccharide of *Aeromonas hydrophila* (chemotype II) lipopolysaccharide

2.2.1. Bacterial culture

Aeromonas hydrophila Chemotype II, strain N^o: SJ-48R was originally isolated from canned milk, and it was obtained from the National Collection of Marine Bacteria, Aberdeen, Scotland (strain NCMB86). It was isolated from cells that were grown to a stationary phase in Trypticase Soy Broth, without added dextrose, and it was supplied by Baltimore Biological Laboratories.

2.2.2. Extraction and purification of the core oligosaccharide

The lipopolysaccharide which is shown in **Figure 2.2** was extracted by the aqueous phenol method⁷⁷ and purified by electro dialysis.⁷⁸ The core oligosaccharide was obtained by mild hydrolysis of the lipopolysaccharide with acetic acid, and it was purified by gel exclusion chromatography using Sephadex G-50 and Sephadex G-15.

2.2.3. Permethylation procedure for the core oligosaccharide

2.2.3.1. The Hakomori methylation method

The first methylation analysis of the core oligosaccharide was carried out according to the method of Hakomori.⁷⁹ A sample (5 mg) was dissolved in 1.0 mL of DMSO under stirring at room temperature. 1.0 mL of dimethylsulfinyl anion (preparation: 50mg NaH/oil 50:50 washed with hexane to remove the oil, 1.0 mL DMSO was added, and finally stirred at 60°C for 90 min.) was added to the mixture and the solution was left under stirring at room temperature for about 1 h.

Finally, 1.0 mL of cold methyl iodide (MeI) was added and the mixture was stirred for 4 h. The permethylated core oligosaccharide was purified using a Sephadex LH-20 column and was eluted with chloroform. The solvent was then evaporated and the residue was weighed and dissolved in methanol for mass spectrometric analyses.

2.2.3.2. The Ciucanu & Kerek methylation method

The second methylation analysis of the core oligosaccharide was carried out according to the method of Ciucanu & Kerek.⁸⁰ The carbohydrate sample (2.0 mg) was dissolved in 0.15 mL of DMSO (Me₂SO), 10.0 mg of finely powdered sodium hydroxide (NaOH), and 0.5·10⁻¹ mL of cold methyl iodide (MeI) were added. The mixture was then stirred for 6 minutes in a closed vial at room temperature. The reaction was stopped by adding 0.5 mL of water and 0.5 mL of chloroform. Finally the chloroform layer was washed with water (3 × 5 mL) and dried with Na₂SO₄.

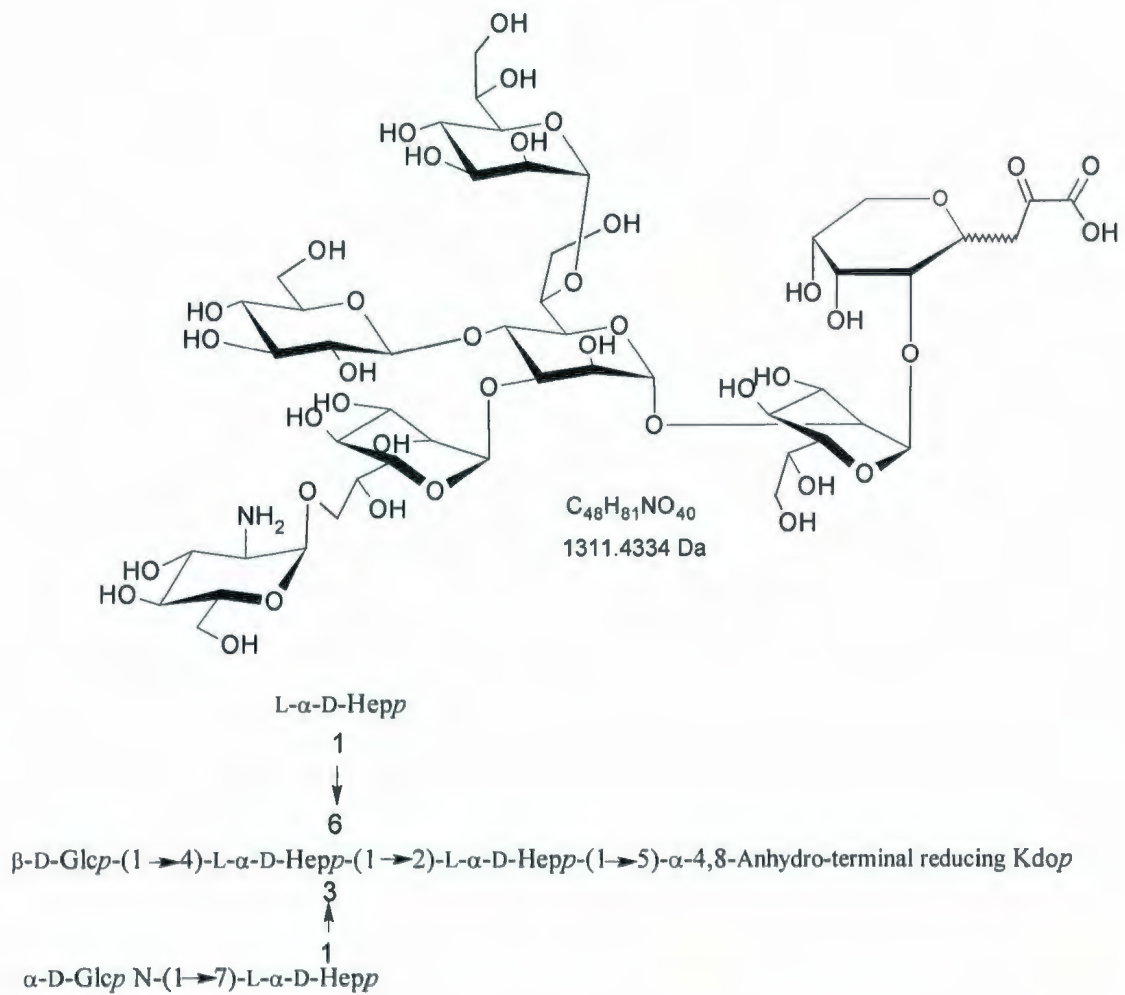


Figure 2.2: Structure of the core oligosaccharide of *Aeromonas hydrophila* (chemotype II) lipopolysaccharide, strain SJ-48R.

2.3. Electrospray quadrupole orthogonal time-of-flight mass spectrometry

Mass spectra of the pure core oligosaccharide mixture were acquired in positive- and negative-ion modes while the mass spectra of the permethylated derivatives of the cleaved core oligosaccharide were acquired in the positive-ion mode. For positive-ion analyses, samples were dissolved in water/methanol/formic acid (90/9.9/0.1) and for negative-ion analyses, samples were dissolved in water. The permethylated derivative samples were dissolved in methanol. An Applied Biosystems, API QSTAR XL QqTOF-MS/MS spectrometer was used for these experiments. The mass range in m/z of this tandem mass spectrometer analyzer varies from 5 to 40,000 and the resolution is 10,000 FWHM in the positive-ion mode. The machine is composed of a Time-of-Flight (TOF) analyzer which is a reflectron, with an effective path of 2.5 m. The sample solution is infused into the mass spectrometer at a rate of $10 \mu\text{L}\cdot\text{min}^{-1}$ using an integrated Harvard syringe pump (Harvard Apparatus, Hollister, MA). The turbo Ionspray source was operated at 5.5 kV at a temperature of 80°C . The principal parameters for ESI-MS in the positive-ion mode were: Declustering Potential (DP1) = 60-80 volt; Focusing Potential (FP) = 200 volt; Declustering Potential (DP2) = 10 volt. The principal parameters for ESI-MS in the negative-ion mode were: Declustering potential (DP1) = -30 volt; Focusing Potential (FP) = -105 volt; Declustering Potential (DP2) = -10 volt. In ESI (+)-CID-MS/MS, the Collision Energy (CE) was about 70 eV and in ESI (-)-CID-MS/MS, the Collision Energy (CE) was about -60 eV.

For all experiments, in both positive-and negative-ion mode the typical parameters were kept more or less constant.

2.4. Matrix-assisted laser desorption ionization mass spectrometry

2,5-Dihydroxybenzoic acid was used as matrix for the MALDI-MS experiment. The DHB (10.0 mg) were dissolved in 1.0 mL of a mixture which was composed of 90% Milli-Q water and 10% methanol for a concentration of 10.0 mg.mL⁻¹. For MALDI-MS analyses the samples were prepared by mixing equal volumes of a saturated DHB solution and a solution of 1.0 mg.mL⁻¹ of the core oligosaccharide mixture. Then 1.0 µL of this solution was placed onto the sample plate. The experimentations were conducted in the same device (QSTAR XL instrument) equipped with a N₂ laser (25 Hz). The spectra were acquired by irradiation of the analytes with desorption laser set at a soft power energy (25% power energy).

CHAPTER 3: GAS-PHASE FRAGMENTATION STUDY OF A SERIES OF BIOTIN REAGENTS USING AN ELECTROSPRAY IONIZATION TANDEM MASS SPECTROMETRY QqTOF-HYBRID INSTRUMENT

3.1. Introduction

During the past few decades, biotin reagents (**Figure 2.1**) have been developed specifically to be attached covalently to proteins via the intermediacy of a cleavable connector.⁸¹⁻⁸⁴ Biotin (**Figure 1.12**), which is also known as either vitamin H or as vitamin B₇, is a water-soluble B-complex vitamin which has an empirical formula of C₁₀H₁₇N₂O₃S.⁶⁵ Biotin itself is a small molecule, with a nominal mass of 244 Da, and is composed of a tetrahydroimidizalone ring fused to a tetrahydrothiophene ring substituted at the C-2 position with valeric acid.⁸⁵

The biotin polyethylene oxide-*N*-hydroxysuccinimide reagent (BPEN) can acylate amino groups of proteins and other compounds via reaction of the *N*-hydroxysuccinimide ester. BPEN covalently labeled compounds can be selectively separated from complex mixtures by adsorbing the target compounds onto the immobilized glycoprotein, avidin.⁸⁵ The high affinity of biotin for avidin provides the basis for many established procedures for the detection and isolation of biotin-associated proteins.⁸¹⁻⁸⁵ It has also become possible to apply this affinity system to the detection of specific DNA sequences by using biotinylated DNA as hybridization probes.⁶⁶ There have been a multitude of reports dealing with the identification of intact protein-biotin complexes by matrix-assisted laser desorption/ionization mass spectrometry (MALDI-MS).⁶⁶⁻⁶⁹

Biotin plays an important role as one of the most efficient non-radioactive DNA labels which can be detected by MALDI-MS using, for example, the biotin–protein–conjugated-streptavidin system.^{71,86} It was observed that DNA MS sequencing requires stringent purity of the analytes that are introduced in the mass spectrometer. Approaches for purifying DNA samples which rely on the strong interaction of biotin and the protein streptavidin on solid surfaces such as magnetic beads have been widely used. In addition, there also have been numerous reports on the ESI-MS characterization of labeled oligonucleotides using biotin.⁷³

The gas-phase mass spectrometric fragmentations of the biotin linkers themselves have not been well studied. Therefore, a systematic and comprehensive study of the biotin linkers using electrospray ionization is necessary. This will establish blueprints and diagnostic fragmentation schemes for ESI-MS and CID-MS/MS analyses and allow quality control and quality assurance of biotinylated DNA and protein complexes. In this study, five commercially-available synthetic biotin linker molecules (*1-5*) (**Figure 2.1**) were investigated. They are defined in the following descriptions:

The psoralen-PEO-Biotin (or psoralen-BPE, *1*) containing the reactive psoralen-group ($C_{11}H_5O_3$) (**Figure 2.1**), which is designed to efficiently label nucleic acids. In addition, the psoralen group can either intercalate into the helices of DNA, or stack along with the bases of single-stranded DNA or RNA. Upon photoactivation, the psoralen group cross-links with the 5,6- double bond of pyrimidine bases.^{87,88}

The *p*-aminobenzoyl biocytin **2** (**Figure 2.1**) is composed of a *p*-aminobenzamide attached to the C-2 position of the hexanoic acid, which is, in turn, attached through C-6 to the spacer (**Figure 2.1**). The biotin reagent **2** preferably reacts

with the phenolic residue of tyrosine and/or with the imidazole ring of histidine.⁸⁹ It is also used to biotinylate DNA through the guanidine at the N-8 position.⁹⁰

The photoactivatable biotin **3** (**Figure 2.1**) contains the *p*-azido-*o*-nitro-aniline group attached on one extremity of the C-3 position of the propyl chain of *N*-1,1'-[(propyl)(propylamine)]-methylamine, whereas the N-4 position of the propylamine chain is attached via an amide linkage to biotin. The *p*-azido-*O*-nitro-aniline portion of this biotin linker will react with a variety of functional groups (primary and secondary amines, sulfhydryl and carbonyl groups).^{91,92}

The biotin-PEO-biotin or biotinyl-hexaethyleneglycol dimer **4** (**Figure 2.1**) is a homobifunctional reagent containing two biotin moieties separated by a diamine-polyethylene oxide (PEO) spacer arm. The PEO spacer arm imparts high water solubility to this reagent. It may be used to connect multiple biotin-binding protein molecules such as the proteins avidin and streptavidin.⁹³

The Sulfo-SBED **5** (**Figure 2.1**) which is composed of the (sulfosuccinimidyl-2-[6-(biotinamido)-2-(*p*-azidobenzamido)-hexanoamido]-ethyl-1,3-dithiopropionate) is a hetero-bifunctional crosslinker, containing both an *N*-hydroxysuccinimide (NHS) ester. The NHS ester is reactive toward primary amines, and a photoactivatable aryl azide group.⁹⁴⁻⁹⁶

In a continuation of our research work on the gas-phase MS fragmentation breakdown of novel biomolecules,⁹⁷⁻¹⁰⁰ the ESI-MS and CID-MS/MS fragmentations of the five different biotin linkers **1-5** are presented in this section.

In this study the highly purified commercial biotin linkers **1-5** were introduced by infusion into the electrospray ionization source without any need for prior chromatographic separation.

3.2. ESI-QqTOF-MS analysis of the biotin reagents 1-5

The ESI-QqTOF-MS analyses of this series were all recorded in the positive ion mode, (DPI = 60-120 volt) and afforded in all cases the expected $[M+H]^+$ protonated molecules. The formation of the protonated molecules was enhanced by the addition of a trace amount of 0.1% formic acid. The product ion scans of the precursor protonated molecules selected from the five biotin linkers are shown in **Figures 3.(1-5)** and in **Schemes 3.(1-5)**. The ESI-MS of the psoralen-PEO-biotin **1** produced the $[M+H]^+$ protonated precursor ion **1a** at m/z 689.2854 and the $[M+Na]^+$ sodiated adduct at m/z 711.2645 (**Fig. 3.1(a)**). The ESI-MS of the *p*-aminobenzoyl biocytin **2** formed the $[M+H]^+$ protonated precursor ion **2a** at m/z 492.2277 (**Fig. 3.2(a)**). The ESI-MS of the photoactivatable biotin **3** afforded the $[M+H]^+$ protonated precursor ion **3a** at m/z 534.2630 (**Fig. 3.3(a)**). The ESI-MS of the PEO biotin dimer **4** afforded the $[M+H]^+$ protonated precursor ion **4a** at m/z 733.3634, and the $[M+H\text{-biotinyl group}]^+$ ion **4b** at m/z 507.2832 (**Fig. 3.4(a)**). Finally, the ESI-MS of the Sulfo SBED **5** afforded the $[M+H]^+$ protonated precursor ion **5a** at m/z 880.1853, and ions which are formed during the ionization process: $[M+H-Na]^+$ **5b** at m/z 858.2060, the $[M+H\text{-}(Sodiated\ Sulfonated\ N\text{-hydroxysuccimide})]^+$ **5d** at m/z 681.2302, and the $[(\text{biotinyl group})\ C_6H_{10}NO\ (\text{photoactivatable aryl azide group})]^+$ **5f** at m/z 500.2018 (**Fig. 3.5(a)**).

In order to confirm the gas-phase fragmentation study of biotin linkers, the ESI-MS of deuterated biotin linkers was also carried out. The H/D exchange for each individual linker was shown to be total (100%). For example, during the ESI-MS analysis of the deuterated biotin linker **1** it was observed that all four exchangeable H

atoms are replaced by D atoms. Moreover, the additional H⁺ charge is also replaced by D⁺. Thus, the mass shift for a full H/D exchange localized at the NH-group of the molecule *I* is +5 Da, and it was assigned as [C₃₃H₄₀D₅N₄O₁₀S]⁺ at *m/z* 694.3250.

3.3. CID-MS/MS analysis of biotin reagents *I-5*

Low-energy collision-induced dissociation CID-MS/MS analyses of the different precursor protonated species [M+H]⁺ were conducted with different collision energies. **Tables A.(1-5)** which are shown in Appendix A, summarize the formation of the various diagnostic product ions observed in the CID-MS/MS analyses of the precursor protonated molecules [M+H]⁺ selected from the various biotin linkers *I-5* and, as well, observed in the *quasi*-MS³ analysis of some second generation product ions. The various coding used for the product ion tagging was based on the nature of the linker, the type of photoreactive group and/or the photoactivatable group. In addition, the CID-MS/MS analyses of the different deuterated precursor species were also achieved to confirm the formation of the major product ions.

3.3.1. CID-MS/MS of the [M+H]⁺ ion at *m/z* 689.2854 selected from the psoralen-PEO-biotin linker *I* and *quasi*-MS³ analysis of the precursor [M+H-photoreactive psoralen group]⁺ ion *Ib* at *m/z* 487. 2507

The product ion scan of the selected protonated precursor ion at *m/z* 689.2854 for the biotin linker *I* (shown as **Figure 3.1(a)**) was recorded with a Collision Energy (CE) of 26 eV and a Declustering Potential (DP1) of 60 V (**Fig.3.1(b)** & **Table A.1** (Appendix A)). The protonated precursor ion at *m/z* 689.2859 eliminates the photoreactive psoralen group [(C₁₁H₆O₄), (202 Da)] to produce the product ion *Ib* at

m/z 487.2507. The precursor ion also eliminates more complex neutral portions corresponding to the photoreactive group attached to part of the linker arm: $C_{12}H_{19}N_3O_2S$ (269Da), $C_{16}H_{29}N_3O_5S$ (375 Da), and $C_{21}H_{24}NO_8$ (419 Da) fragments to afford, respectively, the various product ions: *Ic*, *Id*, and *Ie* at m/z , 420.1844, 314.1022, and 270.1402 (**Fig.3.1(b)** & **Table A.1** (Appendix A)). The formation of this series of product ions has been tentatively assigned as follows. The protonated molecular ion eliminates the photoreactive psoralen group (9-hydroxy-7*H*-furo [3,2-*g*]chromen-7-one) to afford the product ion *Ib* which has been assigned as the $[M+H-(\text{photoreactive psoralen group})]^+$ at m/z 487.2507. The product ion *Ie* at m/z 270.1402 is produced by the loss of the neutral fragment $[(C_{21}H_{24}NO_8), (419 \text{ Da})]$; it was assigned as the $[(\text{biotinyl group})C_2H_5N]^+$. The precursor ion can also eliminate, from the opposite side, a neutral fragment formed by the biotin group and associated fragmented portions occurring from the fission of the spacer arm, such as the $[C_{12}H_{19}N_3O_2S]$ and the $[C_{16}H_{29}N_3O_5S]$ to create the product ions: $[(\text{psoralen group})C_{10}H_{20}NO_4]^+$ *Ic* at m/z 420.1844 and $[(\text{psoralen group})C_6H_{11}NO_2]^+$ *Id* at m/z 314.1022, respectively.

CID-nozzle fragmentation of the protonated molecule *Ia* recorded with different declustering potential (DP1 = 60, 100, 120 V) increased the fragmentation of the protonated molecules into product ions, which allowed to record *quasi-MS*³ of product ion *Ib*. Thus, second-generation product ion scans occurring from the precursor ion $[M+H-\text{photoreactive psoralen group}]^+$ *Ib* at m/z 487.2587 afforded the following series of product ions: *Ie-j* respectively, at m/z 270.1291, 261.1818, 227.0859, 218.1403, 156.1082, and 112.0760 (**Fig.3.1(c)** & **Table A.1** (Appendix A)). The creation of this series of product ions was tentatively described as follows

(Scheme 3.1). The product ion at m/z 261.1818 was created from the precursor ion by elimination of a neutral portion [(C₁₀H₁₆N₃O₂S), (226 Da)] belonging to the biotin group and was assigned as *If* [C₁₂H₂₅N₂O₄]⁺. The product ion at m/z 227.0859 assigned as *Ig* [biotinyl group]⁺ ion can be formed two different ways, either from the precursor ion by the loss of the full spacer [(C₁₂H₂₄N₂O₄), (260 Da)], or from the product ion *Ie* by elimination of aziridine (43 Da). The product ion *Ih* at m/z 218.1403, assigned as [C₁₀H₂₀NO₄]⁺, was created from either the precursor ion by elimination of [C₁₂H₁₉N₃O₂S], (269 Da)] corresponding to the biotinyl spacer fragment or from the product ion *If* by the loss of aziridine. The product ion *Ii* at m/z 156.1082 assigned as [C₈H₁₄NO₂]⁺ was formed from the precursor by elimination of [(C₁₄H₂₅N₃O₄S), (331 Da)] which corresponds to the biotinyl group attached to portion of the spacer arm. In addition, the product ion *Ii* can be formed from the product ion *Ih* by elimination of ethylene glycol (42 Da). Finally the product ion at m/z 112.0760 assigned as *Ij* [C₆H₁₀NO]⁺ spacer fragment ion was formed from the product ion *Ii* by elimination of acetaldehyde (44 Da).

All the proposed structures assigned to the various product ions were verified by conducting separate CID-MS/MS analysis of the selected pentadeuterated-psoralen-polyethylene oxide-biotin ion at m/z 694.3096. As a result, CID-MS/MS of the precursor ion at m/z 694.3250 afforded this series of product ions: *Ib'* at m/z 491.2892, *Ic'* at m/z 423.1951, *Id'* at m/z 315.1136 and *Ie'* at m/z 273.1491. This series of product ions exhibited respectively upward shifts of 4, 3 and 1 Da from the original product ions obtained for the non-labeled precursor ion *Ia* (Table A.1 (shown in Appendix A)). This result confirmed our original assignments of the product ions.

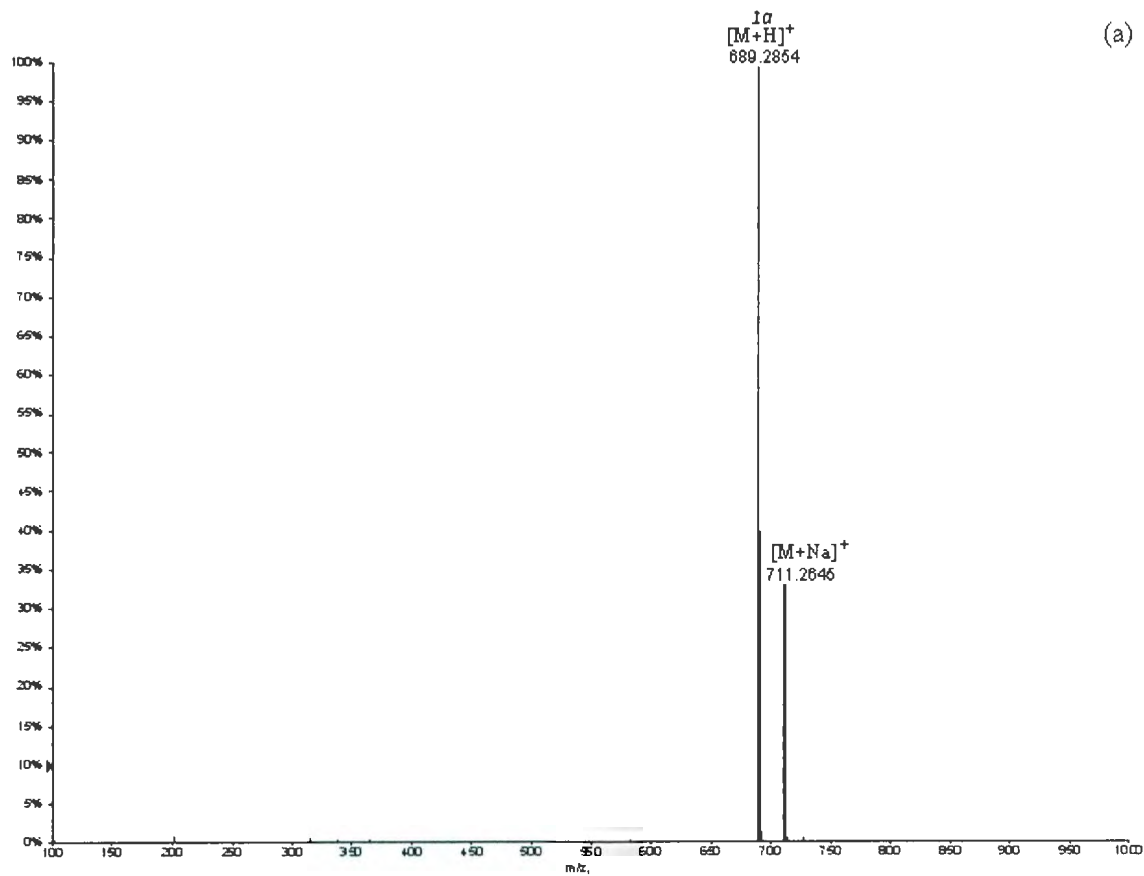


Figure 3.1: (a) ESI-QqTOF-MS (+) of the psoralen-PEO-biotin *1*.

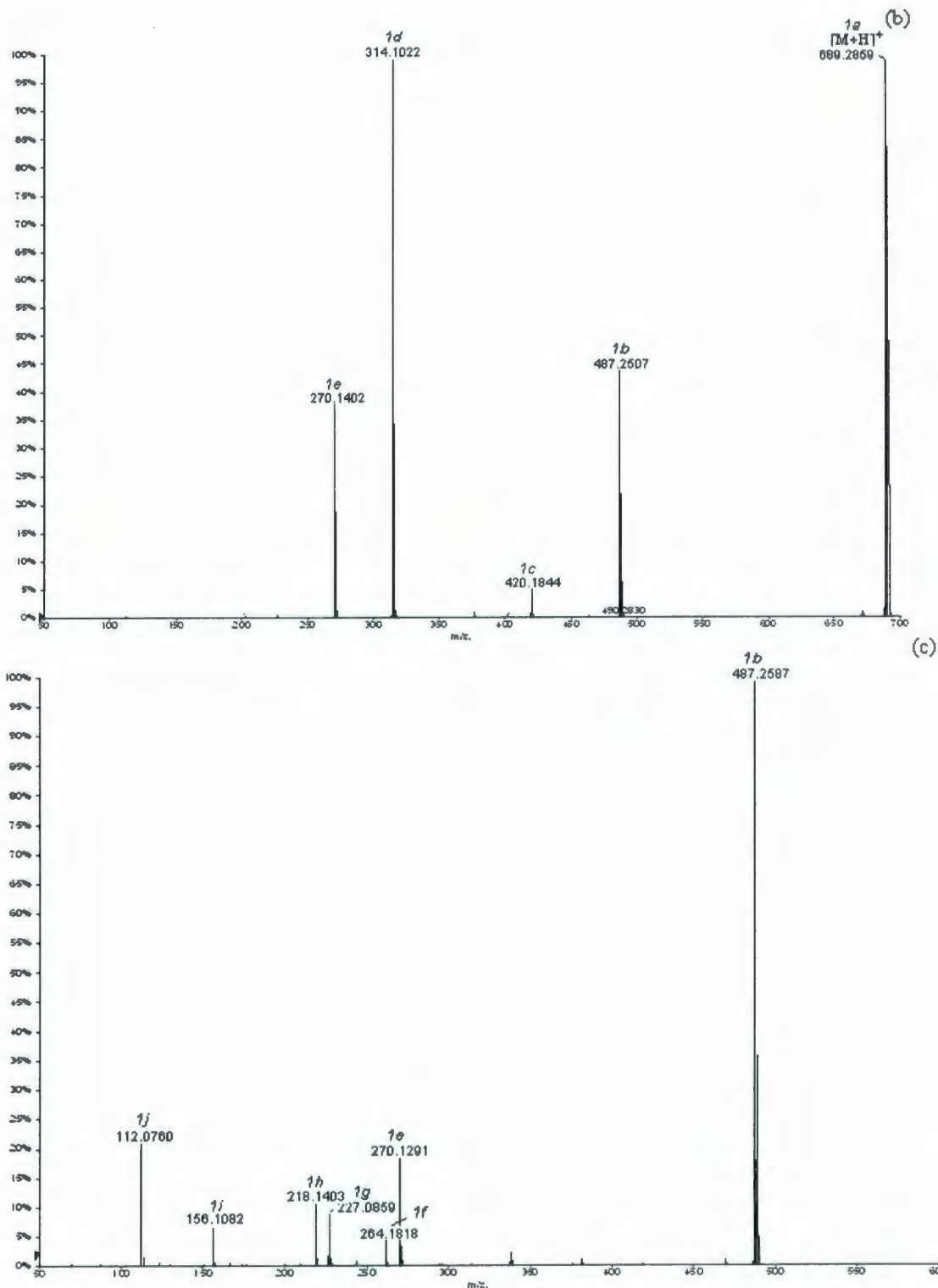
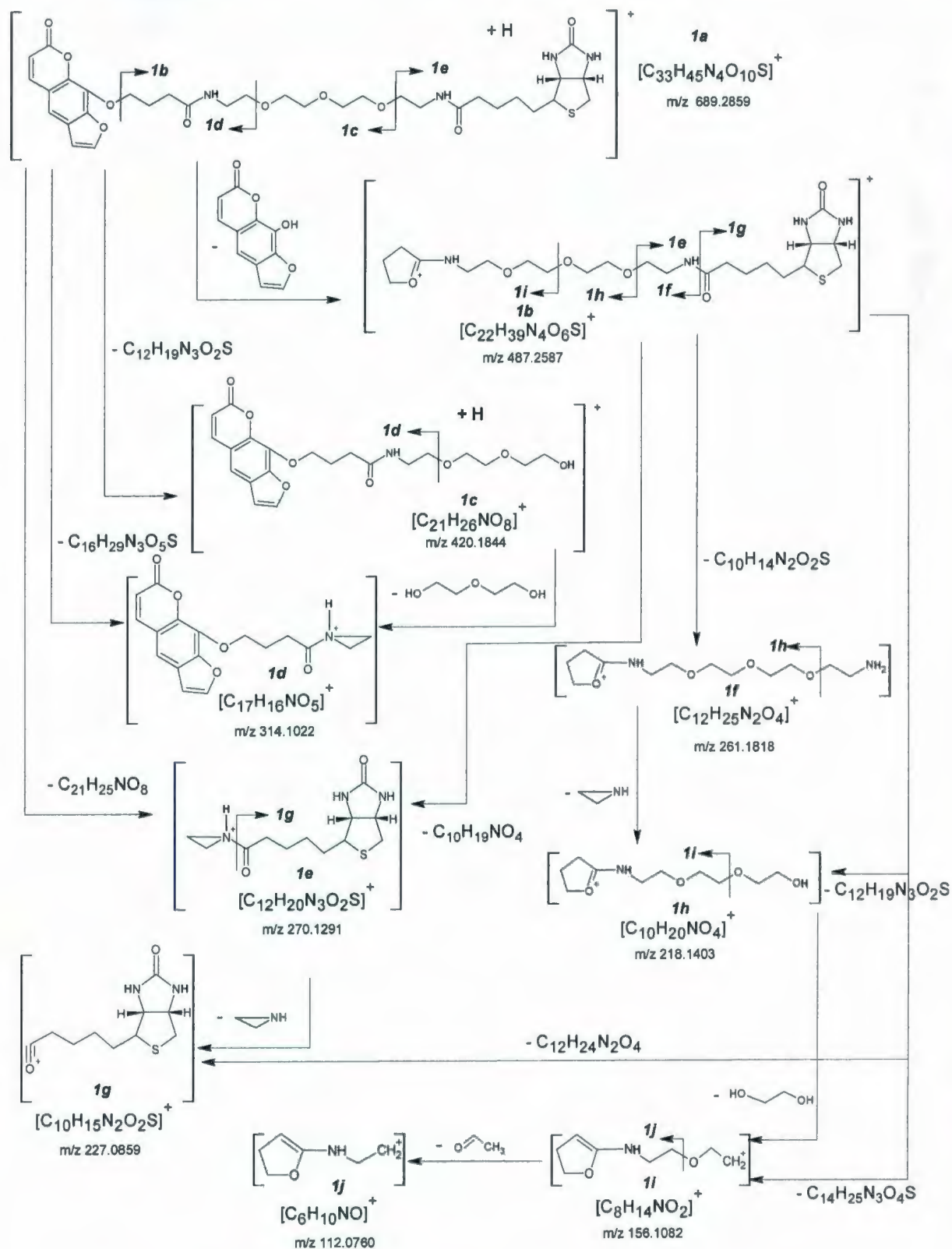


Figure 3.1 (continued): (b) CID-MS/MS of the selected protonated precursor ion at m/z 689.2854 from psoralen PEO Biotin I; (c) quasi-MS³ of the selected ion *1b* at m/z 487.2507 from psoralen PEO Biotin I.



Scheme 3.1: The proposed fragmentation routes of the psoralen-PEO-biotin **1** obtained during the CID-MS/MS of the protonated precursor ion **1a** at m/z 689.2859 and the quasi-MS³ of the precursor ion **1b** at m/z 487.2587.

3.3.2. CID-MS/MS of the $[M+H]^+$ precursor ion at m/z 492.2277 selected from the *p*-aminobenzoyl biocytin linker 2

The product ion scan of the selected protonated molecule at m/z 492.2277 for the biotin linker 2 (shown as **Figure 3.2(a)**) was recorded with a CE of 30 eV and a DPI of 60 V. It afforded the product ions at m/z 474.2172, 310.1598, 227.0860, 120.0447 and 84.0809 (**Fig.3.2(b)**). The structural identities of the major product ions are indicated in **Table A.2** (Shown in Appendix A) and their geneses are showed in **Scheme 3.2** and are explained as follows: The precursor ion at m/z 492.2278 loses water to afford the product ion **2b** at m/z 474.2172 assigned as the $[M+H-H_2O]^+$ ion. This latter product ion eliminates carbon monoxide and *p*-aminobenzamide to give the product ion **2c** at m/z 310.1598 assigned as the $[(\text{biotinyl group})C_5H_9N]^+$ ion. The product ion **2c** can eliminate the neutral pyridine derivative (2,3,4,5-tetrahydropyridine) $[(C_5H_9N), (83 \text{ Da})]$ to give the product ion **2d** at m/z 227.0860 assigned to the $[\text{biotinyl group}]^+$ ion. The product ion **2c** can also lose the biotinyl fragment $[(C_{10}H_{15}N_2O_2S), (227 \text{ Da})]$ followed by protonation to form the product ion **2f** at m/z 84.0809 and this was assigned as the pyridine derivative $[2,3,4,5\text{-tetrahydropyridine} + H]^+$ ion. Note that the product ion **2d** can also be formed directly by cleavage of the opposite side of the precursor ion with elimination of the photoreactive group attached to the full spacer arm $[(C_{13}H_{19}N_3O_3), (265 \text{ Da})]$. Finally, the product ion **2e** at m/z 120.0447 is formed from the precursor ion by elimination of the neutral biotinyl group attached to the full spacer arm molecule $[(C_{16}H_{28}N_4O_4S), (372 \text{ Da})]$, corresponding to the charged photoreactive group $[p\text{-aminobenzoyl}]^+$. The proposed CID-MS/MS fragmentation routes are tentatively shown in **Scheme 3.2**.

All the exact mass assignments of the product ions were verified by conducting separate CID-MS/MS analysis of the octadeuterated-*p*-aminobenzoyl-biocytyl ion at m/z 500.2951 (**Table A.2** (shown in Appendix A)).

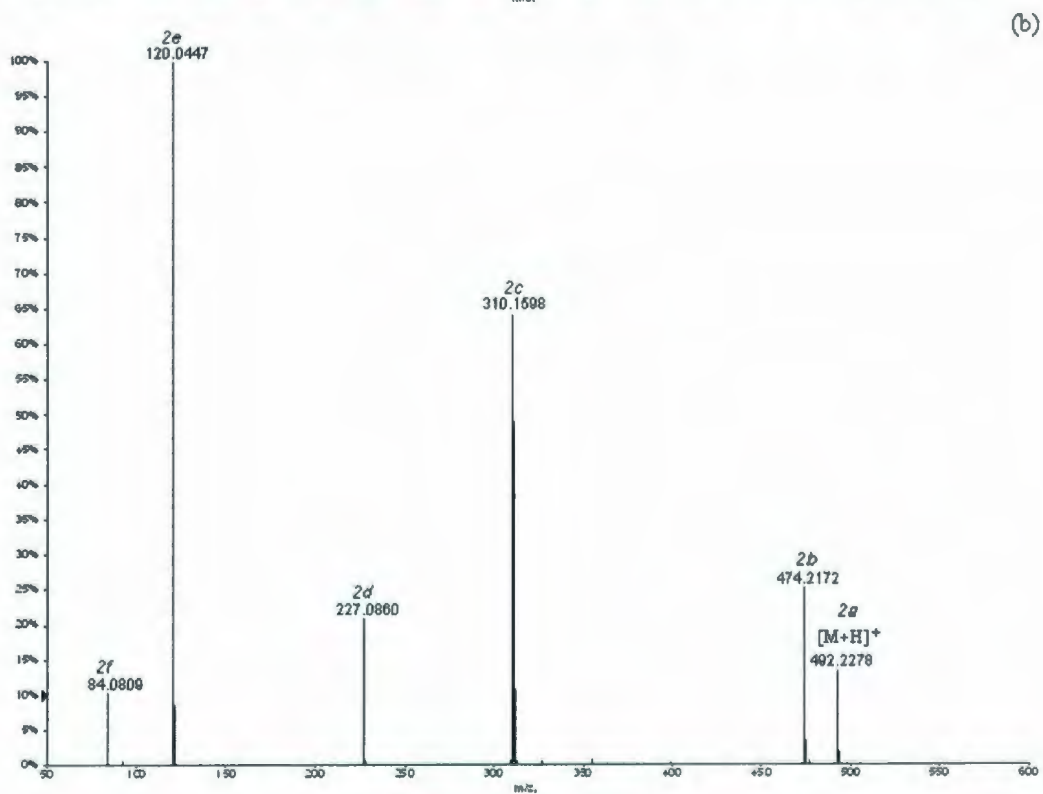
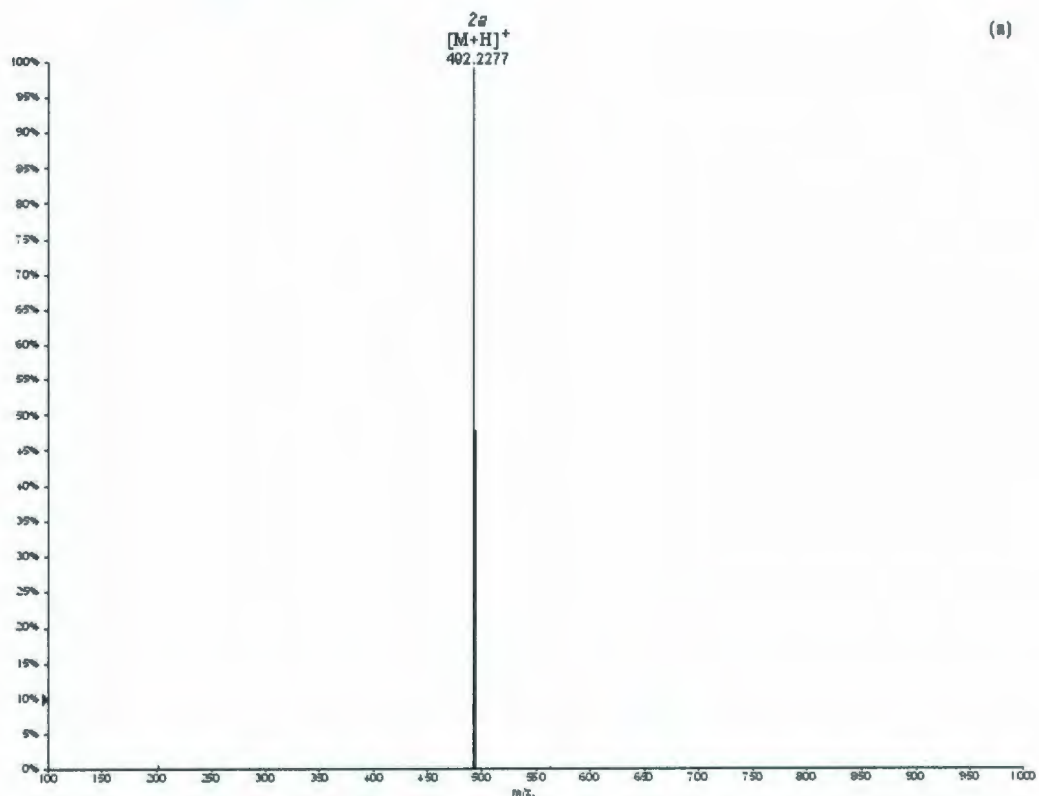
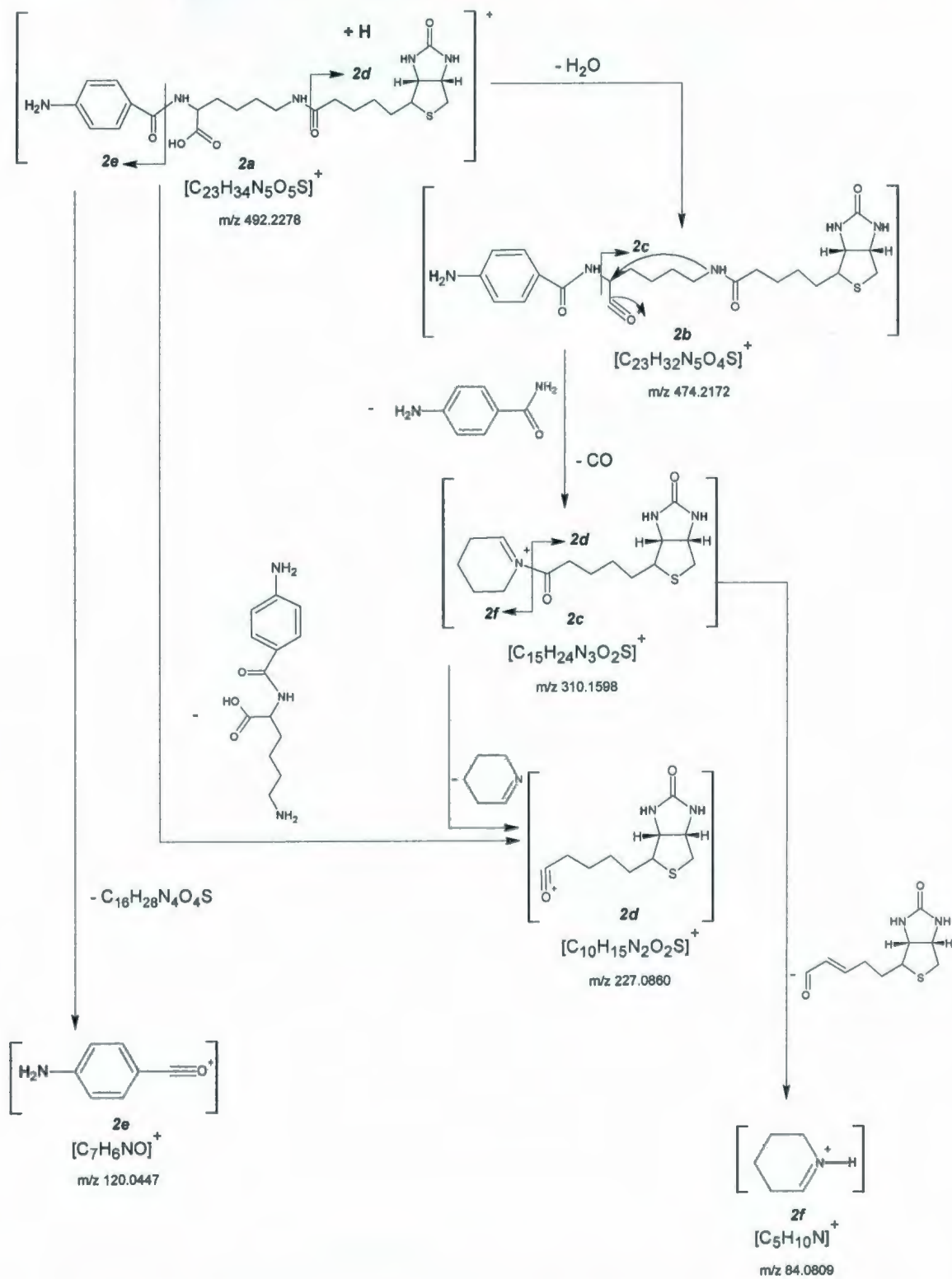


Figure 3.2: (a) ESI-QqTOF-MS (+) of the *p*-aminobenzoyl biocytin **2**; (b) CID-MS/MS of the selected protonated precursor ion **2a** at m/z 492.2277 from *p*-aminobenzoyl biocytin **2**.



Scheme 3.2: The proposed fragmentation routes of the *p*-aminobenzoyl-biocytin **2** obtained during the CID-MS/MS of the protonated precursor ion **2a** at m/z 492.2278.

3.3.3. CID-MS/MS of the $[M+H]^+$ ion at m/z 534.2630 selected from the photoactivatable biotin linker **3**

The CID-MS/MS analysis of the selected protonated precursor ion **3a** at m/z 534.2630 for the biotin linker **3** (shown as **Figure 3.3(a)**) was recorded with a CE of 30 eV and a DPI of 60 V. It produced the major product ions observed at m/z 353.2059, 327.1898, 284.1441, 227.0806, 84.0839, and 58.0667 (**Figure 3.3(b)** & **Table A.3** (shown in Appendix A)). The proposed CID-MS/MS fragmentation routes of the precursor ion are tentatively shown in **Scheme 3.3**. The protonated precursor ion $[M+H]^+$ at m/z 534.2561 consecutively eliminates the photoactivatable *p*-azido-*o*-nitro-aniline group $[(C_6H_5N_5O_2), (179 \text{ Da})]$ and a hydrogen molecule to form the product ion **3b** at m/z 353.2059 assigned as the $[(\text{biotinyl group})C_7H_{14}N_2]^+$ ion. The product ion **3c** at m/z 327.1898 was formed from the precursor ion by elimination of the $[(C_8H_9N_5O_2), (207 \text{ Da})]$ neutral fragment formed by the photoactivatable group and the spacer arm; it was assigned as the $[(\text{biotinyl group})C_5H_{12}N_2]^+$ ion. The product ion **3d** at m/z 284.1441 was created from the product ion **3b** by elimination of the neutral fragment $[(C_4H_9N), (71 \text{ Da})]$ and was assigned as $[(\text{biotinyl group})C_3H_7N]^+$ or the $[C_{13}H_{22}N_3O_2S]^+$ ion. Note that this product ion **3d** can be formed from the precursor ion directly by loss of the $[(C_{10}H_{14}N_6O_2), (250 \text{ Da})]$. The product ion **3e** at m/z 227.0806 was formed from the precursor ion by elimination of a neutral fragment formed by the photoactivatable group and the complete spacer arm $[(C_{13}H_{21}N_7O_2), (307 \text{ Da})]$ and was assigned as $[\text{biotinyl group}]^+$ or the $[(C_{10}H_{15}N_2O_2S)]^+$ ion. The product radical ion **3f** at m/z 84.0839 is formed from the product ion **3c** by elimination of the biotinyl group $[C_{10}H_{16}N_2O_2S, (227 \text{ Da})]$ and a

methyl radical, and it was assigned as $[\text{C}_4\text{H}_8\text{N}_2]^+\cdot$ radical ion. Finally the product ion **3g** at m/z 58.0667 is formed from the product ion **3d** by elimination of a neutral fragment $[(\text{C}_{10}\text{H}_{14}\text{N}_2\text{O}_2\text{S}), (226 \text{ Da})]$, and it was assigned as $[\text{C}_3\text{H}_8\text{N}]^+$ ion.

All the exact mass assignments of the product ions were verified by conducting separate CID-MS/MS analysis of the pentadeuterated-photoactivatable biotin ion at m/z 539.2868 (**Table A.3** (shown in Appendix A)).

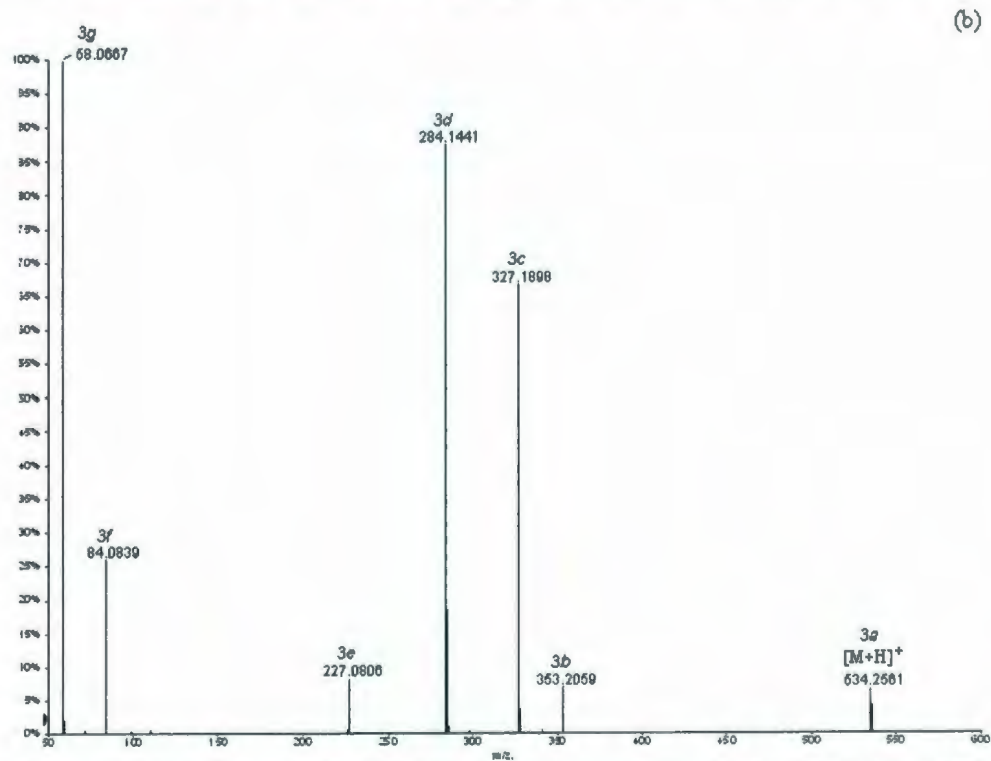
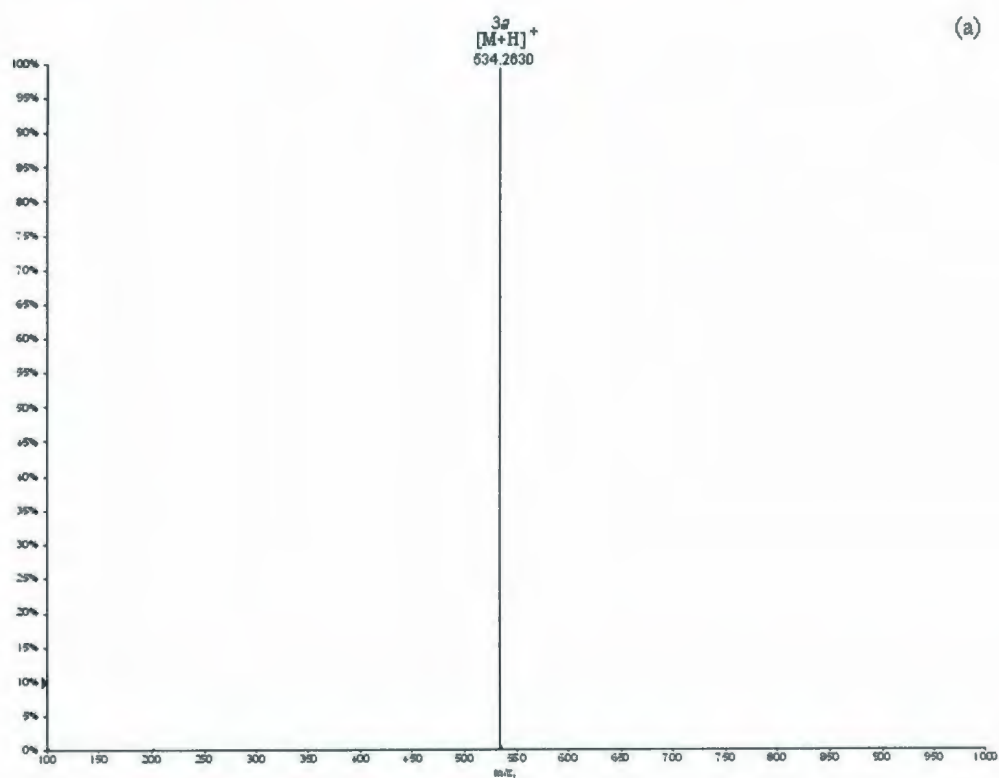
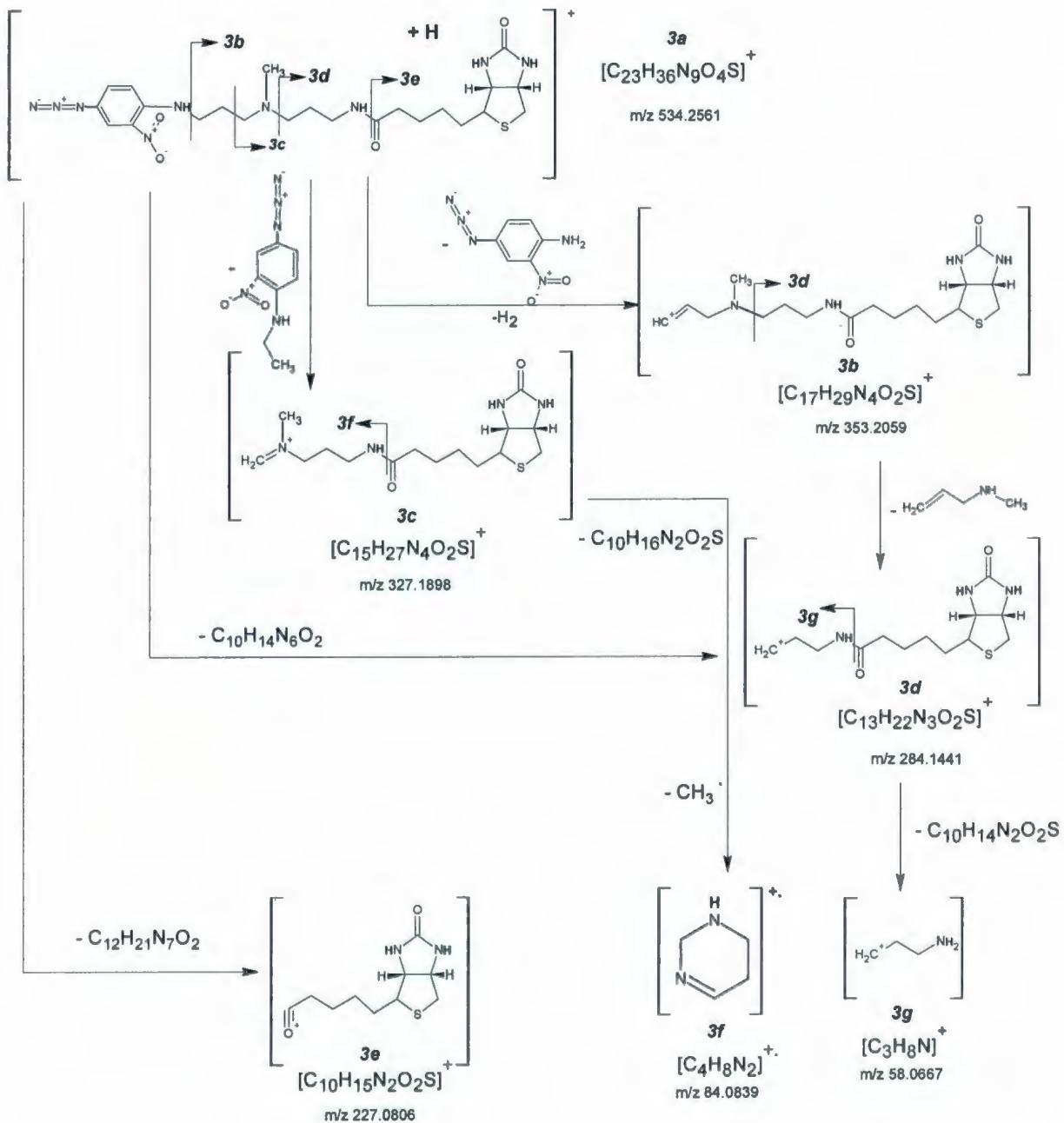


Figure 3.3: (a) ESI-QqTOF-MS (+) of the photoreactive biotin **3**; (b) CID-MS/MS of the selected protonated precursor ion $3a$ at m/z 534.2630 from photoreactive biotin **3**.



Scheme 3.3: The proposed fragmentation routes of the photoactivatable biotin **3** obtained during the CID-MS/MS of the protonated precursor ion **3a** at m/z 534.2561.

3.3.4. CID-MS/MS of the protonated molecule $[M+H]^+$ ion at m/z 733.3634 selected from the PEO-biotin dimer linker **4 and *quasi-MS³* analysis of $[M+H\text{-biotinyl group}]^+$ precursor ion **4b** at m/z 507.2832**

The product ion scan of the selected protonated molecule **4a** at m/z 733.3634 for the biotin linker **4** (shown as **Figure 3.4(a)**) was recorded with a CE of 26 eV and a DPI of 60 V. It created a series of product ions which were assigned as follow: **4c**, **4e**, and **4g** at m/z 464.2415, 270.1283, and 227.0852 respectively (**Fig.3.4(b)** & **Table A.4** (shown in Appendix A)). Furthermore, *quasi-MS³* of the selected precursor ion at m/z 507.2832 (DPI = 80 V, CE = 38 eV) afforded the following series of product ions: **4d** at m/z 281.2060, **4e** at m/z 270.1301, **4f** at m/z 238.1639, and **4g** at m/z 227.0850 (**Fig.3.4(c)** & **Table A.4** (shown in Appendix A)). The schemes describing the tentative geneses of the MS/MS and *quasi-MS³* product ions are shown in **Scheme 3.4**.

All the exact mass assignments of the product ions were verified by conducting separate CID-MS/MS analysis of the heptadeuterated-PEO-BiotinDimer ion at m/z 740.4083. (**Table A.4** (shown in Appendix A))

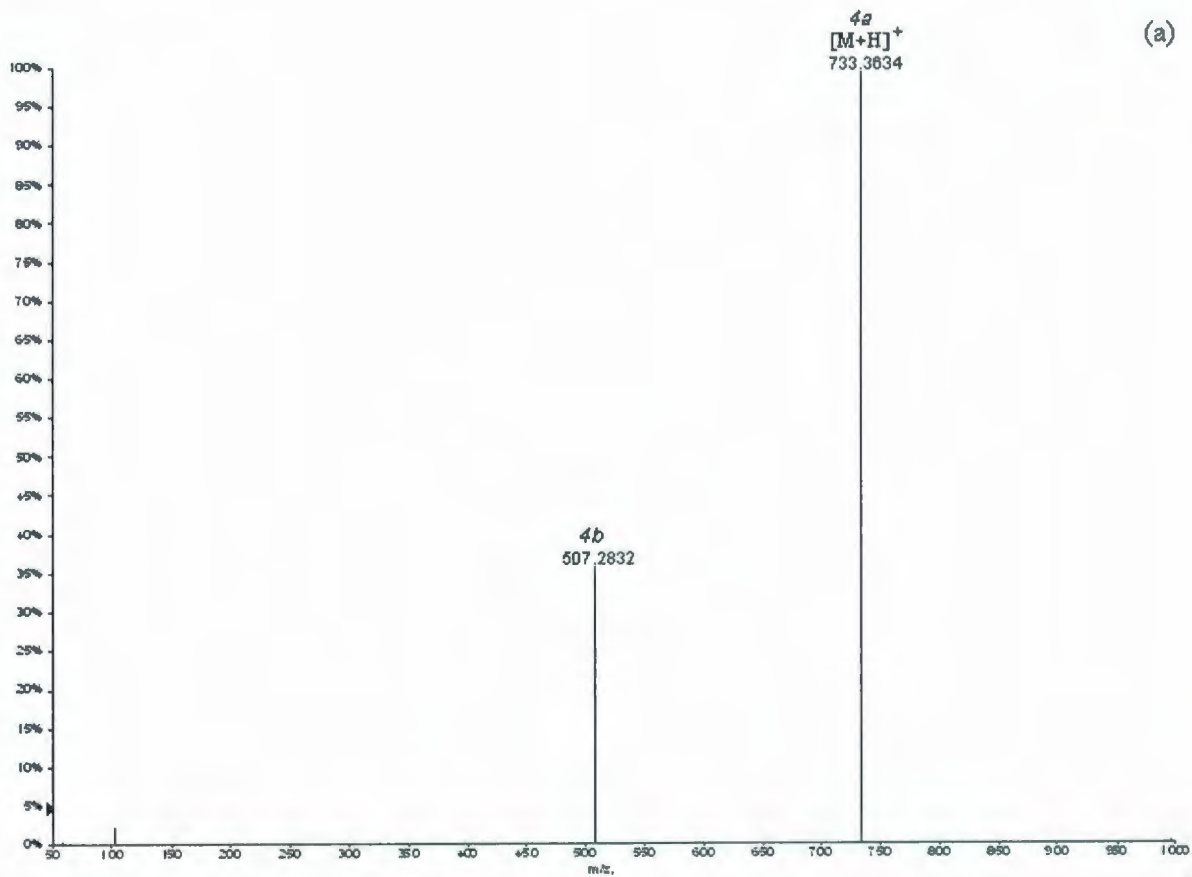


Figure 3.4: (a) ESI-QqTOF-MS (+) of the PEO-biotin Dimer 4.

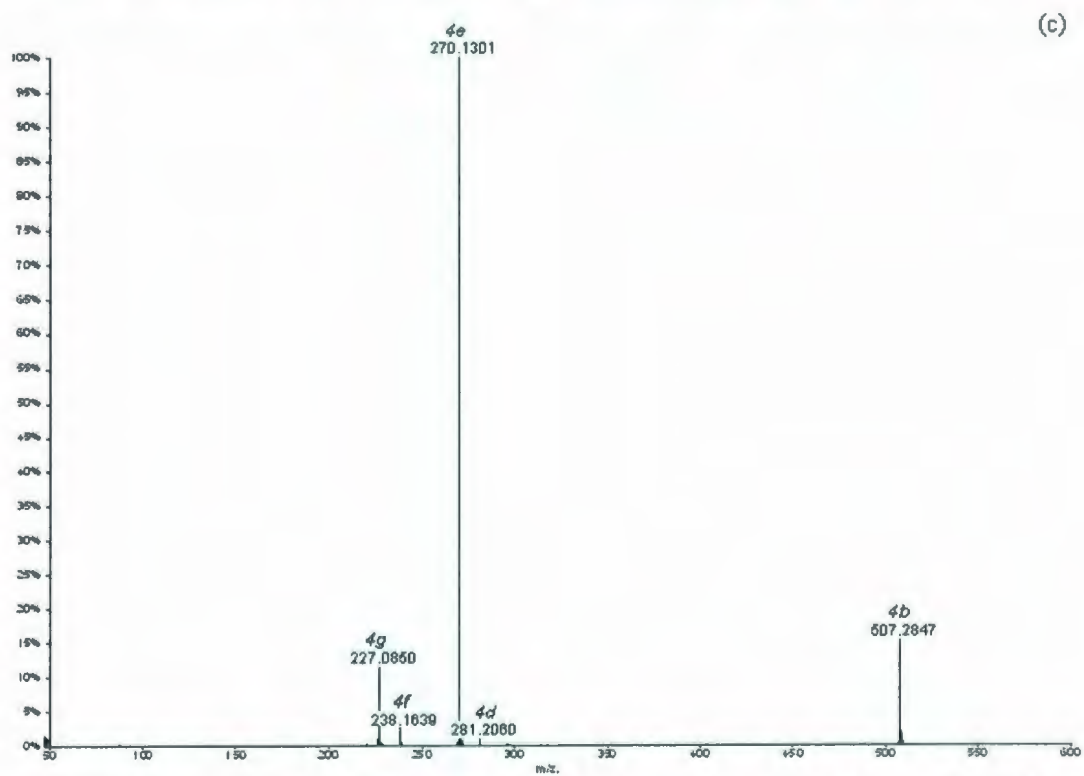
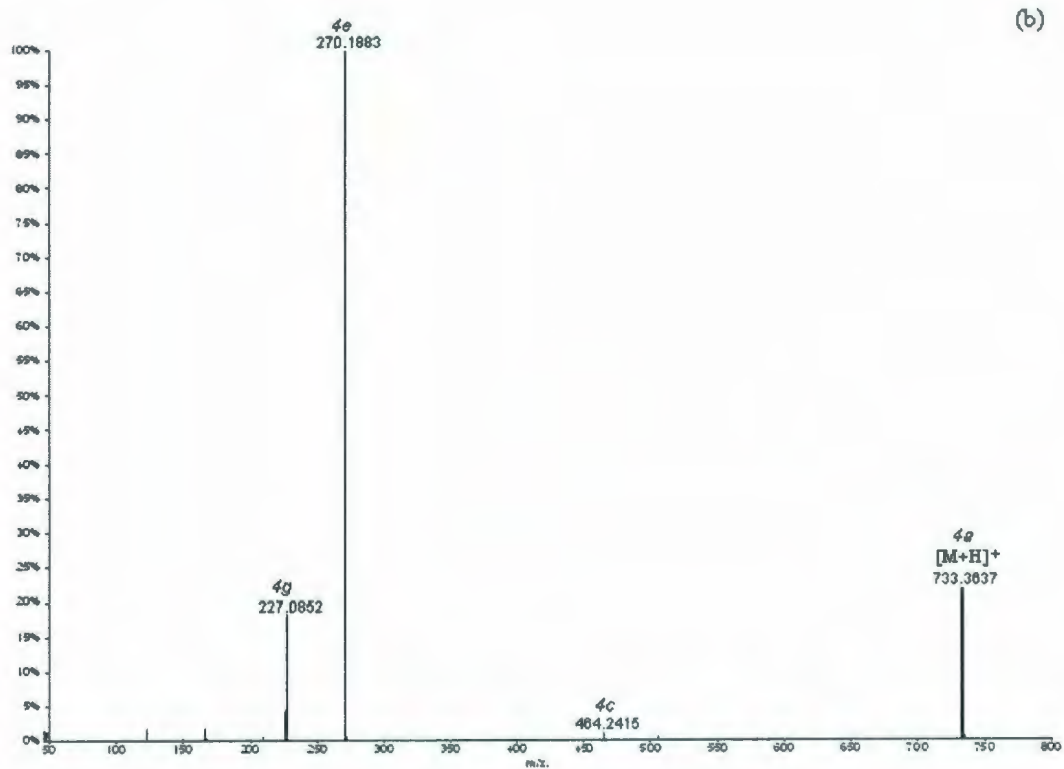
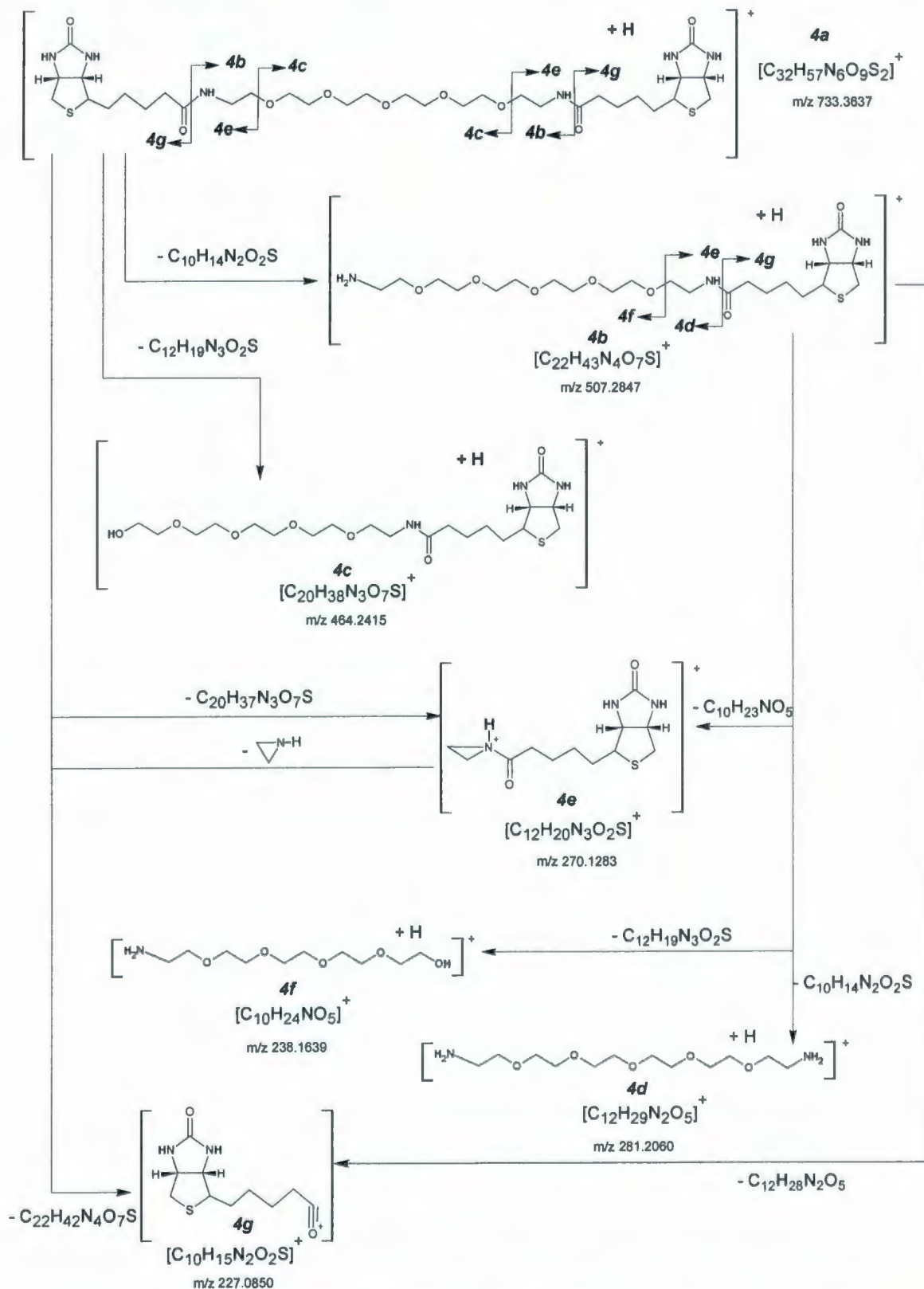


Figure 3.4 (continued): (b) CID-MS/MS of the selected protonated precursor ion **4a** at m/z 733.3634 from PEO Biotin Dimer **4**; (c) quasi-MS³ of the selected ion **4b** at m/z 507.2832 from PEO Biotin Dimer **4**.



Scheme 3.4: The proposed fragmentation routes of PEO-biotin Dimer **4** obtained during the CID-MS/MS of the protonated precursor ion **4a** at m/z 733.3637 and the ion **4b** at m/z 507.2847.

3.3.5. CID-MS/MS of the protonated molecule $[M+H]^+$ at m/z 880.1853 obtained from the Sulfo SBED biotin linker **5**

The product ion scans of the selected protonated molecule **5a** at m/z 880.1853 for the biotin linker **5** (shown as **Figure 3.5(a)**) was recorded with a CE of 35 eV and a DP1 of 80 V. It afforded the major product ions at m/z 852.1804, 522.0827, 494.0780, 444.2029, 350.1410, 227.0851, 120.0454 and 84.0788 (**Fig.3.5(b)**). The proposed CID-MS/MS fragmentation routes of the Sulfo SBED biotin protonated precursor ion at m/z 880.1818 are shown in **Scheme 3.5 (a)** and **Table A.5** (Appendix A).

3.3.5.1. *Quasi-MS³* analysis of the $[M+2H-Na]^+$ ion at m/z 858.2060 and the [biotinyl group $C_6H_{10}NO$ (photoactivatable aryl azide group)]⁺ ion **5f** at m/z 500.2018

The product ion scan of the selected precursor ion $[M+2H-Na]^+$ **5b** at m/z 858.2060 was recorded with a CE of 35 eV and a DP1 of 80 V. It afforded the following series of product ions: **5d**, **5f**, **5h**, **5i**, **5j**, **5l**, and **5m**, respectively, at m/z 681.2292, 500.2061, 472.2045, 444.2082, 427.1759, 310.1586, and 227.0852 (**Fig.3.5(c)** & **Table A.5** (shown in Appendix A). The tentative fragmentation routes occurring from the dissociation of the $[M+2H-Na]^+$ ion at m/z 858.2064 are shown in **Scheme 3.5 (b)**. Moreover, a *quasi-MS³* product ion scan of the selected precursor **5f** [biotinyl group $C_6H_{10}NO$ (photoactivatable aryl azide group)]⁺ ion at m/z 500.2018 has been performed and has afforded the following series of product ions: **5h**, **5i**, **5j**, **5l**, **5m**, and **5n**, respectively, at m/z 472.2045, 444.2082, 427.1759, 310.1586, 227.0852,

and 120.0456 (**Fig.3.5(d)**), confirming the structure assigned to these product ions.

The tentative fragmentation routes are shown in **Scheme 3.5 (b)**.

All the exact mass assignments of the protonated molecules and the product ions were verified by conducting separate CID-MS/MS analysis of the hexadeuterated sodiated-Sulfo-SBED biotin ion at m/z 886.2174 (shown in **Table A.5** (Appendix A)).

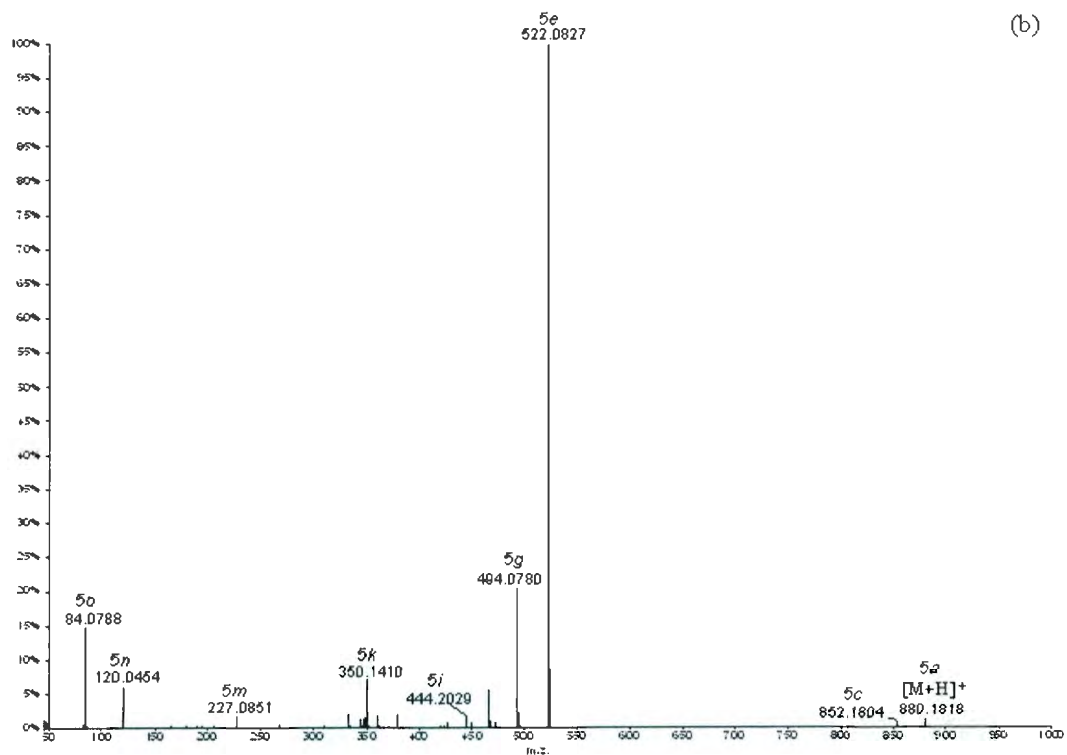
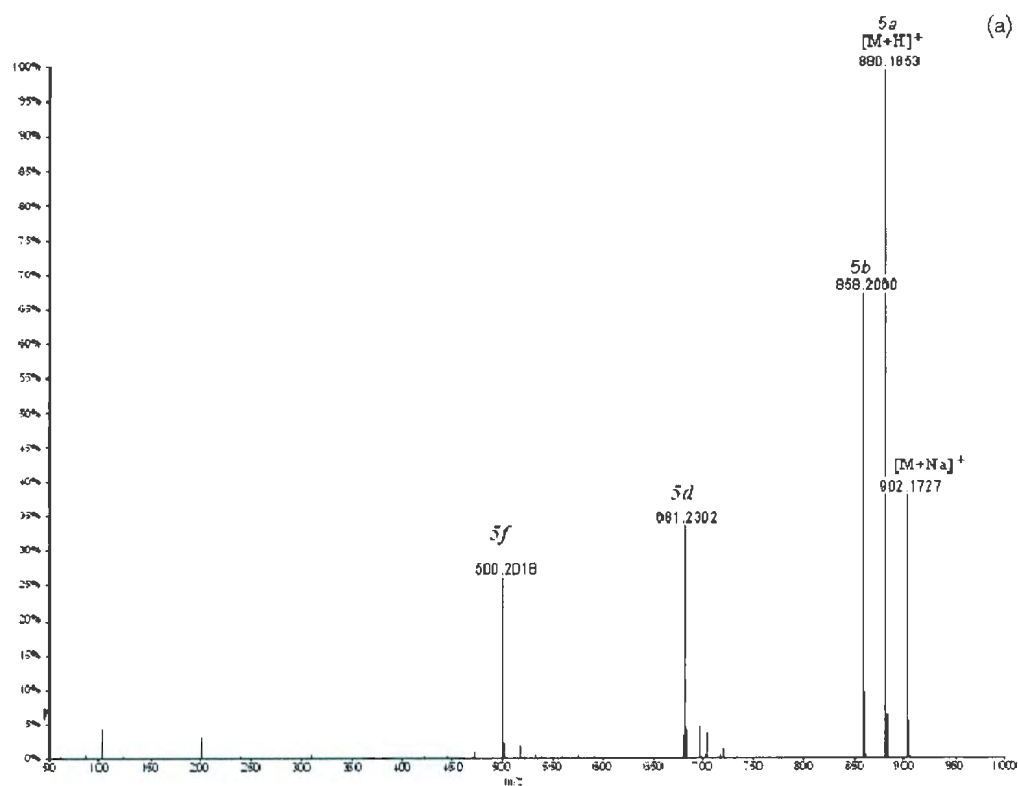


Figure 3.5: (a) ESI-QqTOF-MS (+) of the Sodiated Sulfo SBED 5; (b) CID/MS/MS of selected protonated precursor ion 5a at m/z 880.1853 from sodiated sulfo-SBED 5.

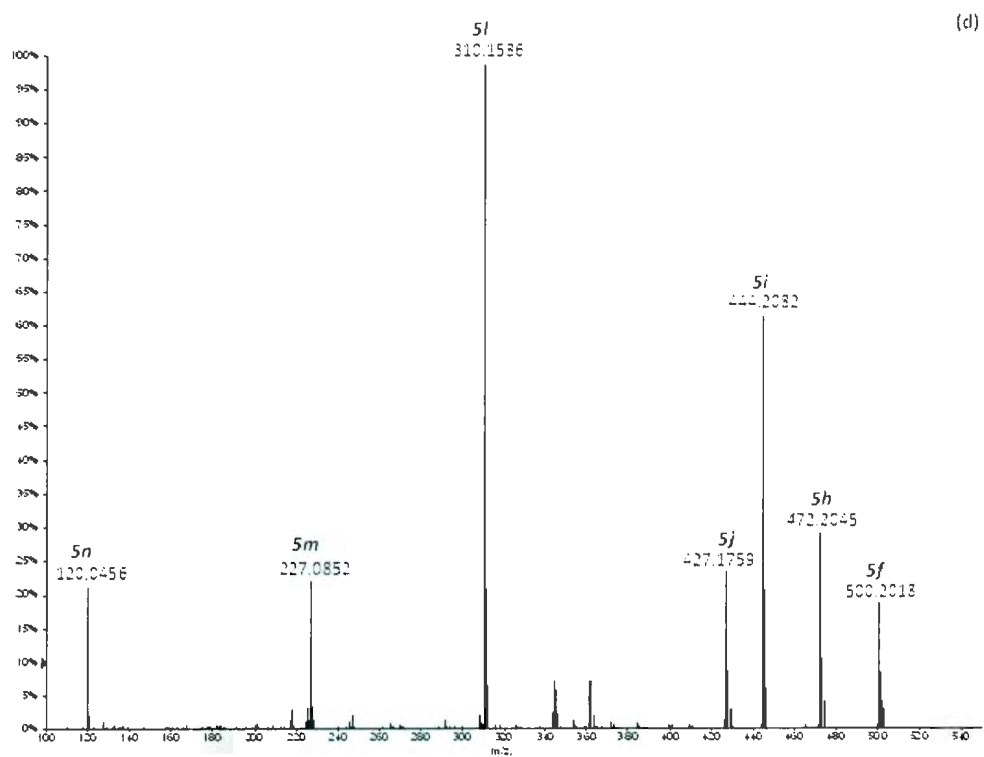
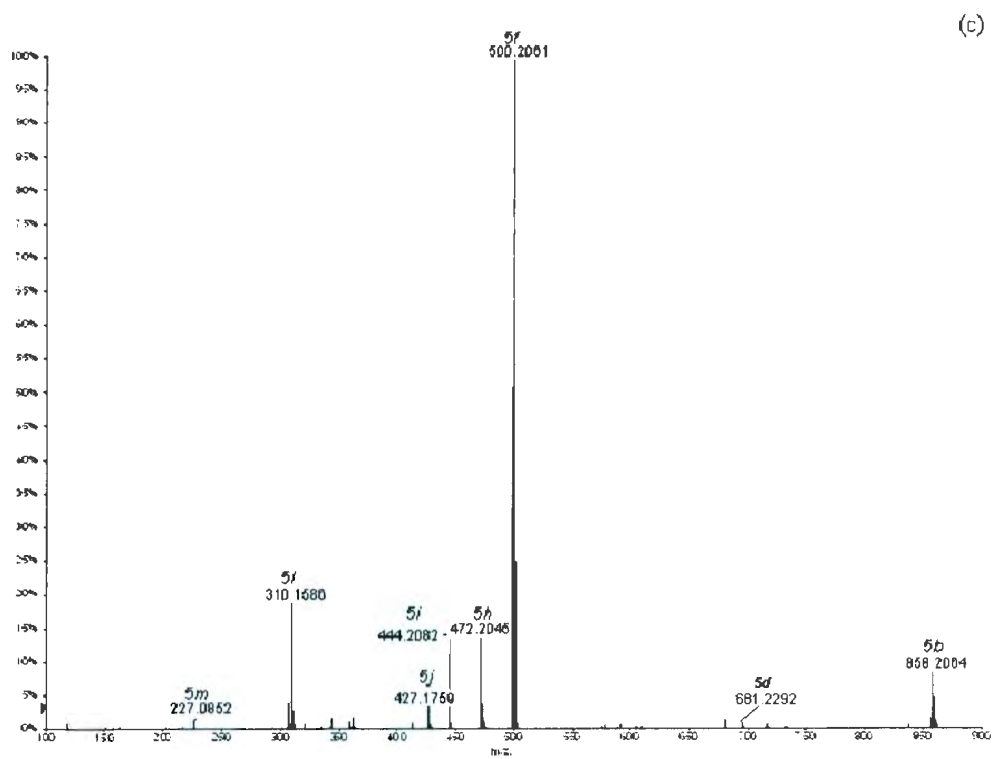
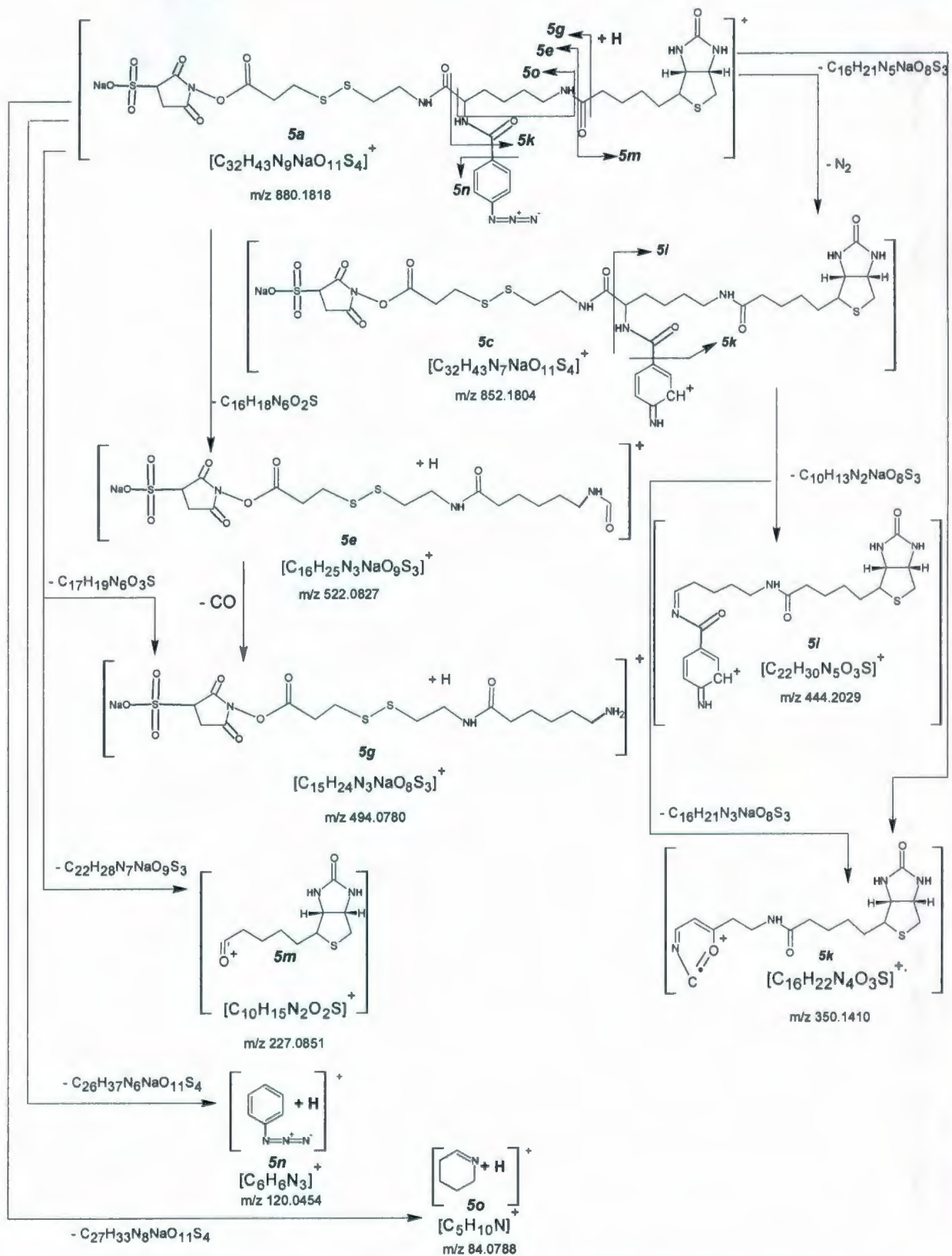
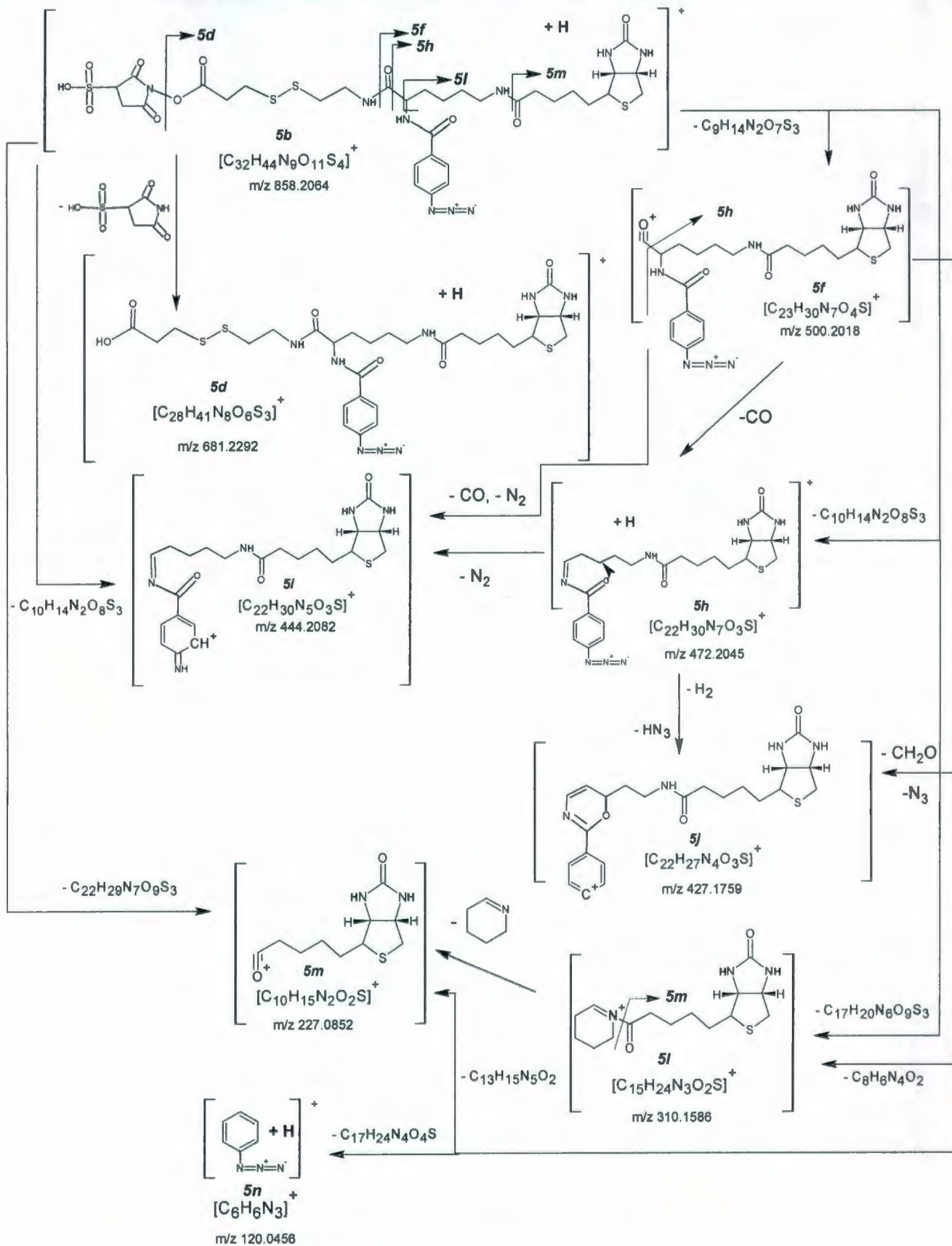


Figure 3.5 (continued): (c) *Quasi-MS*³ of the selected ion **5b** at *m/z* 858.2060 from sodiated sulfo-SBED **5**; (d) *quasi-MS*³ of the selected ion **5f** at *m/z* 500.2018 from sodiated sulfo-SBED **5**.



Scheme 3.5 (a): The proposed fragmentation routes of the sodiated sulfo SBED **5** obtained during the CID-MS/MS of the protonated precursor ion **5a** at m/z 880.1818.



Scheme 3.5 (b): The proposed fragmentation routes of the sodiated sulfo-SBED **5** during the *quasi-MS*³ of the precursor ions: **5b** at m/z 858.2064 and **5f** at m/z 500.2018.

3.4. Conclusion

In this study, the gas-phase fragmentations of the commercially available biotinyl reagents using ESI-MS and CID-MS/MS analyses with a QqTOF-MS/MS hybrid instrument have been examined. The results presented in this study demonstrated that during ESI-MS and CID-MS/MS analyses, the biotin reagents follow a similar fragmentation pattern and that the cleavages usually can occur at either end of the spacer arm of the biotin reagents. In general, the CID-MS/MS fragmentation routes of the five precursor protonated molecules obtained from the biotin linkers *1-5* afforded a series of product ions formed essentially by similar routes.

As expected, it was noticed that increasing the collision energy (CE) of the CID-MS/MS analyses resulted in the enhancement of gas-phase fragmentation of the spacer arm. We have also noted that a quick scrutiny of **Table A.(1-5)** (shown in Appendix A) will indicate the presence of common product ions. It is essential to mention that the product ion assigned as the [biotinyl group]⁺, [C₁₀H₁₅N₂O₂S]⁺ at *m/z* 227.08 is present in all MS/MS analyses of all five biotin linkers.

The genesis of the MS/MS fragmentations and the structural identities of the product ions are shown in **Figures 3.(1-5)** and **Schemes 3.(1-5)**. This fragmentation pattern can be used to easily predict the fragmentation patterns of new compounds with the same general backbone structure. In addition to the proposed mechanisms of the CID-MS/MS, fingerprints of these biotin reagents were confirmed by performing similar MS/MS analyses on the labeled deuterated biotin reagents. The ESI-MS and CID-MS/MS fingerprints of the series of biotin reagents presented in this manuscript

are indispensable blueprints necessary for our continuing studies, as we have produced biotinylated DNA which will be used for further applications.

CHAPTER 4: CONFIRMATION AND CHARACTERIZATION OF THE PRESENCE OF THE 4-O-PHOSPHORYLATED KDO REDUCING END GROUP OF THE LPS CORE OLIGOSACCHARIDE OF *AEROMONAS HYDROPHILA* (CHEMOTYPE II) USING TANDEM MASS SPECTROMETRY

4.1. Introduction

Lipopolysaccharides (LPSs) are amphiphilic molecules contained in the outer leaflet of the external membrane of gram-negative bacteria. They are anchored in the membrane by the lipid part (lipid A), which is covalently linked to an oligosaccharide fragment (core) that, in turn, is bonded to a polysaccharide part (*O*-antigen, or *O*-side chain). Due to their outward location, the LPSs are involved in mechanisms of interaction with the surroundings. Despite the fact that gram-negative bacteria colonize very different organisms and environments, LPSs show a common architectural structure. This suggests that the molecular structures of the LPS components can play an important role in host or environment specificity.¹⁰¹⁻¹⁰⁶

The *Vibrionaceae* family belongs to the major group of *Proteobacteria*, which are inhabitants of fresh or salt water. Several species are pathogenic, including the type species *Vibrio cholerae*, which is the agent responsible for cholera. Most bioluminescent bacteria belong to this family, and are typically found as symbiotes of deep-sea animals.¹⁰¹ The inability to detect Kdo in LPSs from the genera *Vibrio* and *Aeromonas*, which belong to aquatic Gram-negative bacteria family of the *Vibrionaceae*, was first pointed out by Jackson & Redmond¹⁰² in 1971 and subsequently by Jann *et al.*,¹⁰³ and by Hisatsune *et al.*, for *V. cholera* in 1982.¹⁰⁴

Accordingly, it was commonly assumed that Kdo was absent from the LPS of all members of the *Vibrionaceae* family of gram-negative bacteria, and its absence was established by being negative to the thiobarbiturate-based colorimetric assay. This assay, also called the Weissbach reaction,¹⁰⁵ was used as a characteristic for taxonomic classification.^{103.104} Contrary to this accepted view, however, Banoub *et al.* first reported the presence of one residue of Kdo (or Kdo-like substance) in LPSs of the *Vibrionaceae*, family in the early 1980s).^{106a}

Phosphorylated Kdo units have been isolated from, and detected in, a number of LPS preparations. Upon strong acid hydrolysis, Kdo derivatives phosphorylated in position O-5, were released from the LPS of *V. cholerae* Ogawa and Inaba.¹⁰⁷ The phosphorylated Kdo was identified by gas-liquid chromatography and mass spectrometry, after reduction and permethylation, as Kdo 5-phosphate.¹⁰⁷ Phosphorylated Kdo units have been isolated from various LPS preparations obtained from different types of gram-negative bacteria. Caroff and coworkers have shown that in the LPS-2 of *Bordetella pertussis* endotoxin, the Kdo unit was substituted at O-5 by the inner core oligosaccharide portion and also carried a phosphate substituent on the O-4 position. They established that, following mild hydrolysis of the glycosidic bond of the Kdo unit, the phosphate group was easily released and eliminated. They noticed that the product formed was still attached to the core oligosaccharide portion and could not be identified.¹⁰⁸ Auzaneau *et al.*, have shown that mild acid hydrolysis of a Kdo unit, which was methylated at O-5 and phosphorylated at position O-4, produced a mixture of type-specific 4,8- and 4,7-anhydro-Kdo units.¹⁰⁹

4.2. Analysis of the core oligosaccharide by ESI ((+)/(-))-QqTOF-MS and MALDI-QqTOF-MS

In the present study, the structural reinvestigation of the native core oligosaccharide of *Aeromonas hydrophila* (chemotype II) lipopolysaccharide SJ-48R (**Figure 2.2**) was examined using ESI-MS and MALDI-MS and low-energy collision tandem Mass Spectrometry analyses. A similar core oligosaccharide of *Aeromonas hydrophila* (chemotype II SJ-26R was previously studied by NMR, methylation analysis, partial hydrolysis with acid, periodate oxidation, Smith degradation, nitrous acid deamination, and oxidation with chromium trioxide.^{106b} *Aeromonas hydrophilia* is an opportunistic pathogen causing disease in fresh-water fish, particularly salmonid species and it has been shown that the strains isolated from this pathogenic bacterium could cause infection in humans.¹¹⁰

After releasing the core oligosaccharide from the Lipid A by hydrolysis of the rough LPS with 1% acetic acid, we have previously reported that the single reducing Kdo which contains an O-4 phosphate group eliminates phosphoric acid and produces a homogenous mixture of the non-phosphorylated core oligosaccharide with an olefinic chain on the Kdo residue. This open olefinic Kdo chain cyclizes to produce a mixture of two diastereomers of the 4,8-anhydro- α -keto acid derivatives and two diastereomers of the 4,7-anhydro- α -keto acid derivatives (**Scheme 4.1**). The series of four diastereomers is due to the enol \leftrightarrow keto tautomers. In addition, each diastereomer can exist in either, the α - or β -anomeric form, therefore complicating and increasing the numbers of diastereomers to eight in addition to the core oligosaccharide containing the open olefinic Kdo residue (**Scheme 4.1**). It is important to indicate that this

homogeneous mixture contains nine diastereomers.^{13a,13b} The new study of the native core oligosaccharide of *Aeromonas hydrophila* (chemotype II) lipopolysaccharide SJ-48R presented in this rationale has allowed us to obtain a better understanding of the stereospecific fragmentation pathways of the individual glycosyl unit forming this oligosaccharide in addition to precisely sequence the glycosylation sites and glycones order in this type of core oligosaccharide.

In fact, this structural information, such as sequence patterns of branched oligosaccharides or differentiation of isomeric hexosyl units will be very beneficial for the establishment of the presence of the dephosphorylated Kdo derivatives in LPS fractions belonging to the *Vibrionaceae* family which could be conjugated to proteins via functional crosslinkers that could be used as protective vaccines.^{60,111-114}

To summarize it is known that the Kdo unit is phosphorylated at position O-4. It is also known that this latter Kdo residue produces upon acid hydrolysis, eight diastereomers of 4,8- and 4,7-anhydro derivatives of the enolizable α -keto acids and one oligosaccharide containing the open olefinic Kdo residue (**Scheme 4.1**).^{13a,13b} Therefore an objective of the study was to confirm the presence of the nine isobaric diastereomers during MS and MS/MS analyses of the dephosphorylated core oligosaccharide of *Aeromonas hydrophila* (Chemotype II) SJ48-R homogeneous mixture.^{13a,13b}

The pure dephosphorylated homogeneous core oligosaccharide of *Aeromonas hydrophila* (Chemotype II) of SJ-48R mixture was analyzed by electrospray mass spectrometry in positive and negative-ion mode. In addition, MALDI-MS analysis of pure core oligosaccharide was also undertaken in the positive-ion mode.

The ESI-MS analysis of the core oligosaccharide was realized with a Declustering Potential (DP1) = 70V. **Figure 4.1(a)** shows the presence of the protonated molecule $[M+H]^+$ at m/z 1312.4467, which corresponds to the dephosphorylated Kdo molecule occurring from the native core oligosaccharide forming the series of diastereomers of 4,8- and 4,7-anhydro derivatives of the enolizable α -keto acids and in addition to the oligosaccharide containing the open-chain Kdo residue.

The presence of doubly charged molecules could be detected, resulting from the incorporation of potassium and sodium ions to form the cluster ions: $[M+H+K]^{2+}$ at m/z 675.7113 and $[M+H+Na]^{2+}$ at m/z 667.6237. This obtained result confirms the glycone sequence of the reinvestigated structure of the core oligosaccharide.

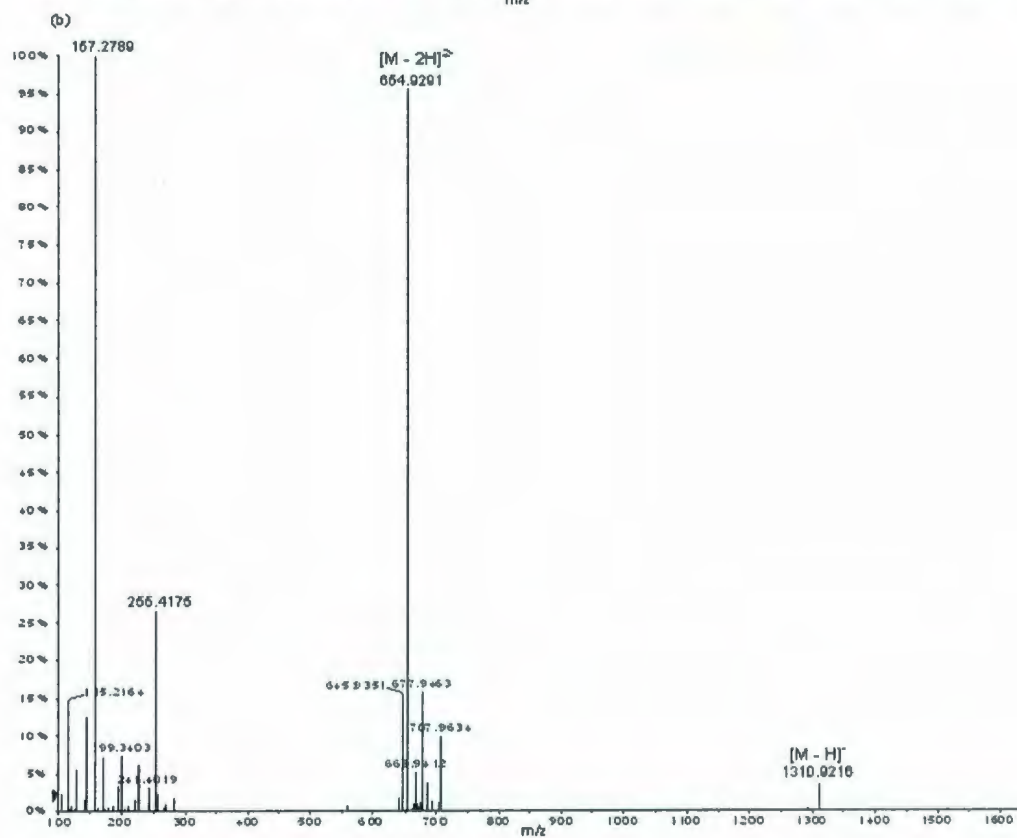
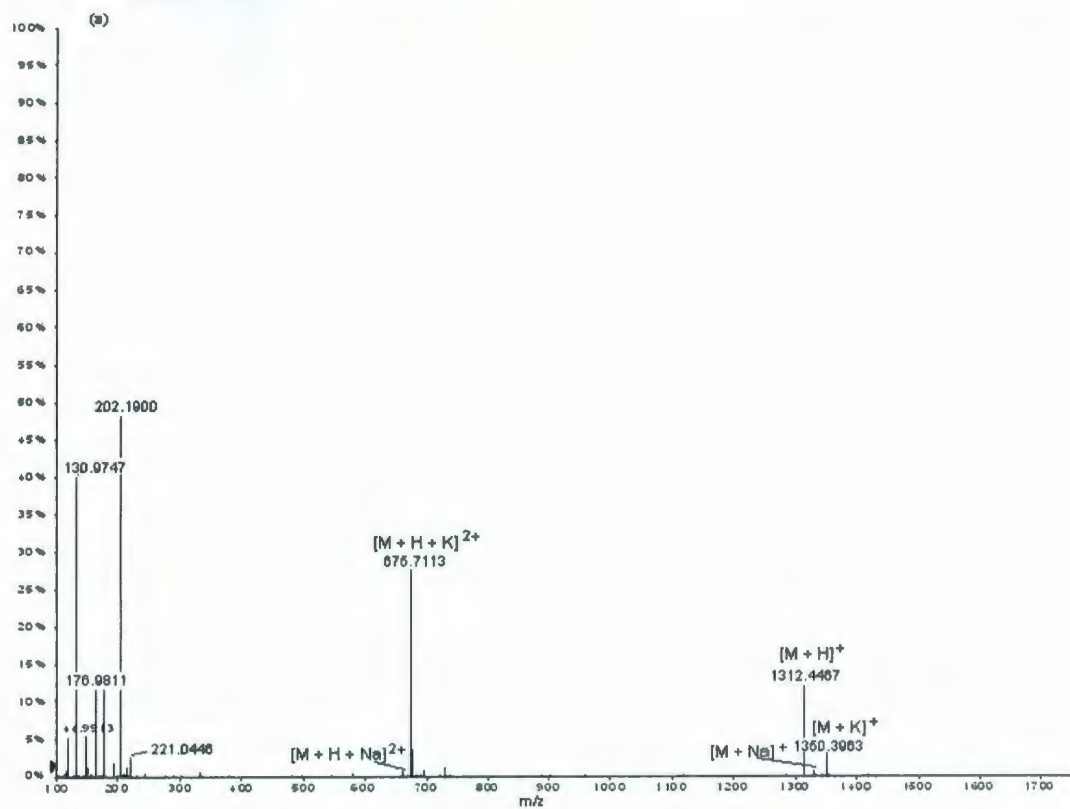
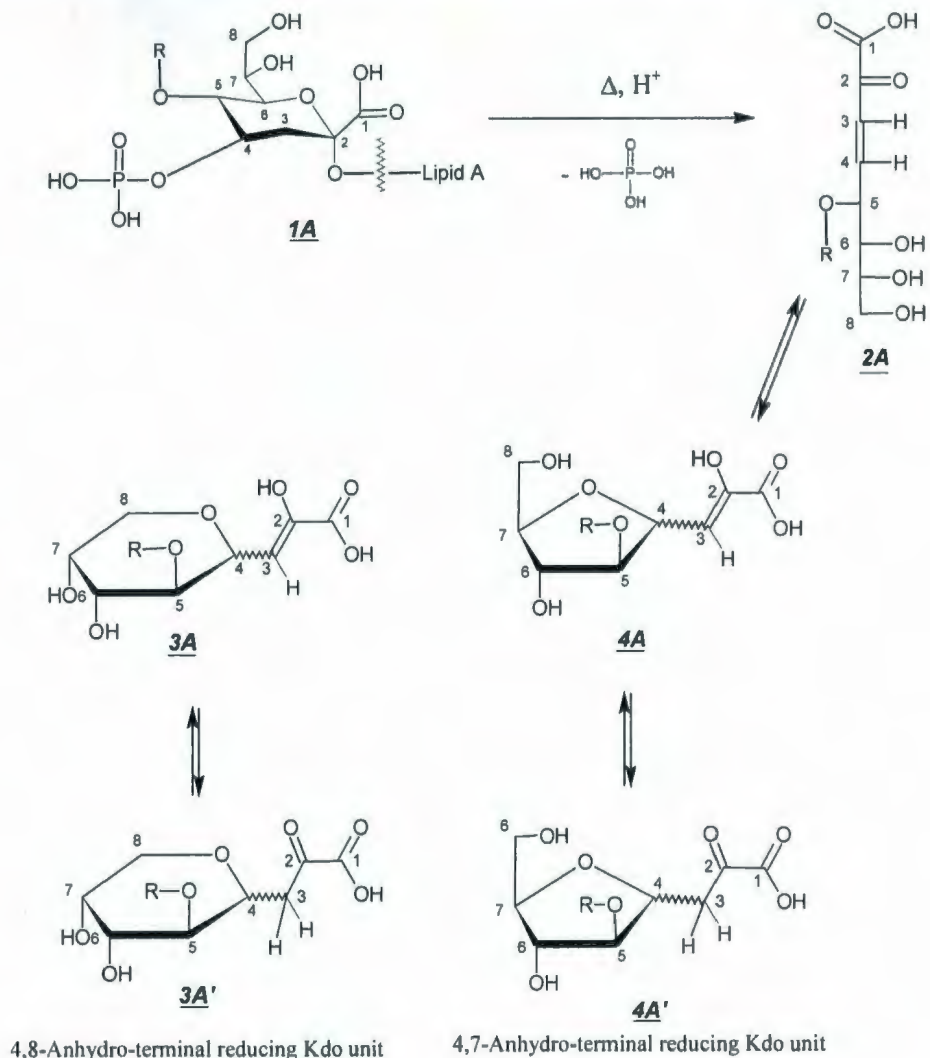
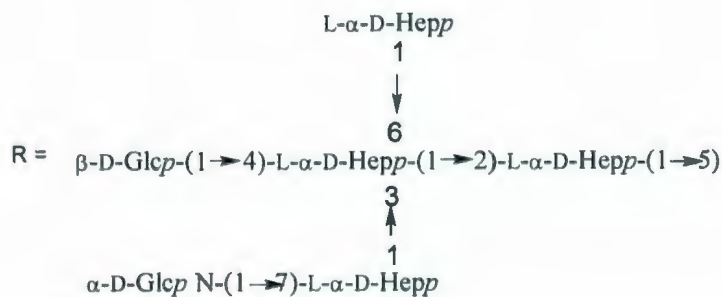


Figure 4.1: (a) ESI-MS (+) of the homogeneous mixture of the native core oligosaccharide; (b) ESI-MS (-) of the molecule characteristic of the native core oligosaccharide.



4,8-Anhydro-terminal reducing Kdo unit

4,7-Anhydro-terminal reducing Kdo unit



Scheme 4.1: Formation of the olefinic *D-arabino*-3-en-2-ulonic acid open chain **2A** after acetic acid treatment and possible structures of the diasteric forms of the 4,8-anhydro (**3A/3A'**)- and 4,7-anhydro (**4A/4A'**) derivatives of the enolizable α -keto-acid.^{13a,13b}

During the ESI-MS analysis, it was noted that the B-type or C-1 glycosidic bond cleavages were favored when we increased the declustering potential voltages to 70 volts.

Low-energy collision dissociation tandem mass spectrometry of the selected protonated molecular ion $[M + H]^+$ at m/z 1312.4467 shown in **Figure 4.2(a)**, demonstrates the various dissociation routes observed with a Declustering Potential 1 (DP1) of 70V and a Collision Energy (CE) of 70eV. As expected, the dissociation of the protonated molecular ion $[M + H]^+$ at m/z 1312.4331 led to the formation of a series of major product ions resulting from Y- and B cleavage types. This CID-MS/MS analysis provided the information related to the branching and the sequence of sugar residues. In addition, we noticed the minor formation of Z-type ruptures, e.g. $[Z_1]^+$ at m/z 203.0533, which correspond to the oxonium ion of the 4,8-anhydro derivatives from the Kdo reducing end group 3A/3A' (**Scheme 4.1**) and the minor formation of A- and X cleavages, e.g. $[^{1,5}X_4 - Y_2]^+$ at m/z 577.1959 and $[^{2,3}A_3]^+$ at m/z 385.1310. Indeed these latter fragments provided cross ring information of some sugar residues. The formation of the product ions occurring from the precursor ion $[M + H]^+$ are shown in **Scheme 4.2 (a)** and **4.2 (b)** and **Table 4.1**. The nomenclature of Domon and Costello is employed to determine the fragmentation routes of the core oligosaccharide.^{46b}

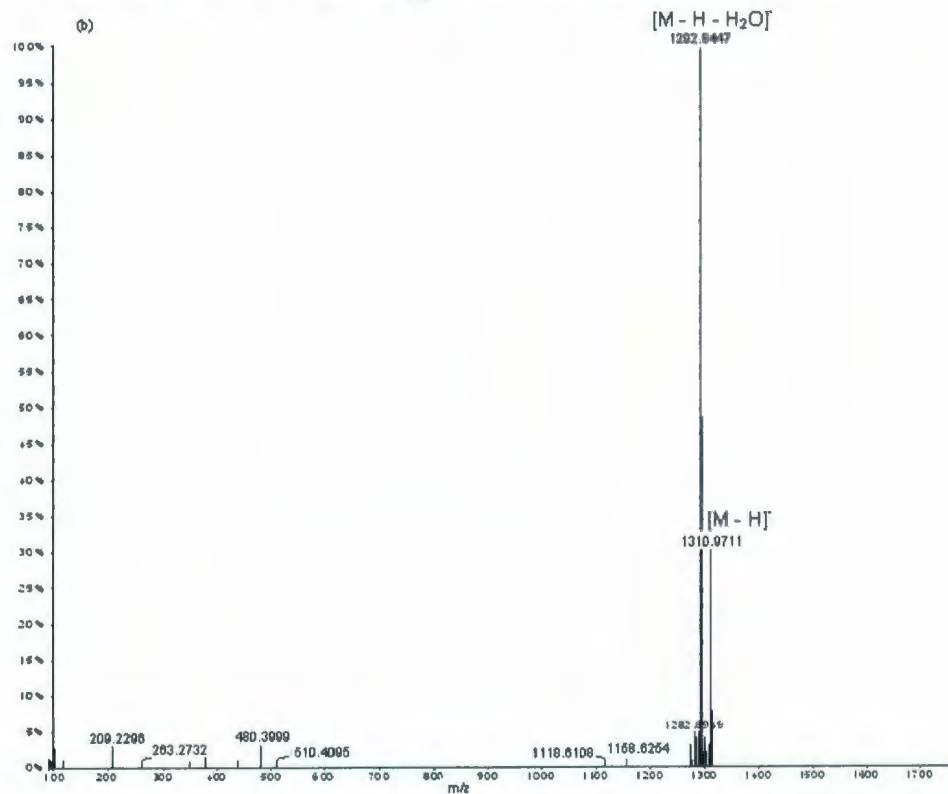
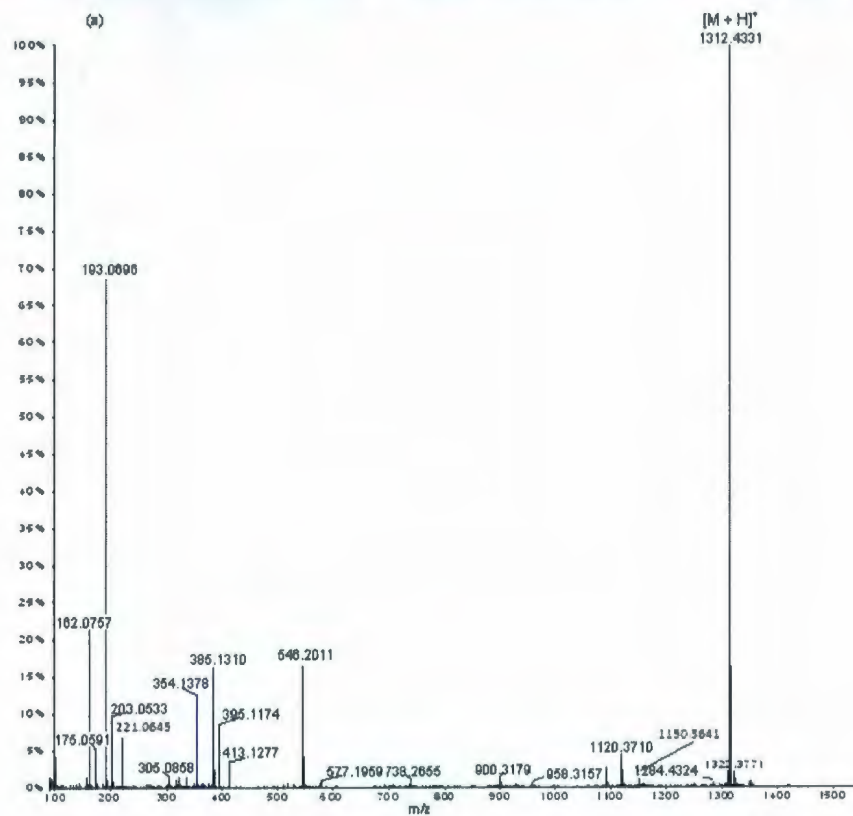


Figure 4.2: (a) ESI (+)-CID-MS/MS of the selected $[M + H]^+$ protonated molecular ion at m/z 1312.4467 from the native core oligosaccharide; (b) ESI (-)-CID-MS/MS of the selected $[M - H]^-$ deprotonated molecular ion at m/z 1310.9216 from the native core oligosaccharide.

In order to confirm the results obtained previously, the homogeneous mixture of the core oligosaccharides was analyzed by electrospray mass spectrometry in the negative-ion mode. The analysis of the core oligosaccharide was realized with a Declustering Potential 1 (DP1) = -30V and Focalized Potential (FP) = (-110)-(-150) V. The full scan ESI-MS data confirmed the presence of the deprotonated molecular ion $[M - H]^-$ at m/z 1310.9216 and the presence of the bis-deprotonated molecular ion $[M - 2H]^{2-}$ at m/z 654.9291 (**Figure 4.1(b)**). Low-energy collision dissociation tandem mass spectrometry of the deprotonated molecular ion $[M - H]^-$ at m/z 1310.9216 is shown in (**Figure 4.2(b)**) and it demonstrates the various dissociation routes of the precursor ion observed with a Declustering Potential 1 (DP1) = -70V and a Collision Energy (CE) = -70eV. The dissociation of the deprotonated molecule $[M - H]^-$ at m/z 1310.9711 led to the formation of a major product ion assigned as $[M - H - H_2O]^-$ ion at m/z 1292.8447 which resulted from an elimination of (H_2O , 18 Da) from the deprotonated precursor ion.

The MALDI-MS analysis (+ ion mode) has shown similar results to the one obtained by ESI-MS, with the exception of the lack of cluster ions such as Na^+ and K^+ (Mass spectra are shown in Appendix B). Furthermore, the MALDI-CID-MS/MS analysis indicate exactly the same formation of the product ions that were observed during ESI-CID-MS/MS analysis (Mass spectra are shown in Appendix B).

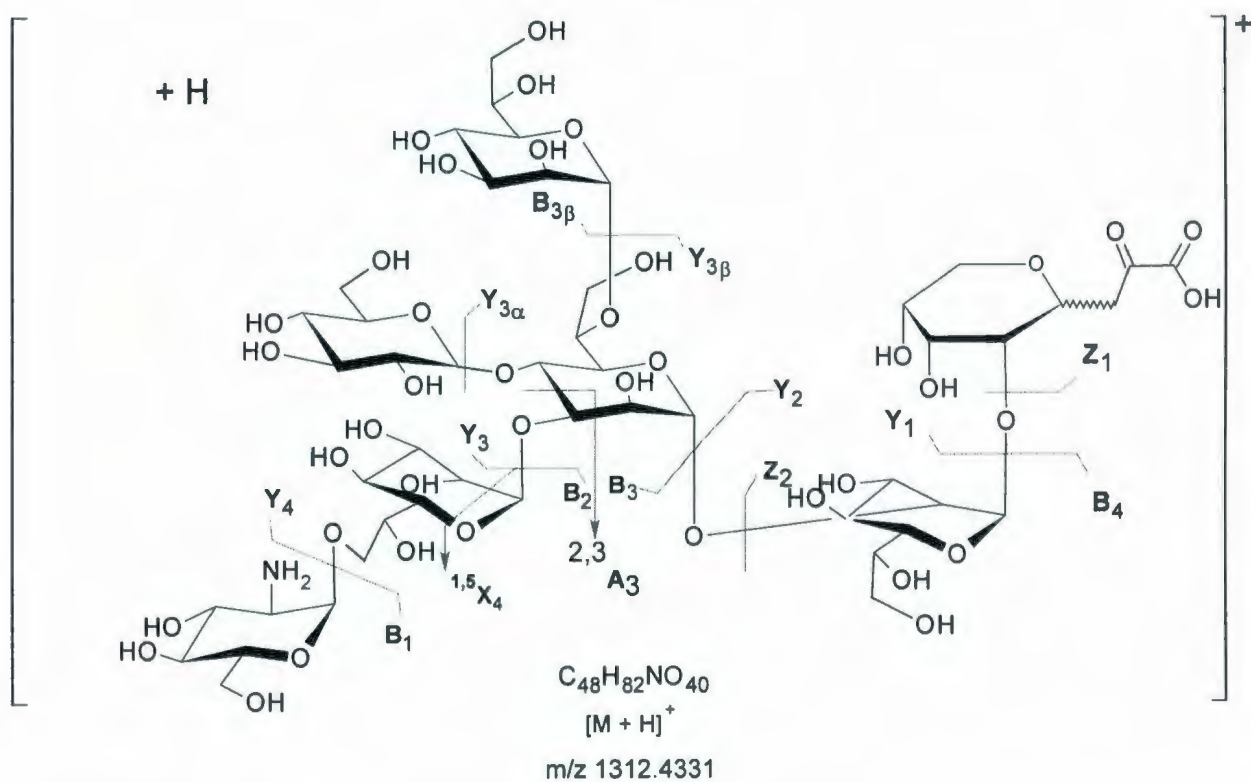
It is important to stress the fact that although the ESI-MS and CID-MS/MS of the precursor molecule in the positive ionization mode seem to indicate very crystal clear simple spectra occurring from a purified compound, this is obviously not the case as a homogeneous mixture exists, of core oligosaccharide containing eight diastereomers of

4,8- and 4,7-anhydro derivatives of the enolizable α -keto acids, and one oligosaccharide containing the open olefinic Kdo residue.

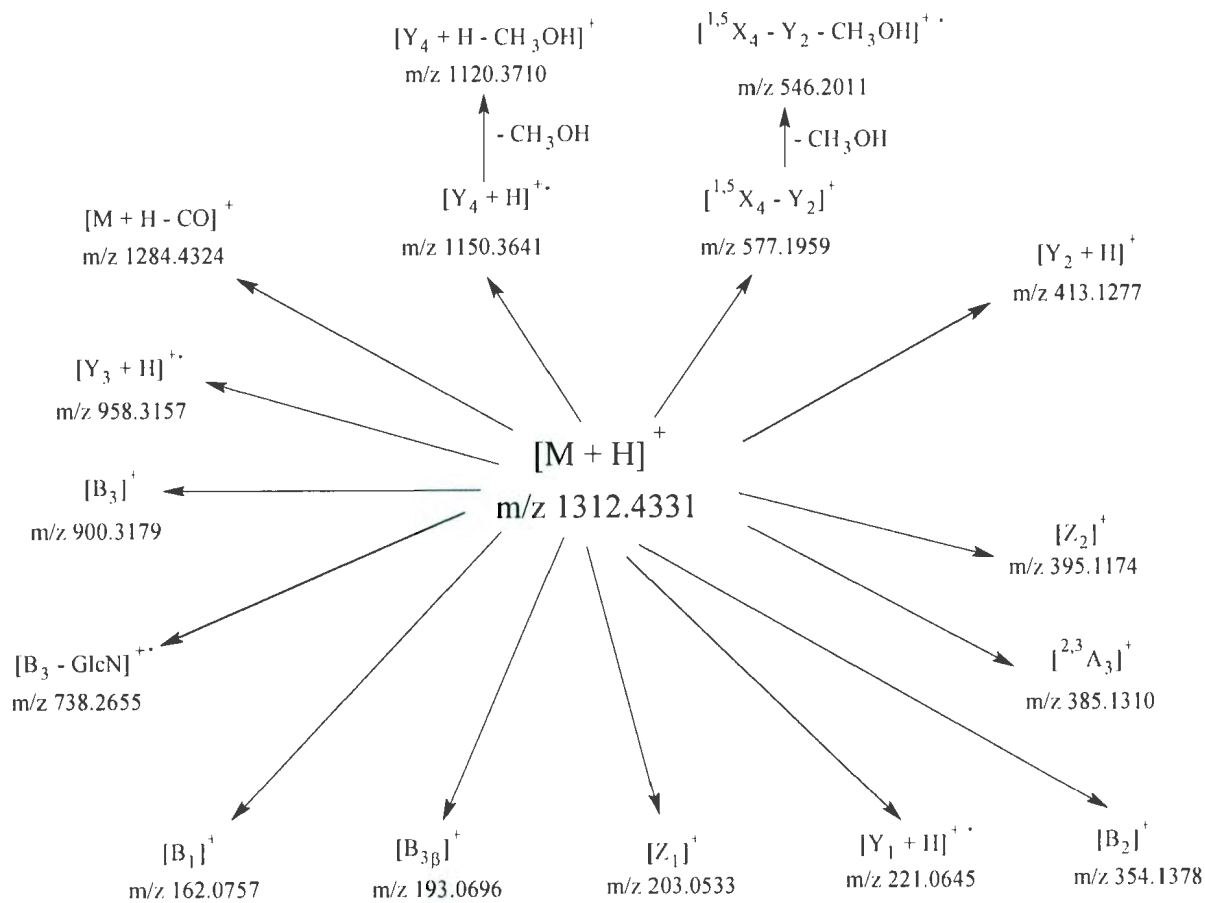
The core oligosaccharide was methylated by the Hakamori method, and the permethylated core oligosaccharide analysis was carried out in order to rationalize the presence of the nine isobaric isomers of this core oligosaccharide, whose existence obviously could not be conclusively proved during the ESI-MS and CID-MS/MS analyses of the native isobaric homogeneous core oligosaccharide.

Table 4.1: List of characteristic fragment ions observed in ESI-QqTOF-CID-MS/MS analysis of the selected protonated molecular ion $[M+H]^+$ at m/z 1312.4467 from the core oligosaccharide of *Aeromonas hydrophila* (Chemotype II).

Fragment ions	Characteristic ions	Calculated m/z	Observed m/z	Relative error ppm
$[M + H]^+$	$[C_{48}H_{82}NO_{40}]^+$	1312.4407	1312.4331	6
$[M + H - CO]^+$	$[C_{47}H_{82}NO_{39}]^+$	1284.4407	1284.4324	7
$[Y_4 + H]^+ \cdot$	$[C_{42}H_{70}O_{36}]^+ \cdot$	1150.3646	1150.3641	0
$[Y_4 + H - CH_3OH]^+$	$[C_{41}H_{68}O_{35}]^+$	1120.3773	1120.3710	6
$[Y_3 + H]^+ \cdot$	$[C_{35}H_{58}O_{30}]^+ \cdot$	958.3013	958.3157	15
$[B_3]^+$	$[C_{33}H_{58}NO_{27}]^+$	900.3196	900.3179	2
$[B_3 - GlcN]^+ \cdot$	$[C_{27}H_{46}O_{23}]^+ \cdot$	738.2429	738.2655	31
$[^{1,5}X_4 - Y_2]^+$	$[C_{21}H_{37}O_{18}]^+$	577.1974	577.1959	3
$[^{1,5}X_4 - Y_2 - CH_3OH]^+ \cdot$	$[C_{20}H_{34}O_{17}]^+ \cdot$	546.1796	546.2011	39
$[Y_2 + H]^+$	$[C_{15}H_{25}O_{13}]^+$	413.1289	413.1277	3
$[Z_2]^+$	$[C_{15}H_{23}O_{12}]^+$	395.1184	395.1174	3
$[^{2,3}A_3]^+$	$[C_{14}H_{27}NO_{11}]^+$	385.1340	385.1310	8
$[B_2]^+$	$[C_{13}H_{24}NO_{10}]^+$	354.1400	354.1378	6
$[Y_1 + H]^+ \cdot$	$[C_8H_{13}O_7]^+ \cdot$	221.0655	221.0645	5
$[Z_1]^+$	$[C_8H_{11}O_8]^+$	203.0555	203.0533	11
$[B_{3\beta}]^+$	$[C_7H_{13}O_6]^+$	193.0712	193.0696	8
$[B_1]^+$	$[C_6H_{12}NO_4]^+$	162.0766	162.0757	6



Scheme 4.2 (a): General fragmentation patterns of the protonated molecular ion $[M+H]^+$ at m/z 1312.4331 from the native core oligosaccharide of *Aeromonas hydrophila* (Chemotype II).



Scheme 4.2 (b): The proposed fragmentation routes of the $[M + H]^+$ protonated precursor ion at m/z 1312.4331 from the native core oligosaccharide of *Aeromonas hydrophila* (Chemotype II).

4.3. Electrospray ionization tandem mass spectrometry analysis of the permethylated core oligosaccharide

4.3.1. ESI-QqTOF-MS analysis of the permethylated native core oligosaccharide

During ESI-QqToF-MS analysis of the permethylated native core oligosaccharide SJ-48, which was performed in methanol, revealed a diagnostic series of eight protonated molecules. Five protonated species were formed by increments of 14 Daltons (at m/z 1676.8630, 1690.8666, 1704.8543, 1718.8338, and 1732.9415) and the presence of an extra three minor satellite signals. There are direct results created from the homogenous mixture of the core oligosaccharide containing the either 4,8- or 4,7-anhydro derivatives of the α -keto acids. A similar series has been previously reported during the analysis of the permethylated core oligosaccharide of *Aeromonas salmonicida* wild and rough mutant LPS forms.^{13a,13b} It is important to stress that this series is not of an artefactual nature, but that it includes and represents real formed compounds which were further analyzed by CID-MS/MS. The double-charged molecules of this series were also observed (**Table 4.2 & Figure 4.3**).

From the ESI-MS shown in **Figure 4.3**, the presence of the protonated precursor ion $[M_1 + H]^+$ at m/z 1676.8630 which resulted from the incorporation of 26 methyl groups of all the hydroxy- and NH-groups of the oligosaccharide chain containing either 4,8- or 4,7-anhydro derivatives of the α -keto acids could be seen. In addition the presence of the protonated precursor ion $[M_2 + H]^+$ at m/z 1690.8666 which resulted from the incorporation of 27 methyl groups of all the hydroxy- and NH₂-groups of the

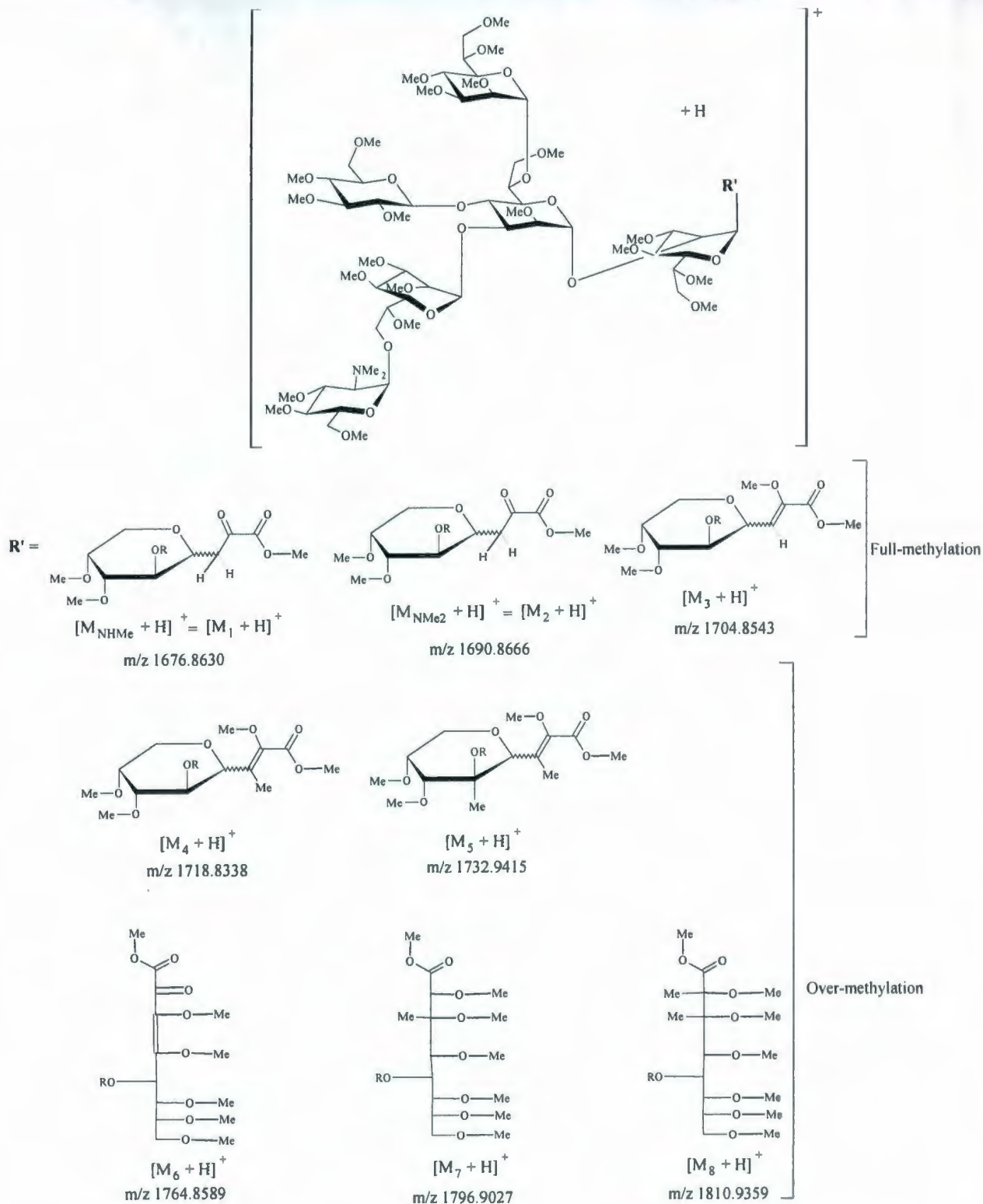
oligosaccharide chain containing either the 4,8- or 4,7-anhydro derivatives of the enolizable α -keto acids could also be observed. This is due to the incorporation of an extra methyl group on the free amino group on the D-glucosamine residue to be dimethylated (NMe₂).^{13a} The protonated precursor ion [M₃ + H]⁺ at m/z 1704.8543 resulted from the incorporation of 28 methyl groups (full methylation) of all the hydroxy- and NH₂-groups of the oligosaccharide chain containing either the 4,8- or 4,7-anhydro derivatives of the enolizable α -keto acids 3A. The protonated precursor ion [M₄ + H]⁺ at m/z 1718.8338 resulted from the incorporation of 29 methyl groups (over methylation) of all the hydroxy- and NH₂-functions of the oligosaccharide chain containing the 4,8-anhydro derivatives of the enolizable α -keto acids in addition to an extra methyl group which arises from the overmethylation of this form of oligosaccharide 3A during Hakomori methylation. The protonated precursor ion [M₅ + H]⁺ at m/z 1732.9415 resulted from the incorporation of 30 methyl groups (over methylation) which was attributed to an additional extra C-methylation on C-3 and C-4 of the 4,8-anhydro Kdo unit 3A. This over-C-methylation has been mentioned as well by Dell *et al.*, using FAB-MS analysis of permethylated core oligosaccharide containing normal Kdo reducing end group (Scheme 4.3).¹¹⁵

It is noteworthy to indicate that the presence of an extra three minor satellite signals which obviously were attributed to the formation of three over-methylated species could be observed. These were the protonated molecules [M₈ + H]⁺ at m/z 1810.9359, [M₇ + H]⁺ at m/z 1796.9027, and [M₆ + H]⁺ at m/z 1764.8589, which resulted from the incorporation of extra methyl groups located on the open olefinic Kdo unit 2A (Scheme

4.3) of the full-methylated core oligosaccharide and which is described below. The presence of these protonated molecules is due to an unusual overmethylation reaction, whose proposed mechanism can be explained as follows. During the Hakamori methylation, it is reasonable to expect that the open olefinic Kdo form 2A (containing a C-3-C-4 double bond) forms a C-2 enol. This C-enol containing the C-3-C-4 double bond can be further oxidized, due to the harsh Hakamori condition, to a reactive β -diketone on C-3 and C-4. This latter β -diketone appears to be prone to be O-methylated; it can also be subjected to extra addition of methyl groups (**Scheme 4.3**).

Thus, when the carbonyl group at C-2 of the open olefinic Kdo unit 2A of the permethylated core oligosaccharide endured an enolization and was subsequently O- and C-methylated, it was postulated that a gas-phase reaction occurs in the ionization chamber during the electrospray process by addition of a solvent methanol to the C-3-C-4 double bond to form the ion $[M_6 + H]^+$ at m/z 1764.8589. The protonated molecule $[M_7 + H]^+$ at m/z 1796.9027 is afforded from the addition of a solvent methanol to the C-3-C-4 double bond of the open olefinic Kdo unit 2A followed by the enolization of the carbonyl group at C-2 which was subsequently O-methylated, and then by an addition of an extra methyl group to the C-3 of the open olefinic Kdo unit 2A (**Scheme 4.3**). Finally the addition of an extra methyl group to the C-4 of the open olefinic Kdo unit 2A affords the protonated molecule $[M_8 + H]^+$ at m/z 1810.9359. Such results were demonstrated in previous investigations of other LPS core oligosaccharide containing 5-O-linked dephosphorylated Kdo residues which were permethylated with the Hakamori method.

¹³a,¹³b However further confirmation was required by conducting CID-MS/MS analyses of these three minor satellite signals of the permethylated core oligosaccharide.



Scheme 4.3: The permethylated core oligosaccharide (Scheme 4.2a) with eight protonated precursor ions: $[M_1+H]^+$, $[M_2+H]^+$, $[M_3+H]^+$, $[M_4+H]^+$, $[M_5+H]^+$, $[M_6+H]^+$, $[M_7+H]^+$ and $[M_8+H]^+$ ions at m/z 1676.8630, 1690.8666, 1704.8543, 1718.8338, 1732.9415, 1764.8589, 1796.9027 and 1810.9359 respectively. The symbol R' represents the full- and over-methylated molecules containing the 4,8-anhydro derivative of the enolizabe α -keto acid terminal and the open olefinic Kdo residue.

4.3.2. A new interpretation of the ESI-QqTOF-MS analysis of the three minor satellite signals of the permethylated core oligosaccharide.

The Hakamori methylation method has long been maligned and has been suspected to form side-products which are caused by the endothermic reactions of the dimethyl anion, the starting material and the methyl iodide.⁷⁹ Certainly, it is well-known that all methylation of carbohydrates occur through successive, base (B)-catalyzed ionization of the hydroxyl groups, followed by reaction with the methylating agent (MeI). For that reason, another type of methylation of the homogeneous core oligosaccharide mixture were performed with the alkali-metal hydroxide method described by Ciucanu & Kerek.⁸⁰ To our surprise and astonishment, after ESI-QqTOF-MS of the permethylated core oligosaccharide was electrosprayed in chloroform, the same series of identical permethylated molecules electrosprayed in methanol were obtained with exactly the same masses, as the one obtained by the Hakamori method. The similarities of these two different methylations of the core oligosaccharide was perplexing until it was realized that the minor satellite signals were DMSO-stable covalent adducts which were effectively formed in solution during the methylation process and not during the electrospray process and the gas-phase formation of these ions. This conclusion was attained after the methylation of the core oligosaccharide by the Hakamori and the Ciucanu & Kerek methods in which the permethylated products were electrosprayed either in methanol or in chloroform solution.^{79,80} In both cases the same results were obtained. To our knowledge, this is the first time that DMSO adducts have been observed in the gas phase, and they have never before been reported.

Consequently, the protonated molecule at m/z 1796.9027, was assigned as the stable covalent DMSO addition product $[M_7 + H]^+$ which had an increment of 78 higher than the protonated molecule $[M_4 + H]^+$ at m/z 1718.8338 (**Figure 4.3**). To be chemically correct, this permethylated $[M_7 + H]^+$ product, is indeed the $[M_4 + H + CH_3SOCH_3]^+$ DMSO covalent product resulting from the Michael addition¹¹⁶⁻¹¹⁸ of the dimsyl anion on the C-2-C-3 double bond of the 4,8-anhydro Kdo-residue (or 4,7-anhydro-residue) followed by an addition of a proton on the double bond. The mechanism formation of this addition product is indicated in **Scheme 4.4 (a)**. It is well-known that the Michael addition reaction is a nucleophilic addition of a carbanion or another nucleophile to an α , β -unsaturated carbonyl compound. It belongs to the larger class of conjugate additions. This is one of the most useful methods for the mild formation of C-C bonds.¹¹⁶⁻¹¹⁸

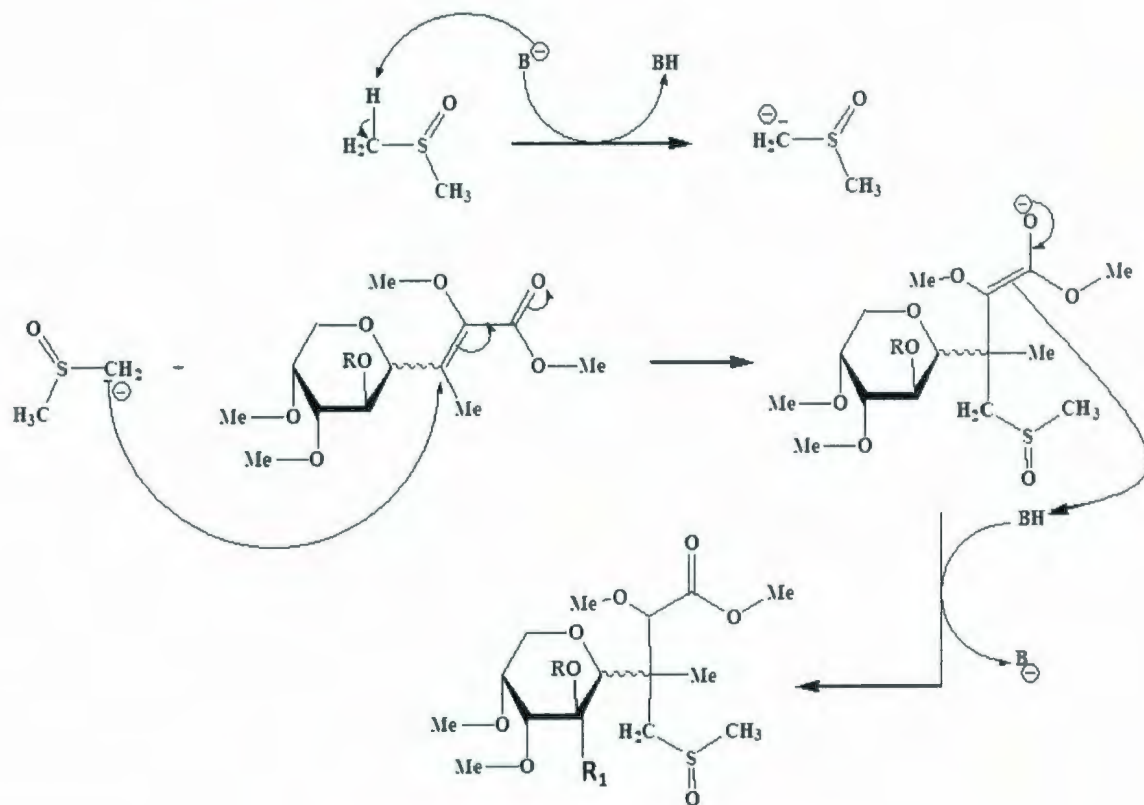
Similarly, the protonated molecule at m/z 1810.9359 assigned as the $[M_8 + H]^+$ ion was the corresponding dimsyl anion addition product of the $[M_5 + H]^+$ ion at m/z 1732.9415 (**Figure 4.3**). Thus the protonated molecules $[M_8 + H]^+$ is the $[M_5 + H + CH_3SOCH_3]^+$ product molecule having an increment of 78 Da higher than the $[M_5 + H]^+$ ion. Once more this was the result of a covalent compound formation resulting from the Michael addition of the dimsyl anion on the C-2-C-3 double bond of the 4,8-anhydro Kdo-residue followed by addition of a proton (**Scheme 4.4 (a)**).

Finally, the identification of the unique covalent addition product of the dimsyl anion to the C-3-C-4 double bond of the open-chain Kdo residue **2A**, followed by a consecutive elimination of a hydrogen molecule, to afford the molecular ion $[M_6]^+$ ion m/z 1764.8589 (**Scheme 4.4 (b)**). It is significant to note, that in this latter molecular ion

[M₆]⁺ the carboxyl group is free and not esterified as a methyl ester. The absence of the methyl ester could be explained by the probable complexation of the C-1 and C-2 carbonyl group with DMSO during the methylation reaction, which will prevent and hinder the esterification reaction.

The confirmation of the different structures of this complete series of permethylated core oligosaccharides and DMSO adducts, was achieved by conducting CID-MS/MS analyses.

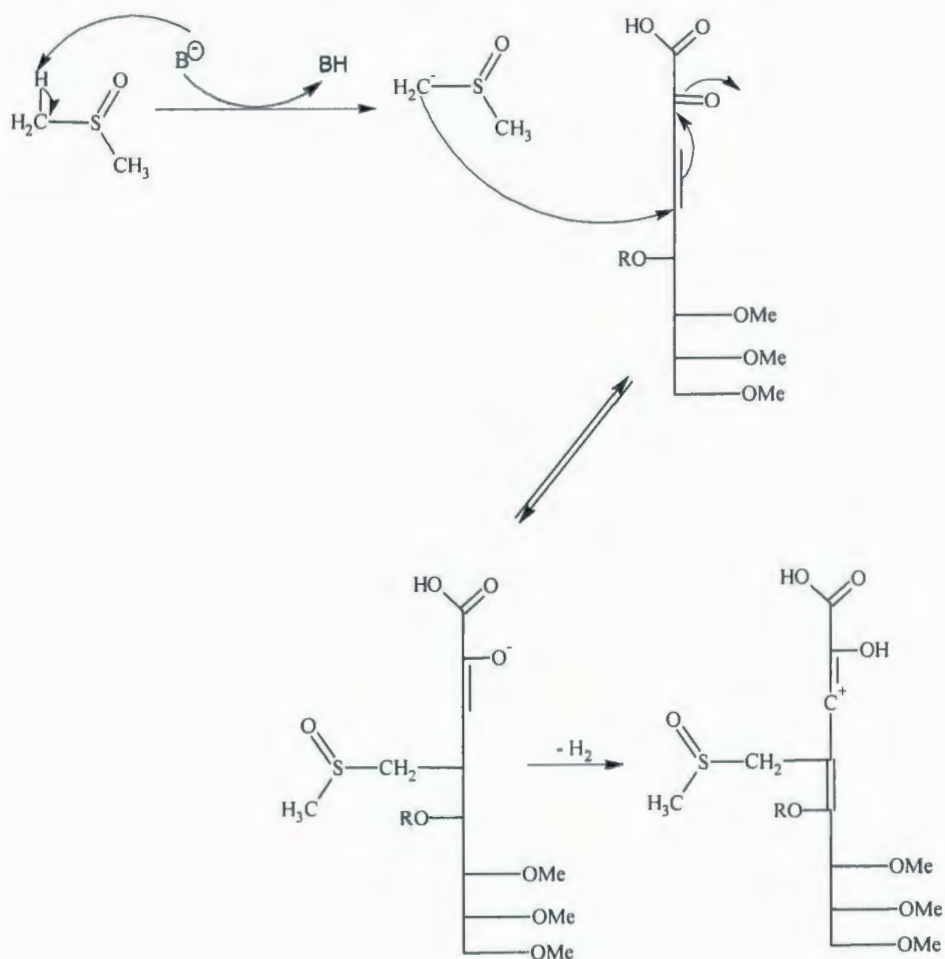
For simplification purposes the Kdo residue in the 4,8-anhydro form is represented in all the schemes.



R= remaining portion of the core oligosaccharide

R₁ = H, Me

Scheme 4.4 (a): Proposed mechanism of the formation of DMSO adducts of the permethylated core oligosaccharide: $[\text{M}_4+\text{H}+\text{CH}_3\text{SOCH}_3]^+$, $[\text{M}_5+\text{H}+\text{CH}_3\text{SOCH}_3]^+$ ions at m/z 1796.9027 and 1810.9359 respectively, resulting from the Michael addition reaction^{117,118} of the dimethyl sulfide anion on the C-2-C-3 double bond of the 4,8-anhydro Kdo-residue.



R= remaining portion of the core oligosaccharide

Scheme 4.4 (b): Proposed mechanism of the formation of DMSO adduct of the permethylated core oligosaccharide: $[\text{M}_6]^+$ ion at m/z 1764.8589, resulting from the Michael addition reaction^{116,117} of the dimethylsulfoniolate anion on the C-3-C-4 double bond of the open olefinic Kdo-residue.

Table 4.2: Diagnostic protonated and sodiated precursor ions and DMSO adducts occurring from the ESI-MS of the permethylated homogenous mixture of the core oligosaccharide of *Aeromonas hydrophila* (Chemotype II).

Incorporat ion of Me groups	Protonated molecules	Characteristic ions	Calculated <i>m/z</i>	Observed <i>m/z</i>	Relative error ppm
	$[M_8 + H]^+$	$[C_{81}H_{152}NO_{42}]^+$	1810.9710		19
30	$[M_5 + H +$ $CH_3SOCH_3]^+$	$[C_{80}H_{148}NO_{41}S]^+$	1810.9242	1810.9359	6
	$[M_7 + H]^+$	$[C_{80}H_{150}NO_{42}]^+$	1796.9626		33
29	$[M_4 + H +$ $CH_3SOCH_3]^+$	$[C_{79}H_{146}NO_{41}S]^+$	1796.9085	1796.9027	3
28	$[M_6 + H]^+$	$[C_{78}H_{142}NO_{42}]^+$	1764.9000		23
27	$[M_6]^+$	$[C_{77}H_{138}NO_{41}S]^+$	1764.8459	1764.8589	7
30	$[M_5 + H]^+$	$[C_{78}H_{142}NO_{40}]^+$	1732.9102	1732.9415	18
29	$[M_4 + H]^+$	$[C_{77}H_{140}NO_{40}]^+$	1718.8419	1718.8338	5
28	$[M_3 + H]^+$	$[C_{76}H_{138}NO_{40}]^+$	1704.8789	1704.8543	14
27	$[M_2 + H]^+$	$[C_{75}H_{136}NO_{40}]^+$	1690.8633	1690.8666	2
26	$[M_1 + H]^+$	$[C_{74}H_{134}NO_{40}]^+$	1676.8476	1676.8630	9
	$[M_8 + Na + H]^{2+}$	$[C_{81}H_{152}NNaO_{42}]^{2+}$	916.9032		29
30	$[M_5 + H +$ $CH_3SOCH_3 +$ $Na]^{2+}$	$[C_{80}H_{148}NNaO_{41}S]^{2+}$	916.9569	916.8762	88
	$[M_7 + Na + H]^{2+}$	$[C_{80}H_{150}NNaO_{42}]^{2+}$	909.9012		42
29	$[M_4 + H +$ $CH_3SOCH_3 +$ $Na]^{2+}$	$[C_{79}H_{146}NNaO_{41}S]^{2+}$	909.9477	909.8630	93
30	$[M_6 + Na + H]^{2+}$	$[C_{78}H_{142}NNaO_{42}]^{2+}$	893.9448	893.8753	78
27	$[M_6 + Na]^{2+}$	$[C_{77}H_{138}NNaO_{41}S]^{2+}$	893.9178		48
30	$[M_5 + Na + H]^{2+}$	$[C_{78}H_{142}NNaO_{40}]^{2+}$	877.8855	877.8548	35
29	$[M_4 + Na + H]^{2+}$	$[C_{77}H_{140}NNaO_{40}]^{2+}$	870.8901	870.8505	45
28	$[M_3 + Na + H]^{2+}$	$[C_{76}H_{138}NNaO_{40}]^{2+}$	863.8952	863.8600	41
27	$[M_2 + Na + H]^{2+}$	$[C_{75}H_{136}NNaO_{40}]^{2+}$	856.9030	856.8625	47
26	$[M_1 + Na + H]^{2+}$	$[C_{74}H_{134}NNaO_{40}]^{2+}$	849.8799	849.8558	28

4.4. ESI-CID-MS/MS analysis of the permethylated core oligosaccharide

4.4.1. ESI-CID-MS/MS analyses of the protonated precursor ions obtained from the permethylated core oligosaccharide

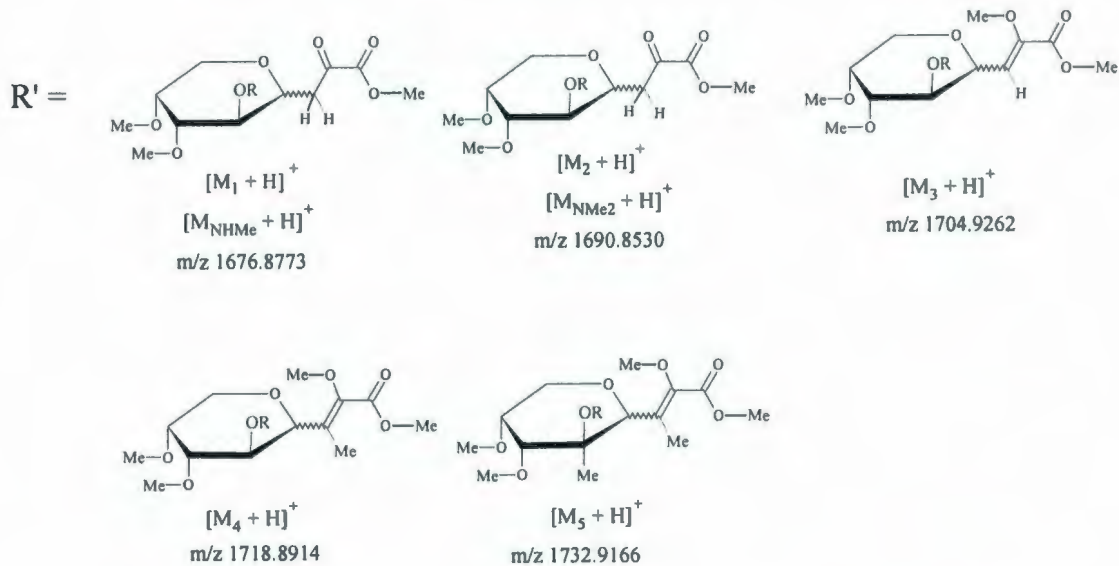
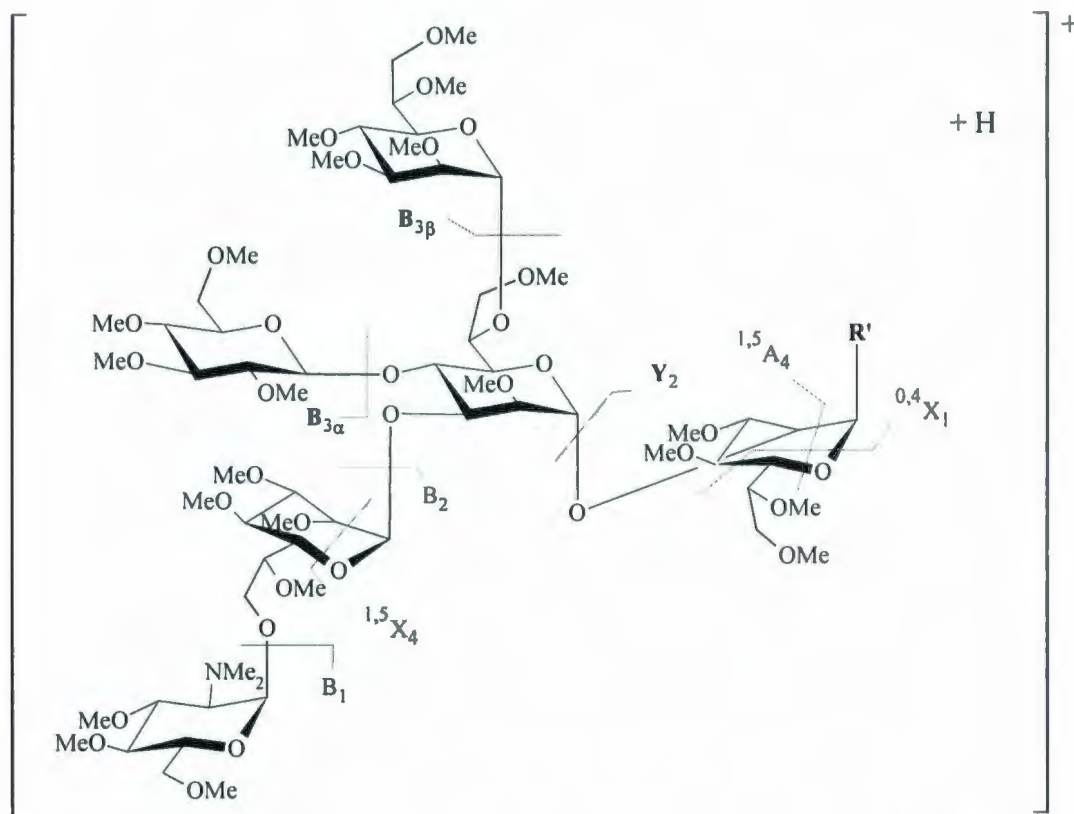
The CID-MS/MS analyses of the selected precursor permethylated molecules extracted from the homogeneous core oligosaccharide containing either the 4,7- or the 4,8-anhydro-Kdo unit are represented as follow: $[M_1 + H]^+$, $[M_2 + H]^+$, $[M_3 + H]^+$, $[M_4 + H]^+$, and $[M_5 + H]^+$ at m/z 1676.8630, 1690.8666, 1704.8543, 1718.8338, and 1732.9415 respectively (**Figure 4.3**). All the CID-fragmentation pathways obtained were similar but not exactly identical to one another, notwithstanding the mass of the selected precursor ion chosen (**Scheme 4.4**).

The CID-MS/MS fragmentation routes of the precursor ions $[M_n + H]^+$ ($n = 1-5$) at m/z 1676.8773, at m/z 1690.8530, at m/z 1704.9262, at m/z 1718.8914, and at m/z 1732.9166, has formed similar product ions (**Figures 4.(4-8)**). For example the CID-MS/MS analysis of the precursor ions $[M_2 + H]^+$ at m/z 1690.8530 has afforded the following product ions: the ion at m/z 728.3389 was assigned as $[^{1,5}X_{3\beta} - B_{3\alpha} - Y_2]^+$ which resulted from the interglycosidic breakage of the methylated L-glycero-D-manno-heptose at position C-1 and C-5 and the simultaneous elimination of 2,3,4,6-tetra-O-methyl glucose residue followed by the loss of 3,4,6,7-tetra-O-methyl heptose-(1→5)-1,6,7-tri-O-methyl 4,8-anhydro-disaccharide derivative of the enolizable α -keto acid terminal. The product ion at m/z 700.3306 assigned as $[^{1,5}X_{3\beta} - B_{3\alpha} - Y_2 - CO]^+$ and was formed from the ion at m/z 728.3544, which eliminated a carbonyl group (28 Da). The product ion at m/z 480.5860 was assigned as $[B_2]^+$ which corresponded to the 3,4,6-tri-O-methyl-2-deoxy-2-

N-dimethyl-glucosaminyl-(1→7)[2,3,4,6-tetra-*O*-methylheptose] disaccharide ion. The product ion at m/z 452.5399 was assigned as $[B_2 - CO]^+$ and resulted from the elimination of a carbonyl group from the product ion at m/z 480.2860. The product ion at m/z 263.1440 was assigned as $[B_{3\beta}]^+$ and corresponded to 2,3,4,6,7-penta-*O*-methyl heptose ion. The product ion at m/z 232.1553 assigned as $[B_1]^+$ corresponded to a 3,4,6-tri-*O*-methyl,*N*-dimethyl-glucosaminyl residue. The product ion at m/z 218.1310 assigned as $[B_{3\alpha}]^+$ corresponded to the 2,3,4,6-tetra-*O*-methyl glucose ion. The product ion at m/z 199.1114 assigned as $[B_1 - CH_3OH]^+$ corresponded to the fragment ion 3,4,6-tri-*O*-methyl,*N*-dimethyl-glucosamine ion, which loses a methanol molecule (32 Da) (**Table 4.3**). The proposed fragmentation routes of all the permethylated protonated precursor ions $[M_n + H]^+$ ($n = 1-5$), are shown in **Scheme 4.5** and **Figures 4.(4-8)**.

Table 4.3: List of similar fragment ions observed during ESI-QqTOF-CID-MS/MS analyses of the permethylated precursor ions: $[M_n + H]^+$ ($n = 1-5$) at m/z 1676.8773, 1690.8530, 1704.9262, 1718.8914, and 1732.9166 respectively of the permethylated core oligosaccharide of *Aeromonas hydrophila* (Chemotype II).

Fragment ions	Characteristic ions	Calculated m/z	Observed m/z	Relative error ppm
$[^{1,5}X_4 - B_{3\alpha} - Y_2]^+$	$[C_{32}H_{56}O_{17}]^+$	728.3544	728.3389	21
$[^{1,5}X_4 - B_{3\alpha} - Y_2 - CO]^+$	$[C_{31}H_{56}O_{16}]^+$	700.3506	700.3306	29
$[B_2]^+$	$[C_{22}H_{42}NO_{10}]^+$	480.569	480.5860	35
$[B_2 - CO]^+$	$[C_{21}H_{42}NO_9]^+$	452.5589	452.5399	42
$[B_{3\beta}]^+$	$[C_{12}H_{23}O_6]^+$	263.1494	263.1440	21
$[B_1]^+$	$[C_{11}H_{22}NO_4]^+$	232.1548	232.1553	2
$[B_{3\alpha}]^+$	$[C_{10}H_{19}NO_4]^+$	218.1386	218.1310	35
$[B_1 - CH_3OH]^+$	$[C_9H_{11}O_5]^+$	199.1208	199.1114	47



Scheme 4.5: The proposed fragmentation routes of the permethylated protonated precursor ions: $[M_1+H]^+$, $[M_2+H]^+$, $[M_3+H]^+$, $[M_4+H]^+$, and $[M_5+H]^+$ ions at m/z 1676.8773, 1690.8530, 1704.9262, 1718.8914, and 1732.9166 respectively. The symbol R' represents the various full- and over-methylated molecules composed of the 4,8-anhydro derivative of the enolizabe α -keto acid terminal residue.

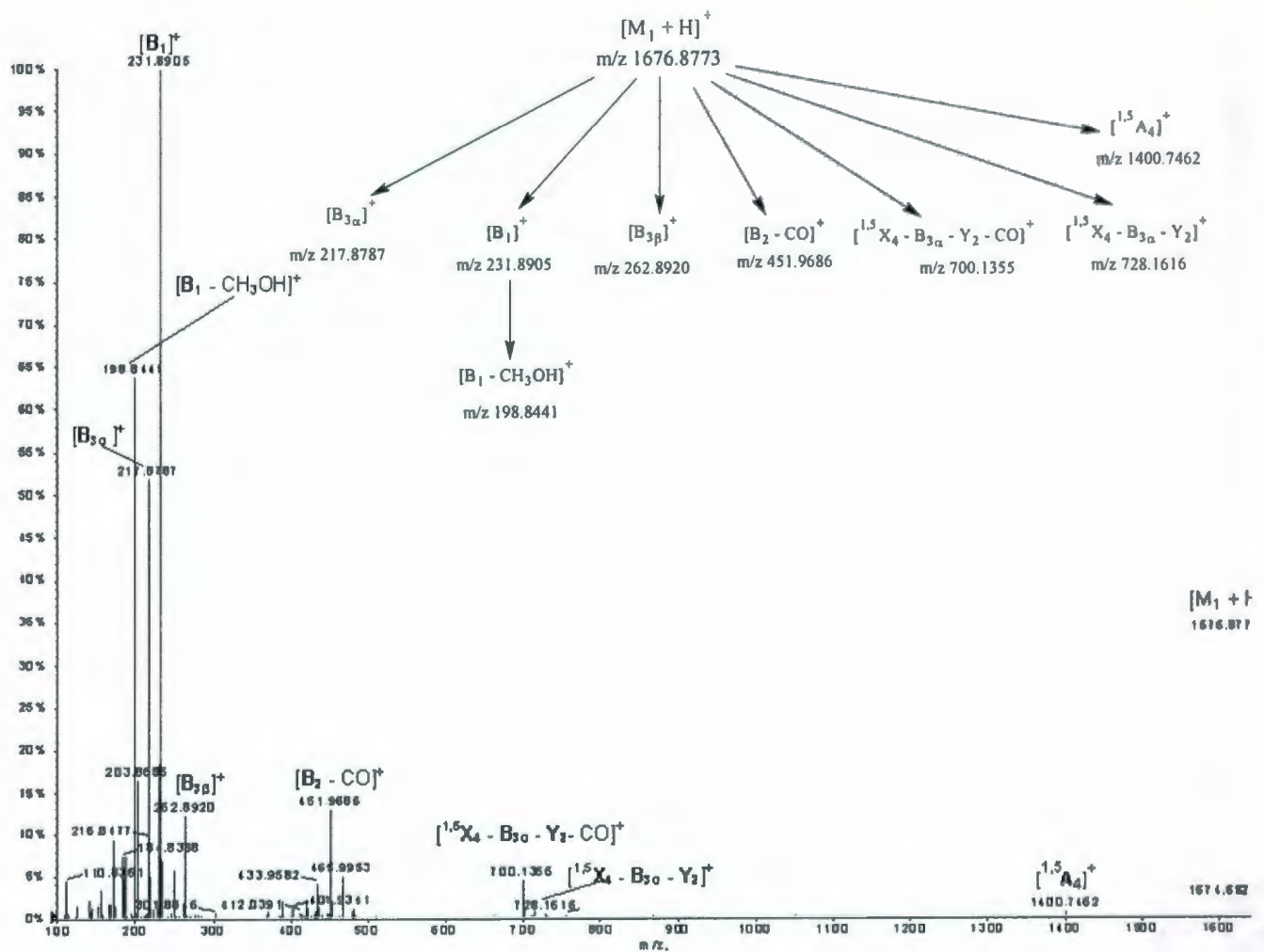


Figure 4.4: ESI-CID-MS/MS of the selected precursor ion at m/z 1676.873 from the permethylated core oligosaccharide.

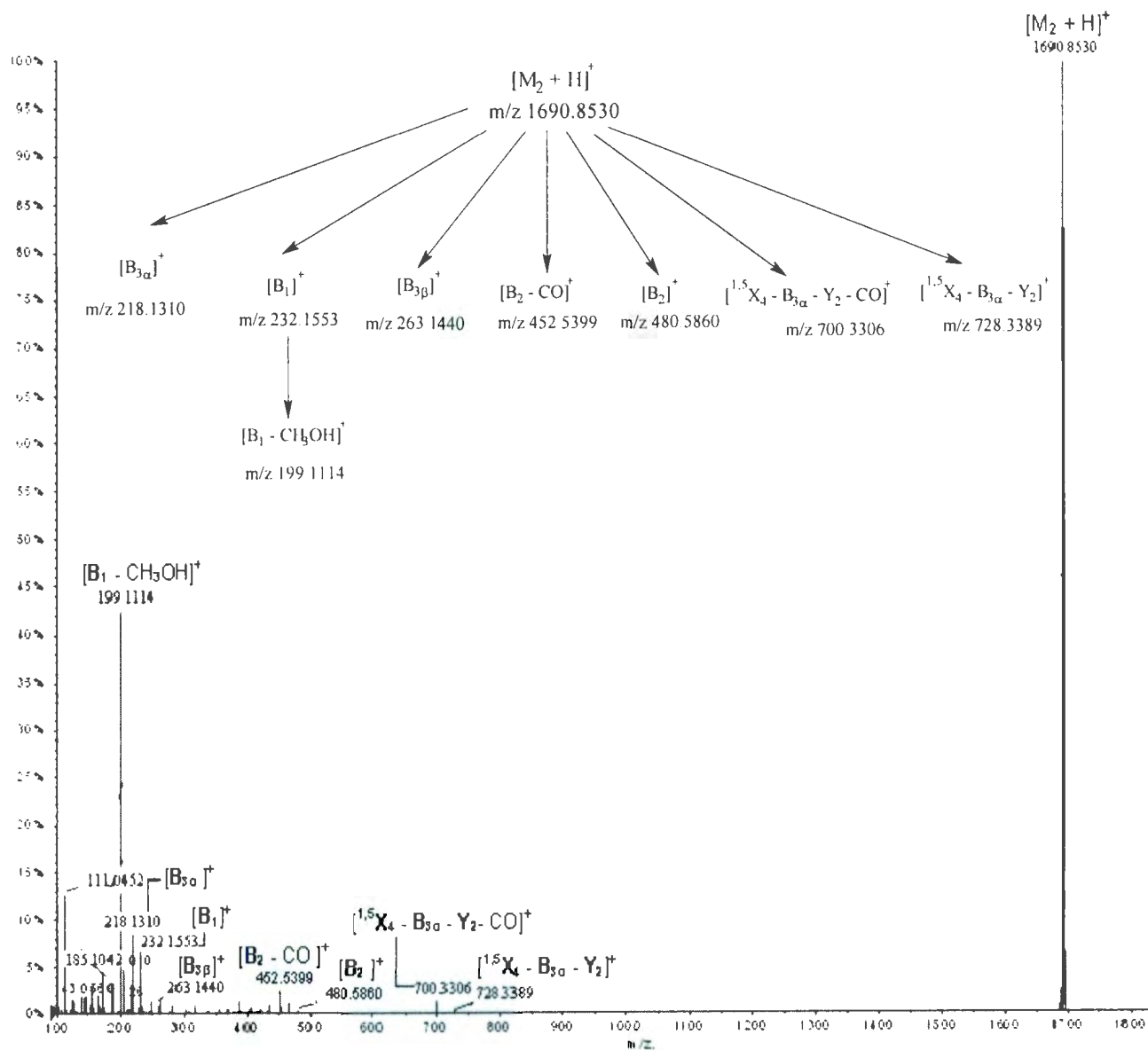


Figure 4.5: ESI-CID-MS/MS of the selected precursor ion at m/z 1690.8666 from the permethylated core oligosaccharide.

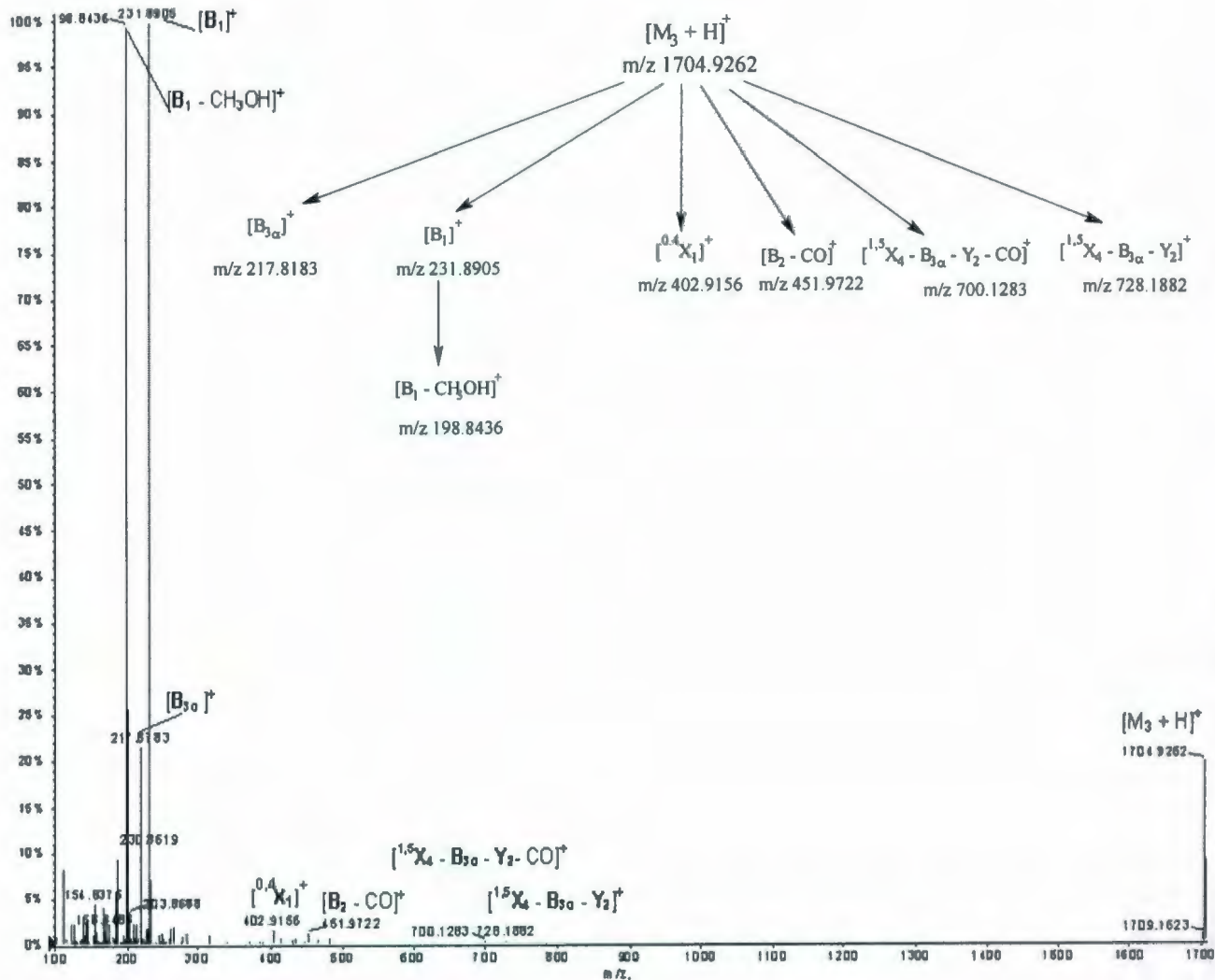


Figure 4.6: ESI-CID-MS/MS of the selected precursor ion at m/z 1704.8543 from the permethylated core oligosaccharide.

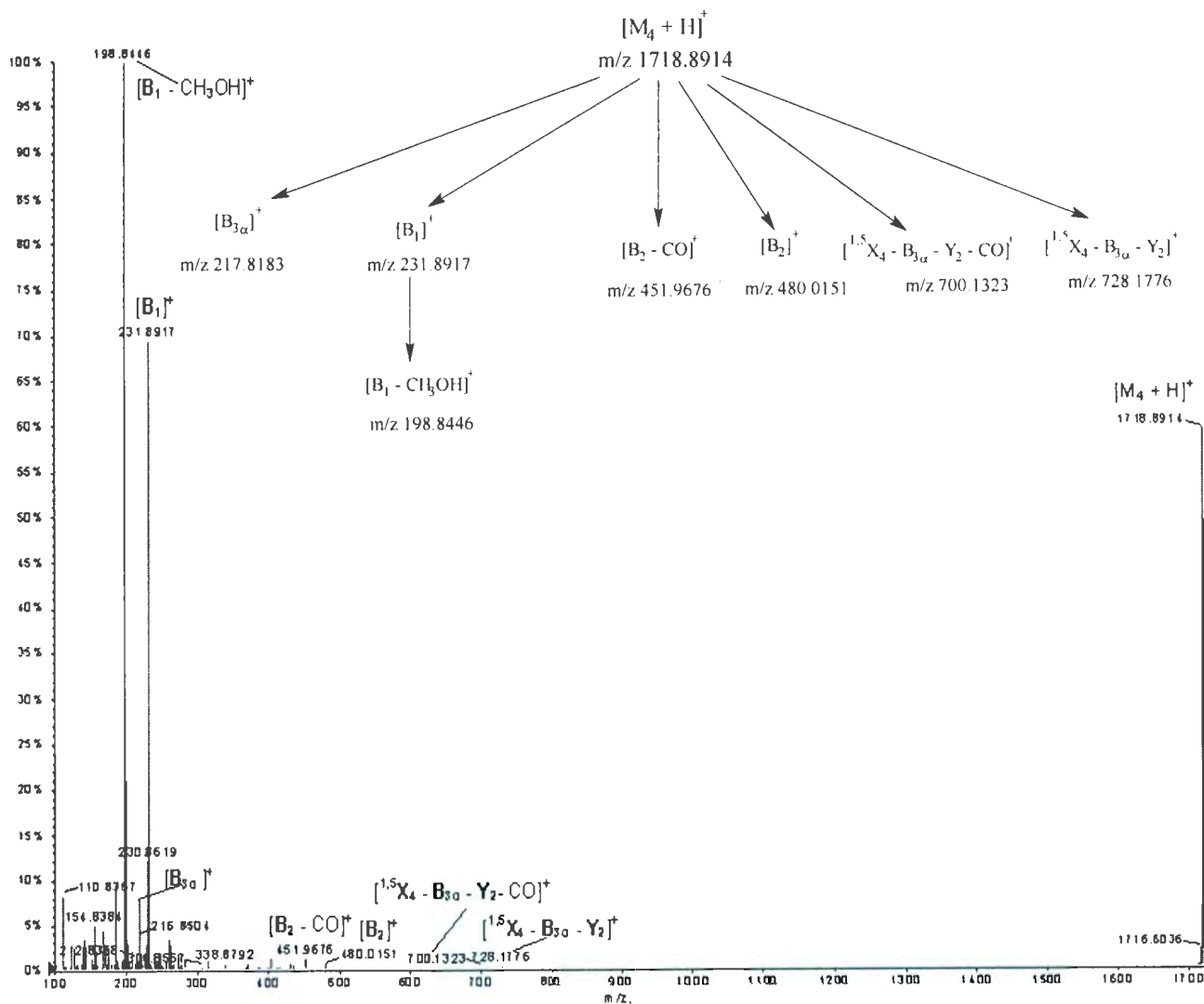


Figure 4.7: ESI-CID-MS/MS of the selected precursor ion at m/z 1718.8338 from the permethylated core oligosaccharide.

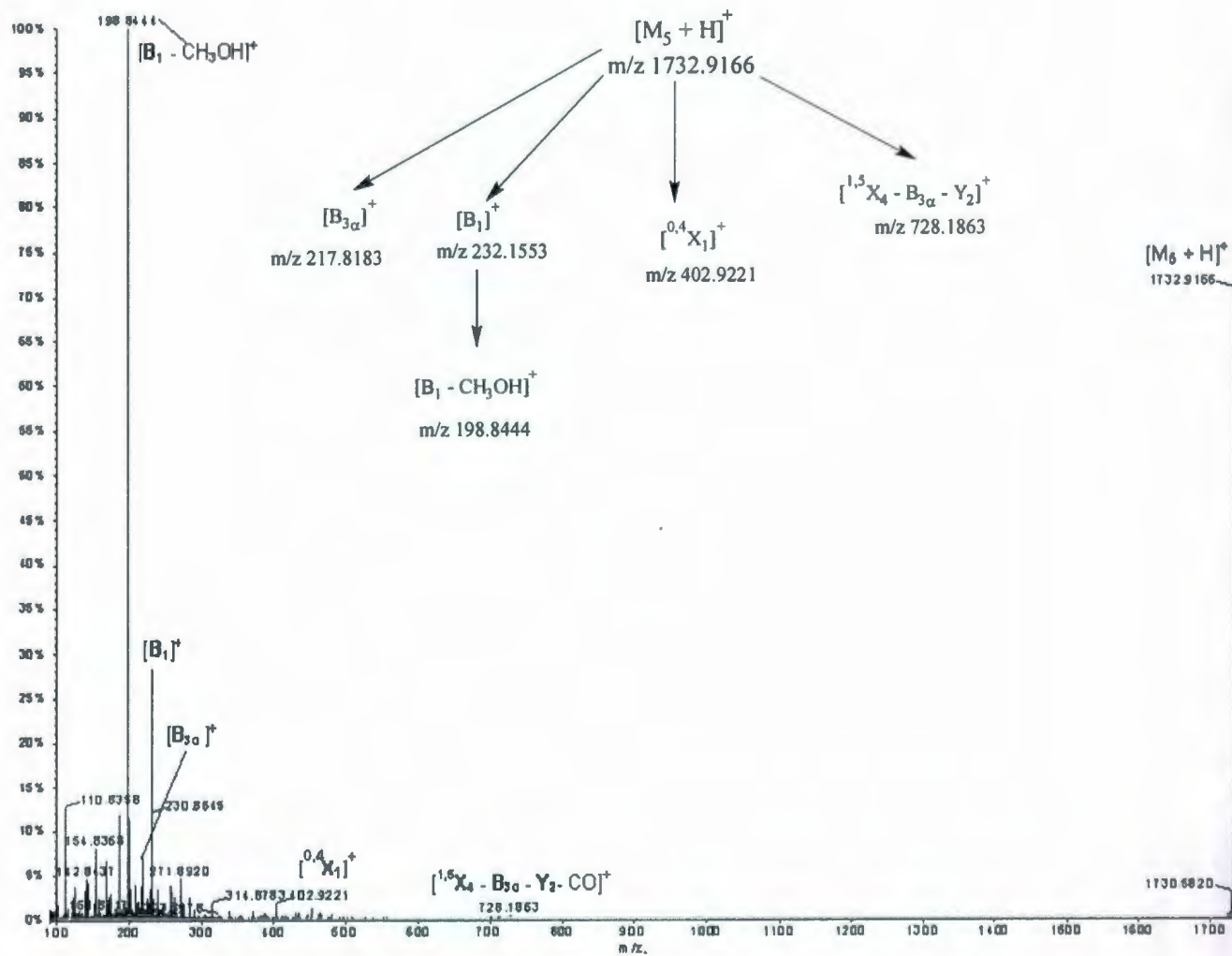


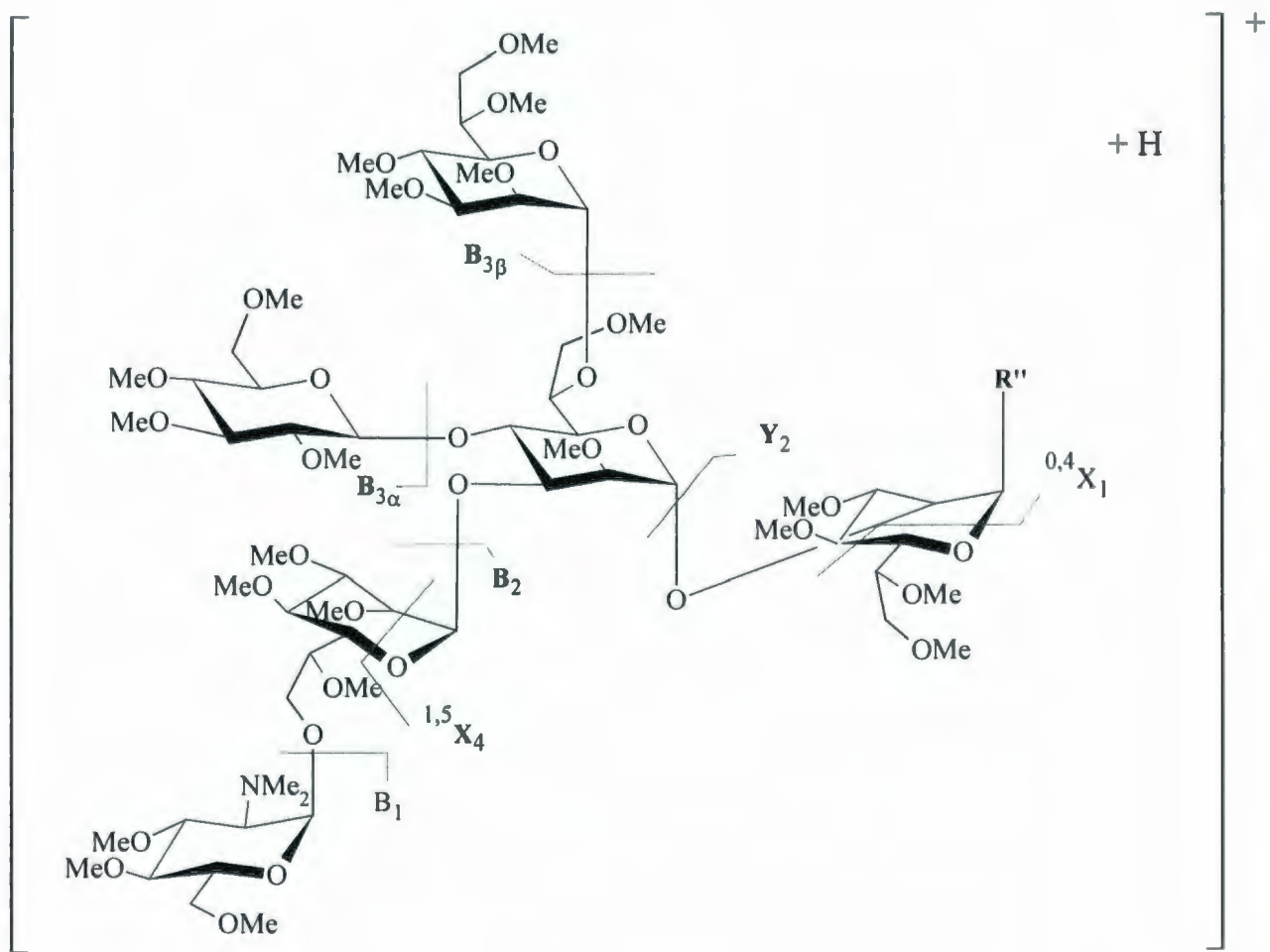
Figure 4.8: ESI-CID-MS/MS of the selected precursor ion at m/z 1732.9415 from the permethylated core oligosaccharide.

4.4.2. ESI-CID-MS/MS analyses of various DMSO adducts of the permethylated core oligosaccharide

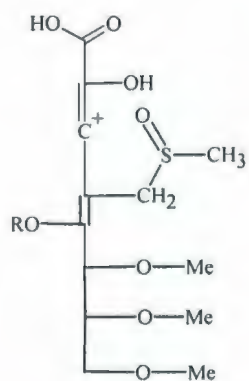
The ESI-CID-MS/MS analyses of the selected precursor ions (shown in **Figure 4.3**) of the DMSO adducts of the permethylated core oligosaccharide at m/z 1764.8589, 1796.9027 and 1810.9359 are shown in **Figures 4.(9-11)**; it illustrated that the CID-fragmentations were almost similar, notwithstanding the different mass of the selected precursor ion. The CID-MS/MS analysis of the precursor ion $[M_6]^+$ at m/z 1764.9647 revealed the presence of low abundances of the same common product ions observed previously, with the exception of the product ion at m/z 1660.8754 (**Figure 4.9**). This latter was created by loss of 104 Da, which was rationalized as the elimination of the terminal CO_2 group (44 Da) followed by two molecules of formaldehyde (60Da).

Similarly, the CID-MS/MS analysis of the precursor ion $[M_4 + H + CH_3SOCH_3]^+$ at m/z 1796.9578 afforded an almost identical spectrum, with the exception of one product ion at m/z 1688.8428 (**Figure 4.10**). This latter was created by elimination of 108 Da, which was rationalized as the loss of the terminal CO_2 molecule (44 Da) followed by two molecules of methanol (64 Da).

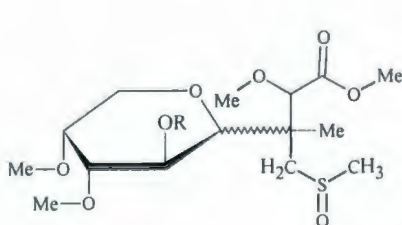
Finally, the CID-MS/MS analysis of the precursor ion $[M_5 + H + CH_3SOCH_3]^+$ at m/z 1810.8907 revealed the presence of low abundances of the same common product ions observed previously, with the exception of one product ion at m/z 1688.8560 (**Figure 4.11**). This latter was created by loss of 122 Da, which was rationalized as the elimination of three molecules of formaldehyde (90 Da) and methanol (32 Da). Note that the common fragmentation routes are shown in **Scheme 4.6**.



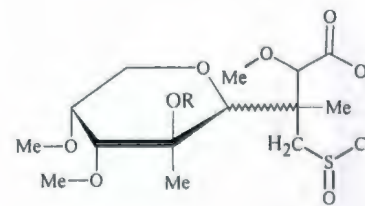
R'' =



$[M_6]^+$
m/z 1764.9647



$[M_4 + H + CH_3SOCH_3]^+$
m/z 1796.9578



$[M_5 + H + CH_3SOCH_3]^+$
m/z 1810.8907

Scheme 4.6: The proposed fragmentation routes of the DMSO adducts of the permethylated core oligosaccharide: $[M_6]^+$, $[M_4+H+CH_3SOCH_3]^+$, and $[M_5+H+CH_3SOCH_3]^+$ ions at m/z 1764.9647, 1796.9578, and 1810.8907 respectively. The symbol R'' represents the various DMSO adducts of the permethylated core oligosaccharide.

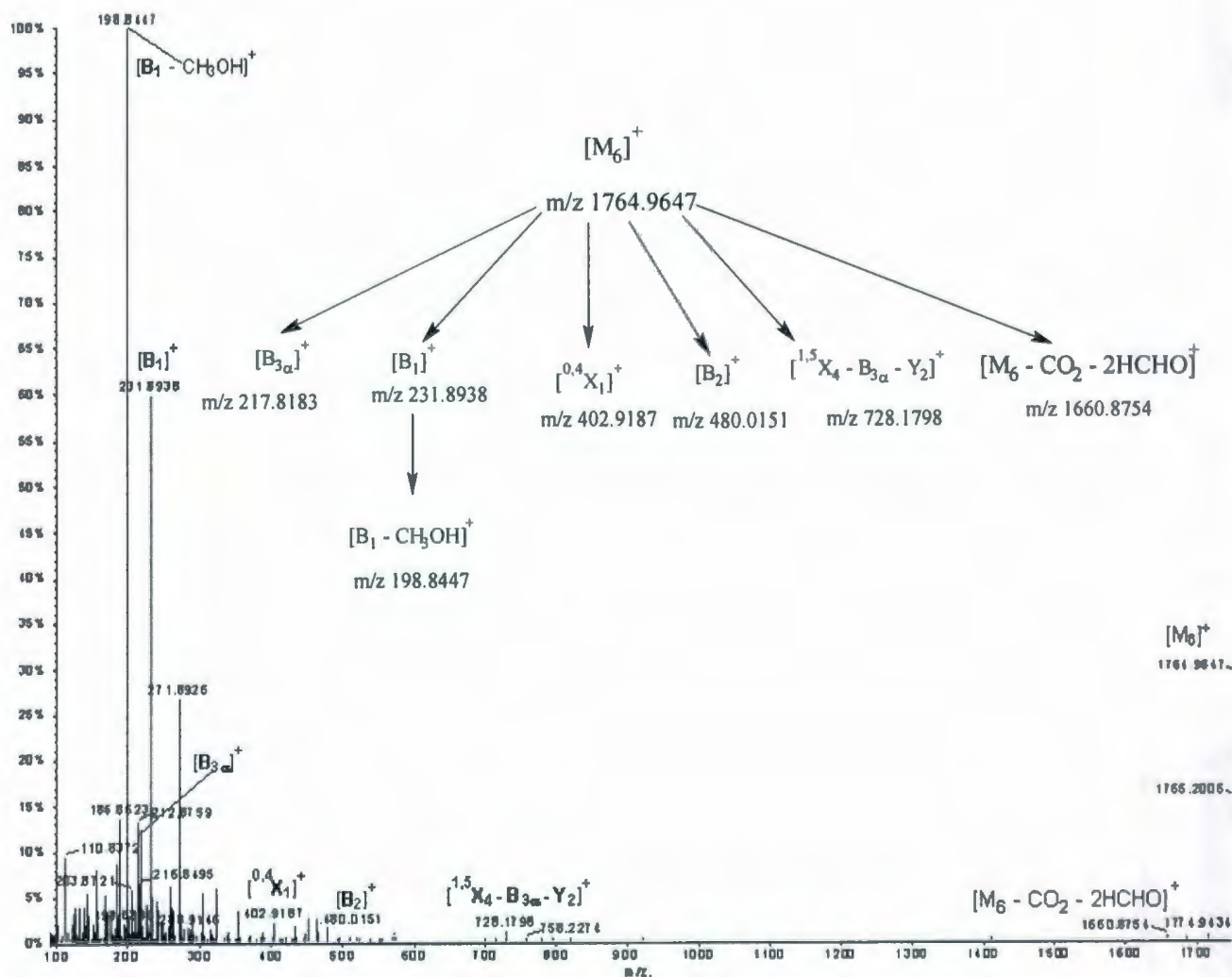


Figure 4.9: ESI-CID-MS/MS of the selected precursor ion at m/z 1764.8589 from the permethylated core oligosaccharide.

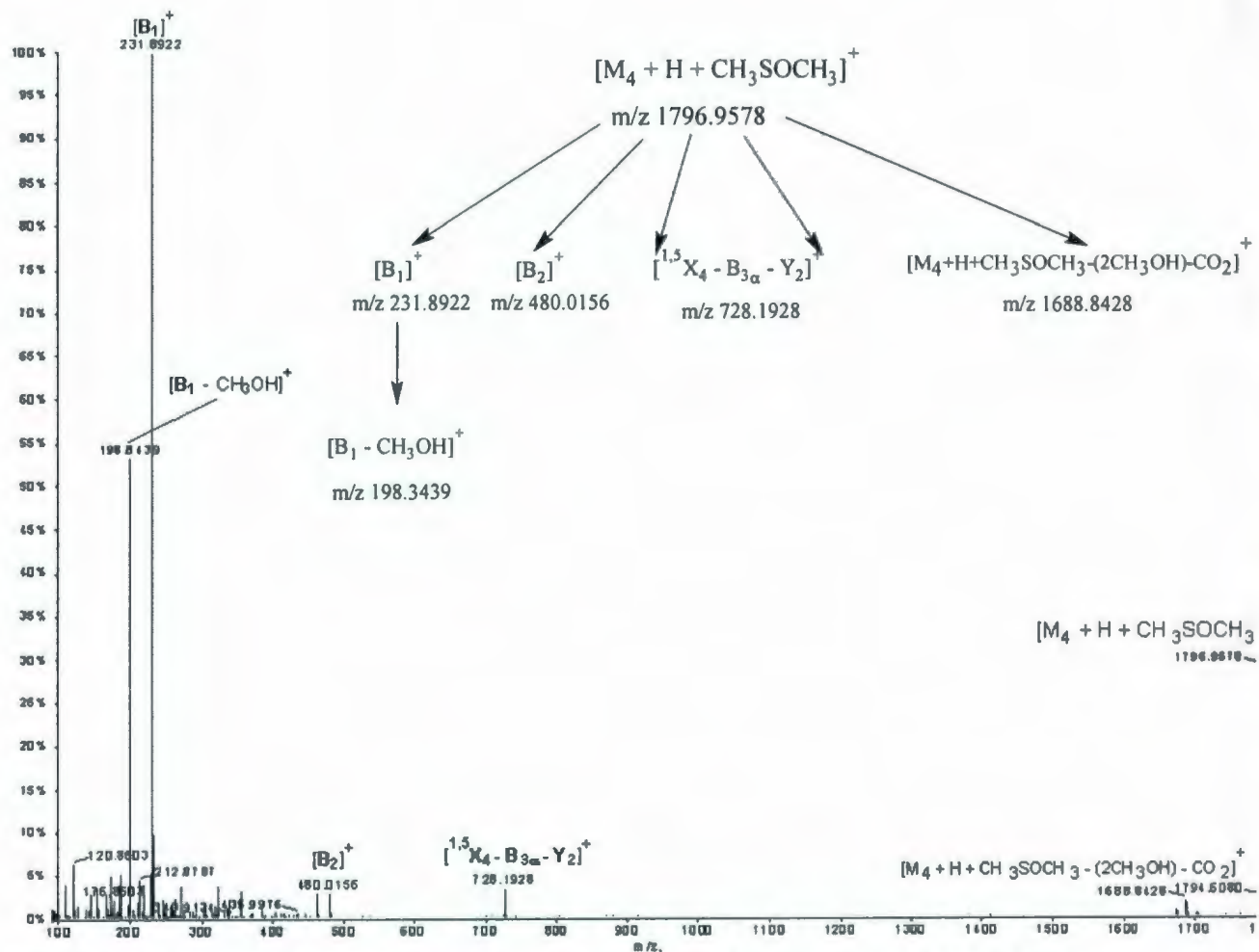


Figure 4.10: ESI-CID-MS/MS of the selected precursor ion at m/z 1796.9027 from the permethylated core oligosaccharide.

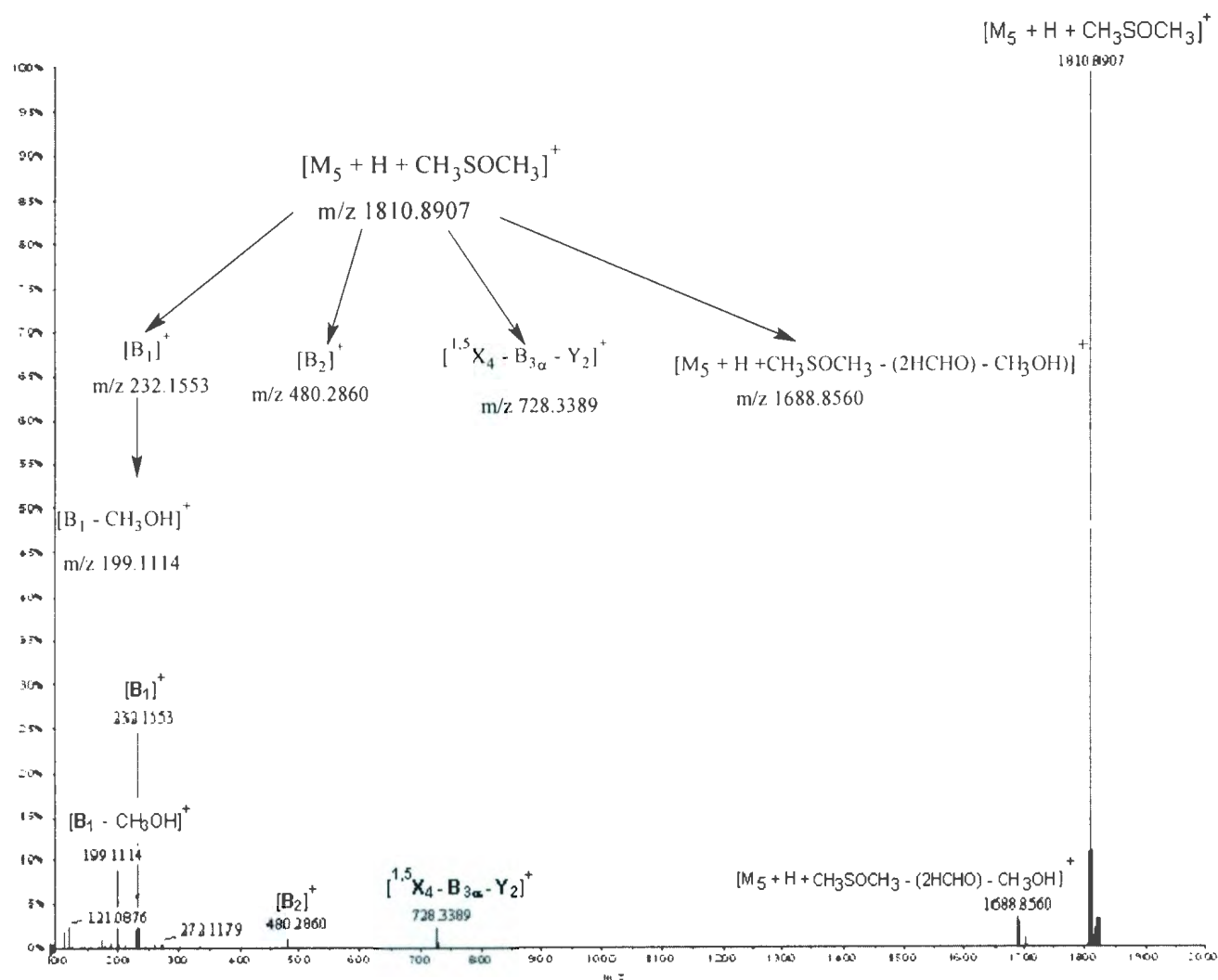


Figure 4.11: ESI-CID-MS/MS of the selected precursor ion at m/z 1810.9359 from the permethylated core oligosaccharide.

In summary, it can be stated that the MS analysis of the permethylated core oligosaccharide highlighted the presence of the two diastomeric forms consisting of the enol↔keto forms obtained from the 4,8- and 4,7- anhydro derivatives of the enolizable α -keto acids. It also revealed the presence of the core oligosaccharide containing the open olefinic Kdo chain with a double bond. Wang *et al.*, reported and confirmed that by using CE-ESI-MS analysis of similar core oligosaccharides, that the core oligosaccharide was a complex mixture, owing to mutarotation of the reducing end 3-deoxy-D-manno-oct-2-ulosonic acid (Kdo) residue and its existence in multiple forms, including 4,7- and 4,8-anhydro forms, which resulted from the partial elimination of the phosphate group of Kdo 4-phosphate present in the native LPS.¹¹⁹

Wang *et al.*, also used ¹H- and ¹³C- NMR spectra and 2D COSY, TOCSY, HSQC, HMBC to study the conformation of the dephosphorylated Kdo residue.¹¹⁹ This latter study confirmed irrevocably the absence of the furanoid form of Kdo in *A. salmonicida* core as one of the unique features of *A. salmonicida* LPS, and is consistent with the deep inner core LPS structure proposed by Banoub *et al.*, which also confirmed the phosphate substitution at the O-4 position of Kdo residue.^{13a, 13b}

4.5. Conclusion

The core oligosaccharide of *Aeromonas hydrophila* (chemotype II) SJ-48R lipopolysaccharide was studied using MALDI-MS, ESI-MS, and CID-MS/MS analyses. This investigation led to a better understanding of the structure of this unique type of natural bacterial core oligosaccharide belonging to the *Vibrionaceae* family.

These LPSs contain a series of isobaric diastereomers of the 4,8- and 4,7-anhydro derivative α -keto acids and one open-chain Kdo residue containing a double bond at C-3-C-4. During the Hakamori methylation of the core oligosaccharide, it was noted that beside the inclusion of the predicted number of methyl groups, corresponding to the complete methylation of all the hydroxyl and NH_2 groups of the oligosaccharide, that incorporation of extra C-Methyl groups on the 4,8- and 4,7-anhydro derivatives α -keto acids of the permethylated core oligosaccharide were observed at: $[\text{M}_4 + \text{H}]^+$ at m/z 1718.8338, and $[\text{M}_5 + \text{H}]^+$ at m/z 1732.8415. These two protonated permethylated species underwent a covalent addition reaction to the C-2-C-3 double bond with the dimsyl anion from DMSO solvent (**Scheme 4.4 (a)**). Furthermore, addition of the dimsyl anion on the C-3-C-4 double bond of the open olefinic Kdo residue via a Michael addition was observed (**Scheme 4.4 (b)**). It was also noted that the olefinic open Kdo chain of the core oligosaccharide **2A** may form a *cis*-1,2-*O*-DMSO complex which would prevent the methylation of the C-1 carboxylic group.

The ESI-CID-MS/MS study of the native homogeneous core oligosaccharides allowed the determination of the sequence of all the constituent glycones and also permitted the confirmation of the exact position of attachment of the various glycones.

It should be noted that the ESI-CID-MS/MS of the fully permethylated core oligosaccharide did not give a very clear picture for establishing the glycone sequences and its attachment positions. However, it allowed for the proof of the existence of the two isobaric forms of the Kdo residue of the core oligosaccharide containing the 4,8- and 4,7-anhydro derivative α -keto acids, in addition to an olefinic open Kdo residue. In addition, it has been shown for the first time that the core oligosaccharides containing the 5-*O*-substituted 4-*O*-phosphorylated Kdo residue form covalent adducts to the C-2-C-3 double bond of the 4,8-anhydro Kdo and to the C-3-C-4 double bond of the olefinic open chain Kdo residue, whose existence has been confirmed by ESI-MS and CID-MS/MS.

Finally, the results obtained in this study are significant for gas-phase fragmentation studies and provide a "unique" blueprint for understanding the gas-phase reactivities and cleavage occurring from this type of LPS core oligosaccharide containing a 4-*O*-phosphorylated and 5-*O*-substituted Kdo.

GENERAL CONCLUSION

The entire work presented in this study has been performed with the aid of tandem mass spectrometry.

The gas-phase fragmentations of a series of biotin reagents which are commercially available compounds were studied. The decomposition pathways of the protonated species were proposed, supported by deuterium labeling experiments. These results have produced a primary publication in *Rapid Communications in Mass Spectrometry*.¹¹³

The molecular structure of the homogenous mixture of the native core oligosaccharide of *Aeromonas hydrophila* (chemotype II) LPS was studied by ESI-MS and MALDI-MS. This core oligosaccharide was shown to contain isobaric diastereomers of the 4,8- and 4,7-anhydro- α -keto acid forms and one open-chain Kdo residue containing a double bond at C-3-C-4. The characteristic glycone sequence was confirmed by ESI-CID-MS/MS analysis of the native core oligosaccharide. The presence of the non-phosphorylated Kdo was demonstrated during the analysis of the homogeneous mixture of the permethylated core oligosaccharide. The collision-induced dissociation of the complete permethylated core has been reported.

The ESI-MS and CID-MS/MS analyses of the permethylated core oligosaccharides showed distinctive fragmentation patterns. The series of the full permethylated protonated molecules and the formation of two additional protonated molecules containing two different C-Me groups were rationalized. The presence of

covalent DMSO adducts, which were the result of an addition reaction of the dimethyl sulfide anion on the C-2-C-3 double bond of the 4,8-anhydro- α -keto acid form and on the C-3-C-4 double bond of the olefinic open-chain Kdo residue, were shown and reported in the literature for the first time.

REFERENCES

1. Kitson, F. G.; Larsen, B. S.; McEwen, C. N. *Gas chromatography and mass spectrometry*, A practical Guide; Academic Press: San Diego, 1996.
2. Barber, M.; Bordoli, R. S.; Sedgwick, R. D., Tyler, A. Fast Atom Bombardment of Solids as an Ion Source in Mass Spectrometry. *Nature*. 1981, 293, pp 270-275.
3. Morris, H. R.; Panico, M.; Barber, M.; Bordoli, R. S.; Sedgwick, R. D.; Tyler, A. Fast Atom Bombardment: A New Mass Spectrometric Method For Peptide Sequence Analysis. *Biochem. Biophys. Res. Commun.* 1981, 101, pp 623-631.
4. Shackleton, C.H.; Straub, K.M. Direct Analysis of Steroid Conjugates: The Use of Secondary in Mass Spectrometer. *Steroids*. 1982, 40, pp 35-51.
5. Tanaka, K.; Waki, Y.; Ido, Y.; Akita, S.; Yoshida, Y.; Yoshida, T. Protein and Polymer Analyses up to m/z 100000 by Laser Ionization Time-of-flight Mass Spectrometry. *Rapid. Commun. Mass. Spectrom.* 1988, 2, pp 151-153.
6. Karas, M. B.; Ingehod, A.; Nordhoff, E.; Stahl, B.; Strupat, K.; Hillenkamp, F. Principles and Applications of Matrix-assisted UV-laser Desorption/Ionization Mass Spectrometry. *Anal. Chim. Acta.* 1990, 241, pp 175-185.
7. Yamashita, M.; Fenn, J. B. Electrospray Ion Source. Another Variation on the Free-Jet Theme. *J. Phys. Chem.* 1984, 88, pp 4451-4459.

8. Fenn, J. B.; Mann, M.; Meng, C. K.; Wong, S. F.; Whitehouse, C. M. Electrospray Ionization for Mass Spectrometry of Large Biomolecules *Science*. **1989**, 246, pp 64-71.
9. Tanaka, K. The Origin of Macromolecule Ionization by Laser Irradiation (Nobel Lecture). *Angew. Chem. Int. Ed.* **2003**, 42, pp 3860-3870.
10. Louris, J. N.; Brodbelt-lusting, J. S.; Cooks, R. G.; Glish, G. L.; Van-Berkel, G. J.; McLuckey, S. A. Ion Isolation and Sequential Stages of Mass Spectrometry in a Quadrupole Ion Trap Mass Spectrometer. *Int. J. Mass. Spectrom. Ion. Processes*. **1990**, 96, pp 117-137.
11. Yost, R. A.; Enke, C. G. Selected Ion Fragmentation with a Tandem Quadrupole Mass Spectrometer. *J. Am. Chem. Soc.* **1978**, 100, pp 2274-2275.
12. Cohen, M. A.; Jahouh, F.; Sioud, S.; Rideout, M. R., Morgan, M. J.; Banoub, H. Quantification of Greenland Halibut Serum Vitellogenin: a trip from the deep sea to the mass spectrometer. *R. commun. Mass. Spectrom.* **2009**, 23, pp 1049-1060.
13. (a) Banoub, J. H.; El-Aneed, A.; Cohen, A. M.; Martin, P. Characterization of the O-4 Phosphorylated and O-5 Substituted Kdo Reducing End Group and Sequencing of the Core Oligosaccharide of *Aeromonas Salmonicida* ssp *Salmonicida* Lipopolysaccharide Using Tandem Mass Spectrometry. *Eur. J. Mass. Spectrum (Chichester, Eng)*. **2004a**, 10, pp 715-730.
(b) Banoub, J. H.; Cohen, A. M.; El-Aneed, A.; Martin, P.; LeQuart. V. Structural Reinvestigation of the Core Oligosaccharide of a Mutant form of *Aeromonas*

Salmonicida Lipopolysaccharide Containing an O-4 Phosphorylated and O-5 Substituted Kdo Reducing End Group Using Electrospray Quadrupole Time-of-flight Tandem Mass Spectrometry. *Eur. J. Mass. Spectrum (Chichester, Eng)*. **2004b**, 10, pp 541-554.

14. Sinz, A.; Kalkhof, S.; Ihling, C. Mapping Protein Interfaces by a Trifunctional Cross-Linker Combined with MALDI-TOF and ESI-FTICR Mass Spectrometry. *J. Am. Soc. Mass. Spectrom.* **2005**, 16, pp 1921-1931.
15. Harrison, G. A.; Mercer, S. R.; Reiner, J. E.; Young, A. B. A Hybrid BEQQ Mass Spectrometer for Studies in Gaseous Ion Chemistry. *Int. J. Mass. Spectrom. Ion. Processes.* **1986**, 74, pp 13-31.
16. Suckau, D.; Resemann, A.; Schuerenberg, M.; Hufnagel, P.; Franzen, J.; Holle, A. A Novel MALDI LIFT-TOF/TOF Mass Spectrometer for Proteomics. *Anal. Bioanal. Chem.* **2003**, 376, pp 952-965.
17. Mechref, Y.; Novotny, M. V.; Krishnan, C. Structural Characterization of Oligosaccharides Using Maldi-TOF/TOF Tandem Mass Spectrometry. *Anal Chem.* **2003**, 75, pp 4895-4903.
18. Banoub J. H.; Thibault, P.; Mansour, A.; Cohen, A.; Heeley, D. H.; Jackman, D. Characterisation of the Intact Rainbow Trout Vitellogenin Protein and Analysis of its Derived Tryptic and Cyanogen Bromide Peptides by Matrix-Assisted Laser Desorption/Ionisation Time-of-flight-mass Spectrometry and Electrospray Ionisation Quadrupole/Time-of-flight Mass Spectrometry. *Eur. J. Mass. Spectrom. (Chichester, Eng)*, **2003**, 9, pp 509-524.

19. Therisod, H.; Labas, V.; Caroff, M. Direct Microextraction and Analysis of Rough-Type Lipopolysaccharides by Combined Thin-Layer Chromatography and MALDI Mass Spectrometry. *Anal. Chem.* **2001**, *73*, pp 3804-3807.
20. Hurst G. B.; Lankford, T. K.; Kennel, S. J. Mass Spectrometric Detection of Affinity Purified Crosslinked Peptides. *J. Am. Soc. Mass. Spectrom.* **2004**, *6*, pp 832-839.
21. Gut, I. G. DNA Analysis by MALDI-TOF Mass Spectrometry. *Hum. Mutat.* **2004**, *23*, pp 437-441.
22. Harvey, D. J. Matrix-assisted laser desorption/ionization mass spectrometry of carbohydrates and glycoconjugates. *Int. J. Mass. Spectrom.* **2003**, *226*, pp 1-35.
23. Balazy, M. Eicosanomics: Targeted Lipidomics of Eicosanoids in Biological Systems. *Prostaglandins Other Lipid Mediat.* **2004**, *73*, pp 173-180.
24. Karas, M.; Baher, U.; Ingedoh, A.; Nordhoff, E.; Stahl, B.; Strupat, K.; Hillenkamp, F. Principles and Applications of Matrix-assisted UV-laser Desorption/Ionization Mass Spectrometry. *Anal. Chim. Acta.* **1990**, *241*, pp 175-185.
25. Beavis, R. C.; Chait, B. T. Cinnamic Acid Derivatives as Matrices for Ultraviolet Laser Desorption Mass Spectrometry of Proteins. *Rapid. Commun. Mass. Spectrom.* **1989**, *3*, pp 432-435.

26. Beavis, R. C.; Chait, B. T. α -Cyano-4-hydroxycinnamic Acid as a Matrix for Matrix-assisted Laser Desorption Mass Spectrometry. *Org. Mass. Spectrom.* **1992**, *27*, pp 156-158.
27. Beavis, R. C.; Chait, B. T. Velocity Distributions of Intact High Mass Polypeptide Molecule Ions Produced by Matrix Assisted Laser Desorption. *Chem. Phys. Lett.* **1991**, *181*, pp 479-484.
28. Knochenmuss, R.; Zenobi, R. MALDI Ionization: The Role of In-Plume Processes. *Chem. Rev.* **2003**, *103*, pp 441-452.
29. Busch, K. L. Desorption Ionization Mass Spectrometry. *J. Mass. Spectrom.* **1995**, *30*, pp 233-240.
30. Laiko, V. V.; Baldwin, M. A.; Burlingame, A. L. Atmospheric Pressure Matrix-Assisted Laser Desorption/Ionization Mass Spectrometry. *Anal. Chem.* **2000**, *72*, pp 652-657.
31. Laiko, V. V.; Taranenko, N. I.; Berkout, V. D.; Musselman, B. D.; Doroshenko, V. M. Atmospheric Pressure Laser Desorption/Ionization on Porous Silicon. *Rapid. Commun. Mass. Spectrom.* **2002**, *16*, pp 1737-1742.
32. Peng, W. P.; Yang, Y. C.; Kang, M. W.; Tzeng, Y. K.; Nie, Z.; Chang, H. C.; Chang, W.; Chen, C. H. Laser-Induced Acoustic Desorption Mass Spectrometry of Single Bioparticles. *Angew. Chem. Int. Ed.* **2006**, *45*, pp 1423-1426.
33. Dole, M.; Mack, L. L.; Hines R. L.; Mobley R. C.; Ferguson L. D.; Alice M. B. Molecular Beams of Macroions. *J. Chem. Phys.* **1968**, *49*, pp 2240-2249.

34. Meng, C. K.; Mann, M.; Fenn, J. B. Of Protons or Protein. "A Beam's a Beam for a' that." (O.S. Burns). *Z. Phys. D. Atoms, Molecules and Clusters*. **1988**, 10, pp 361-368.
35. Kim H. Y.; Salem N. Jr. Application of Thermospray High-Performance Liquid Chromatography/mass Spectrometry for the Determination of Phospholipids and Related Compounds. *Anal. Chem.* **1987**, 59, pp 722-726.
36. Kebarle P.; Tang L. From Ions in Solution to Ions in the Gas phase - the Mechanism of Electrospray Mass Spectrometry. *Anal. Chem.* **1993**, 65, pp 972A-986A.
37. Blades, T. A.; Ikonomou, G. M.; Kebarle, P. Mechanism of Electrospray Mass Spectrometry. Electrospray as an Electrolysis Cell. *Anal. Chem.* **1991**, 63, pp 2109-2114.
38. Dawson, P. H. *Quadrupole Mass Spectrometry*; Elsevier, NewYork. **1976**, Chaps. 2, 3.
39. El-Aneed, Anas. Mass Spectrometric Analysis and Fingerprint Identification of Natural Lipopolysaccharide Vaccine Candidates and Synthetic Liposomal Cholesteryl Neoglycolipids; Ph. D Thesis, Memorial University of Newfoundland, NL **2006**; pp 15-16.
40. Stephens, W. E. Time-of-flight Mass Analysis. *Phys. Re.* **1946**, 69, 691.
41. Brown, R.S.; Lennon, J. Mass Resolution Improvement by Incorporation of Pulsed ion Extraction in a Matrix-assisted Laser Desorption/Ionization Linear Time-of-flight Mass Spectrometer. *Anal. Chem.* **1995**, 67, pp 1998-2003.

42. Mamyrin, B. A.; Shmikk, D. V. The Linear Mass Reflectron. *Sov. Phys. JETP*. **1979**, 49, pp 762-764.
43. Verentchikov, A. N.; Ens, W.; Standing, K. G. Reflecting Time-of-flight Mass Spectrometer With an Electrospray Ion Source and Orthogonal Extraction. *Anal. Chem.* **1994**, 66, pp 126-133.
44. Jennings, K. R. Collision-Induced Decompositions of Aromatic Molecular Ions. *Int. J. Mass. Spectrom. Ion. Phys.* **1968**, 1, pp 227-235.
45. McLafferty, F. W.; Bente, P. F.; Kornfeld, R.; Tsai, S.; Howe, I. Metastable Ion Characteristics. XXII. Collisional Activation Spectra of Organic Ions. *J. Am. Chem. Soc.* **1973**, 95, pp 2120-2129.
46. (a) Domon, B.; Costello, C. E. Structure Elucidation of Glycosphingolipids and Gangliosides Using High-Performance Tandem Mass Spectrometry. *Biochemistry*. **1988a**, 27, pp 1534-1543.
- (b) Domon, B.; Costello, C. E. A Systematic Nomenclature for Carbohydrate Fragmentations in FAB-MS/MS Spectra of Glycoconjugates. *Glycoconjugate. J.* **1988b**, 5, pp 397-409.
47. Galanos, C.; Luderitz, O. Chemistry of Endotoxins. In *Handbook of Endotoxins* ; Rietschel, E. T., Ed.; Elsevier: Amsterdam, **1984**; Vol. 1, p 46.
48. Rietschel, E. T.; Wollenweber, H. W.; Brade, H.; Zahring, U.; Linder, B.; Seydel, U.; Bradaczek, H.; Barnickel, G.; Labischinski, H.; Giesbrecht, P. Chemistry of

- Endotoxins. In *Handbook of Endotoxins*; Rietschel, E. T., Ed.; Elsevier: Amsterdam, **1984**; Vol. 1, p 187.
49. Holst, O.; Brade, H. Molecular Biochemistry and Cellular Biology. In *Bacterial Endotoxic Lipopolysaccharides*; Morrison, D. C.; Ryan, J. L., Eds.; CRC Press: Boca Raton, FL, **1992**; Vol. 1, p 135.
50. Raetz, C. R.; Whitfield, C. Lipopolysaccharide Endotoxins. *Annu Rev Biochem.* **2002**, 71, pp 635-700.
51. Haeffner-Cavaillon, N.; Caroff, M.; Cavaillon, J. M. Interleukin-1 Induction by Lipopolysaccharides: Structural Requirements of the 3-deoxy-D-manno-2-octulosonic acid (KDO). *Mol. Immunol.* **1989**, 26, pp 485-494.
52. Kubler-Kielb, J.; Vinogradov, E.; Ben-Menachem, G.; Pozsgay, V.; Robbins, J. B.; Schneerson, R. Saccharide/Protein Conjugate Vaccines for Bordetella Species: Preparation of Saccharide, Development of New Conjugation Procedures, and Physico-Chemical and Immunological Characterization of the Conjugates. *Vaccin.* **2008**, 26, pp 3587-3593.
53. Pozsgay, V. Recent Developments in Synthetic Oligosaccharide-Based Bacterial Vaccines. *Current Topics in Medicinal Chemistry -HILVERSUM-*, **2008**, 8, No. 2, pp 126-140.
54. Grandjean, C.; Boutonnier, A.; Dassy, B.; Fournier, J. M.; Mulard, L. A. Investigation Towards Bivalent Chemically Defined Glycoconjugate Immunogens Prepared from Acid-detoxified Lipopolysaccharide of Vibrio Cholerae O1, Serotype Inaba. *Glycoconj. J.* **2009**, 26, pp 41-55.

55. Caroff, M.; Karibian, D. Structure of bacterial lipopolysaccharides. *Carbohydr. Res.* **2003**, 338, pp 2431-2447.
56. Avery, O. T.; Goebel, W. F. Chemo-Immunological Studies on Conjugated Carbohydrate-Proteins. *J. Exp. Med.* **1929**, 50, pp 533-550.
57. Stowell, C. P.; Lee, Y. C. Neoglycoproteins: The Preparation and Application of Synthetic Glycoproteins. *Adv. Carbohydr. Chem. Biochem.* **1980**, 37, pp 225-281.
58. Lee, C. J. Bacterial Capsular Polysaccharides-Biochemistry, Immunity and Vaccine. *Mol. Immunol.* **1987**, 24, pp 1005-1019.
59. Aplin, J. D.; Wriston, J. C. Jr Preparation, Properties, and Applications of Carbohydrate Conjugates of Proteins and Lipids. *CRC Crit. Rev. Biochem.* **1981**, 10, pp 259-306.
60. Banoub, J. H.; Shaw, D. H.; Nakhla, N. A.; Hodder, H. J. Synthesis of Glycoconjugates Derived From Various Lipopolysaccharides of the Vibrionaceae Family. *Eur. J. Biochem.* **1989**, 179, pp 651-657.
61. Chernyak, A.; Kondo, S.; Wade, T. K.; Meeks, M. D.; Alzari, P. M.; Fournier, J. M.; Taylor, R.; Kovac, P. K.; Wade, W. F. Induction of Protective Immunity by Synthetic Vibrio Cholerae Hexasaccharide Derived From V. Cholerae O1 Ogawa Lipopolysaccharide Bound to a Protein Carrier. *J. Infect. Dis.* **2002**, 185, pp 950-962.
62. Pozsgay, V. Oligosaccharide-Protein Conjugates as Vaccine Candidates Against Bacteria. *Adv. Carbohydr. Chem. Biochem.* **2000**, 56, pp 153-199.
63. Green, M. N. Avidin, [Review]. *Adv. Protein. Chem.* **1975**, 29, pp 85-133.

64. Bayer, E. A.; Wilchek, M. Application of Avidin-Biotin Technology to Affinity-Based Separations. *J. Chromatogr.* **1990**, 510, pp 3-11.
65. Gyorgy, P.; Rose, C. S. ; Hofmann, K.; Melville, D. B.; du-Vigneaud, V. *A further Note on the Identity of Vitamin H with Biotin. Science.* **1940**, 92, p 609.
66. Hahner, S.; Olejnik, J.; Lüdemann, H. C.; Krzymańska-Olejnik, E.; Hillenkamp.; Rothschild K. J. Matrix-Assisted Laser Desorption/Ionization Mass Spectrometry of DNA Using Photocleavable Biotin. *Biomol. Engin.* **1999**, 16, pp 127-133.
67. Limbach, P. A.; McCloskey, J. A.; Crain, P. F. The Modified Nucleosides of RNA. *Nucl. Acids. Symp. Ser.* **1994**, 31, pp 127-128.
68. Edwards, J. R.; Itagaki, Y.; Ju, J. DNA Sequencing Using Biotinylated Dideoxynucleotides and Mass Spectrometry. *Nucl. Acids. Res.* **2001**, 29, pp E104-4.
69. Fu, D. J.; Tang, K.; Braun, A.; Reuter, D.; Darnhofer-Demar, B.; Little, D. P.; O'Donnell, M. J.; Cantor, C. R.; Koster, H. Sequencing Exons 5 to 8 of the p53 Gene by MALDI-TOF Mass Spectrometry. *Nature Biotechnology.* **1998**, 16, pp 381-384.
70. Jurinke, C.; van den Boom, D.; Collazo, V.; Lüchow, A.; Jacob, A.; Köster, H. Recovery of Nucleic Acids from Immobilized Biotin-Streptavidin Complexes Using Ammonium Hydroxide and Applications in MALDI-TOF Mass Spectrometry. *Anal. Chem.* **1997**, 69, pp 904-910.
71. Sobin, k.; Ruparel, D. U.; Gilliam, G.; Ju, J. Digital Genotyping Using Molecular Affinity and Mass Spectrometry. *Nat. Rev. Genet.* **2003**, 4, pp 1001-1008.

72. Hawkins, T. L.; O'Connor-Morin, T.; Roy, A.; Santillan, C. DNA Purification and Isolation Using a Solid-Phase. *Nucl. Acids. Res.* **1994**, *22*, pp 4543-4544.
73. Bai, X.; Kim, S. L.; Turro, N. J.; Ju, J. Design and Synthesis of a Photocleavable Biotinylated Nucleotide for DNA Analysis by Mass Spectrometry *Nucl. Acids. Res.* **2004**, *32*, pp 535-541.
74. Ju, J. DNA Sequencing with Solid-Phase-Capturable Dideoxynucleotides and Energy Transfer Primers. *Anal. Biochem.* *309*, **2002**, pp 35-39.
75. Joly, N.; Vaillant, C.; Cohen, A. M.; Martin, P.; Essassi, E. M.; Massoui, M.; Banoub J. Structural Determination of the Novel Fragmentation Routes of Zwitterionic Morphine Opiate Antagonists Naloxonazine and Naloxone Hydrochlorides Using Electrospray Ionization Tandem Mass Spectrometry. *Rapid. Commun. Mass. Spectrom.* **2007**, *21*, pp 1062-1074.
76. Bateman, K. P.; Banoub, J. H.; Thibault, P. Probing the Microheterogeneity of O-Specific Chains From *Yersinia Ruckeri* Using Capillary Zone Electrophoresis/Electrospray Mass Spectrometry. *Electrophoresis.* **1996**, *32*, pp 1818-1828.
77. Westphal, O.; Jann, K. Bacterial lipopolysaccharides. *Methods. Carbohydr. Chem.* **1965**, *5*, pp 83-91.
78. Galanos, C.; Lüderitz, O. Electrodialysis of Lipopolysaccharides and Their Conversion to Uniform Salt Forms. *Eur. J. Biochem.* **1975**, *54*, pp 603-610.

79. Hakomori, S. J. A Rapid Permethylation Of Glycolipid, And Polysaccharide Catalyzed By Methylsulfinyl Carbanion In Dimethyl Sulfoxide. *Biochem (Tokyo)*. **1964**, 55, pp 205-208.
80. Ciucanu, I.; Kerek, F. A simple and Rapid Method for the Permethylation of Carbohydrates. *Carbohydr. Res.* **1984**, 131, pp 209-217.
81. Mouton, C. A.; Pang, D.; Natraj, C. V.; Shater, J. A. A reagent for Covalently Attaching Biotin to Proteins Via a Cleavable Connector Arm *Arch. Biochem. Biophys.* **1982**, 218, pp 101-108.
82. Shimkus, M.; Levy, T.; Herman, T. A Chemically Cleavable Biotinylated Nucleotide: Usefulness in the Recovery of Protein-DNA Complexes from Avidin Affinity Columns. *Proc. Natl. Acad. Sci. USA.* **1985**, 82, pp 2593-2597.
83. Gretch, D. R.; Suter, M.; Stinski, M. F. The Use of Biotinylated Monoclonal Antibodies and Streptavidin Affinity Chromatography to Isolate Herpesvirus Hydrophobic Proteins or Glycoproteins. *Anal. Biochem.* **1987**, 163, pp 270-277.
84. Ghebrehiwet, B.; Bossone, S.; Erdei, K. B. M. Reid. Reversible Biotinylation of C1q with a Cleavable Biotinyl Derivative: Application in C1q Receptor (C1qR) Purification. *J. Immunol. Methods.* **1988**, 110, pp 251-260.
85. Wilchek, M.; Ben-Hur, H.; Bayer, E. A. p-Diazobenzoyl Biocytin: A New Biotinylating Reagent for the Labeling of Tyrosines and Histidines in Proteins. *Biochem. Biophys. Res. Comm.* **1986**, 138, pp 872-879.

86. Muddiman, D. C.; Cheng, C.; Udseth, H. R.; Smith, R. D. Charge-State Reduction with Improved Signal Intensity of Oligonucleotides in Electrospray Ionization Mass Spectrometry. *J. Am. Soc. Mass. Spectrom.* **1996**, *7*, pp 697-706.
87. Cimono, G. D.; Gamper, H. B.; Isaaca, S. T.; Hearst, J. E. Psoralens as Photoactive Probes of Nucleic Acid Structure and Function: Organic Chemistry, Photochemistry, and Biochemistry. *Annu. Rev. Biochem.* **1985**, *54*, pp 1151-1193.
88. Wassarman, D. A. Psoralen Crosslinking of Small RNAs in Vitro. *Mol. Biol. Rep.* **1993**, *17*, pp 143-151.
89. Wilchek, M.; Bayer, E. A. Biotin-Containing Reagents. *Methods. Enzymol.* **1990**, *184*, pp123-138
90. Rothenberg, J. M.; Wilchek, M. p-Diazobenzoyl-Biotin: A New Biotinylating Reagent for DNA. *Nucl. Acids. Res.* **1988**, *16*, p 7197.
91. Lacey, E.; Grant, W. N. Photobiotin as a Sensitive Probe for Protein Labeling. *Anal. Biochem.* **1987**, *163*, pp 151-158.
92. Smith, J. S.; Keller, J. R.; Lohrey, N. C.; McCauslin, C. S.; Ortiz, M.; Cowan, K.; Spence, S. E. Redirected Infection of Directly Biotinylated Recombinant Adenovirus Vectors Through Cell Surface Receptors and Antigens. *Proc. Natl. Acad. Sci.* **1999**, *96*, pp 8855-8860.
93. Wilbur, S. D.; Pathare, P.; HamLin, D. K.; Weerawarna, A. Biotin Reagents for Antibody Pretargeting. 2. Synthesis and in Vitro Evaluation of Biotin Dimers and Trimers for Cross-Linking of Streptavidin. *Bioconj. Chem.* **1997**, *8*, pp 819-832.

94. Pandurangi, R. S.; Karra, S. R. ; Katti, K. V.; Kuntz, R. R.; Volkert, W. A. Chemistry of Bifunctional Photoprobes. 1. Perfluoroaryl Azido Functionalized Phosphorus Hydrazides as Novel Photoreactive Heterobifunctional Chelating Agents: High Efficiency Nitrene Insertion on Model Solvents and Proteins. *J. Org. Chem.* **1997**, *62*, pp 2798-2807.
95. Anderson, G. W.; Zimmerman, J. E.; Callahan, F. M. The Use of Esters of N-Hydroxysuccinimide in Peptide Synthesis, *J. Am. Chem. Soc.* **1964**, *86*, pp 1839-1842
96. Wong, S. S. *Chemistry of Protein Conjugation and Crosslinking*, CRC Press Inc.: Boca Raton, FL, **1991**; p 2526.
97. Banoub, J. H.; Boullanger, P.; Lafont, D.; Cohen, A. ; El Aneed, A.; Rowlands, E. In Situ Formation of C-glycosides During Electrospray Ionization Tandem Mass Spectrometry of a Series of Synthetic Amphiphilic Cholesteryl Polyethoxy Neoglycolipids Containing N-acetyl-D-glucosamine. *J. Am. Soc. Mass. Spectrom.* **2005**, *16*, pp 565-570.
98. Joly, N.; El-Aneed, A.; Martin, P.; Cecchelli, R.; Banoub, J. Structural Determination of the Novel Fragmentation Routes of Morphine Opiate Receptor Antagonists Using Electrospray Ionization Quadrupole Time-of-flight Tandem Mass Spectrometry. *Rapid. Commun. Mass. Spectrom.* **2005**, *19*, pp 3119-3130.
99. Joly, N.; Jarmouni, C.; Massoui, M.; Essassi, E. M.; Martin, P.; Banoub, J. Electrospray Tandem Mass Spectrometric Analysis of Novel Synthetic

- Quinoxalinone Derivatives. *Rapid. Commun. Mass. Spectrom.* **2008**, 22, pp 819-833.
100. Rida, M.; El-Meslouhi, H.; Es-Safi, N. E.; Essassi, E. M.; Banoub, J. Gas-Phase Fragmentation Study of Novel Synthetic 1,5-Benzodiazepine Derivatives Using Electrospray Ionization Tandem Mass Spectrometry. *Rapid. Commun. Mass. Spectrom.* **2008**, 22, pp 2253-2268.
101. Madigan, M.; Martinko, J. *Brock Biology of Microorganism (11 th ed)*. Prentice Hall, **2005**.
102. Jackson, G. D.; Redmond, J. Immunochemical Studies of the O-antigen of *Vibrio cholerae*: The Constitution of a Lipopolysaccharide from K Cholerae 569B (Inaba). *FEBS Lett.* **1971**, 13, pp 117-120.
103. Jann, B.; Jann, K.; Beyaert, G. O. 2-Amino-2,6-Dideoxy-D-Glucose (D-quinovosamine): A Constituent of the Lipopolysaccharides of *Vibrio Cholerae*. *Eur. J. Biochem.* **1973**, 37, pp 531-534.
104. Hisatsune, K.; Kondo, S.; Iguchi, T.; Machida, M.; Asou, Inaguma S.M.; Yamamoto, F. Sugar Composition of Lipopolysaccharides of Family Vibrionaceae. Absence of 2-Keto-3-Deoxyoctonate (KDO) Except in *Vibrio Parahaemolyticus* O6. *Microbiol. Immunol.* **1982**, 26, pp 649-664.
105. Weissbach, A.; Hurwitz, J. The Formation of 2-Keto-3-deoxyheptonic Acid in Extracts of *Escherichia coli* B : I. Identification. *J. Biol. Chem.* **1959**, 234, pp 705-709.

106. (a) Banoub, J. H.; Shaw, D. H.; Michon, F. Hydrolytic Release, and Identification by G.I.C.-M.S. of 3-Deoxy-D-Manno-2-Octulosonic Acid in the Lipopolysaccharides Isolated From Bacteria of the Vibrionaceae. *Carbohydr. Res.* **1983a**, 123, pp 117-122.
- (b) Banoub, J. H.; Choy, Y.; Michon, F.; Shaw, D. H. Structural Investigations on the Core Oligosaccharide of *Aeromonas Hydrophila* (Chemotype II) Lipopolysaccharide. *Carbohydr. Res.* **1983b**, 114, pp 267-276.
107. Brade, H. Occurrence of 2-Keto-Deoxyoctonic Acid 5-Phosphate in Lipopolysaccharides of *Vibrio Cholerae* Ogawa and Inaba. *J. Bacteriol.* **1985**, 161, pp 795-798.
108. Caroff, M.; Lebbar, S.; Szabo, L. Detection of 3-Deoxy-2-Octulosonic Acid in Thiobarbiturate-Negative Endotoxins. *Carbohydr. Res.* **1987**, 161, pp c4-7.
109. Auzanneau, F.; Charon, D.; Szabó, L. Phosphorylated Sugars. Part. 27. Synthesis and Reaction in Acidic Medium of 5-O-Substituted Methyl 3-Deoxy- α -D-Manno-2-Octulopyranosidonic Acid 4-Phosphate. *J. Chem. Soc. Perkin. Trans.* **1991**, 1, pp 509-517.
110. Davis, W. A.; Kane, J. G.; Garagusi, F. Human *Aeromonas* Infections: A Review of the Literature and a Case report of Endocarditis. *Medecine*, **1978**, 3, pp 267-277.
111. Phalipon, A.; Tanguy, M.; Grandjean, C.; Guerreiro, C.; Belot, F.; Cohen, D.; Sansonetti P. J.; Mulard, L. A. A Synthetic Carbohydrate-Protein Conjugate

- Vaccine Candidate against *Shigella flexneri* 2a Infection' *J. Immunol.* **2009**, 182, pp 2241-2247.
112. Robbinsa, J. B.; Schneersona, R. Synthesis, Hypothesis for Vaccine Development: Immunological Characterization of the Conjugates. *Vaccine*, **2008**, 26, pp 3587-3593.
113. Sioud, S.; Genestie, B.; Jahouh, F.; Martin, P.; Banoub, J. Gas-Phase Fragmentation Study of Biotin Reagents Using Electrospray Ionization Tandem Mass Spectrometry on a Quadrupole Orthogonal Time-of-flight Hybrid Instrument. *Rapid Commun. Mass Spectrom.* **2009**, 23, pp 1941-1956.
114. Nakhla, A. N.; Szalai, A. J.; Banoub, J. H.; Keough, K. M. W. Uptake and Biodistribution of Free and Liposomally Incorporated Lipopolysaccharide of *Aeromonas salmonicida* Administered Via Different Routes to Rainbow Trout (*Oncorhynchus Mykiss*). *J. Liposome. Resear.* **1994**, 4, pp 1029-1041.
115. Dell, A.; Azadi, P.; Tiller, P.; Thomas-Oates, J.; Jennings, H. J.; Beurret, M.; Michon, F. Analysis of Oligosaccharide Epitopes of Meningococcal Lipopolysaccharides by Fast-Atom-Bombardment Mass Spectrometry. *Carbohydr. Res.* **1990**, 200, pp 59-76.
116. Bergman, E. D.; Ginsburg, D.; Pappo, R. The Michael reaction. *Org. React*, 10, **1959**, pp 179-556.
117. Cregge, R. J.; Herrmann, J. L.; Schlessinger, R. H. A versatile and reactive Michael receptor for the synthesis of 1,4-dicarbonyl compound. *Tetrahedron Lett*, 14, **1973**, pp 2603-2606.

118. Wang, Z.; Li, J.; Vinogradov, E.; Altman, E. Structural Studies of the Core Region of *Aeromonas Salmonicida* Subsp. *Salmonicida* Lipopolysaccharide. *Carbohydr. Res.* **2006**, 341, pp 109-117.

APPENDIX A

**TABLES OF PRODUCT IONS OBSERVED DURING CID-MS/MS AND *QUASI-*
MS³ ANALYSES OF THE FIVE BIOTIN REAGENTS**

Table A.1: Characteristic product ions observed in the CID-MS/MS of the $[M+H]^+$ ion at m/z 689.2859 and the *quasi*-MS³ analysis of the $[M+H\text{-photoreactive psoralen group}]^+$ ion at m/z 487.2597 from psoralen- PEO-Biotin 1.

Psoralen-PEO-Biotin 1 (Mr. 688.2778 Da)					
CID-MS/MS of the $[M+H]^+$ ion at m/z 689.2854					
Fragment ions	Characteristic ions	Calculated m/z	Observed m/z	Relative error ppm	
$[M+H]^+$	<i>1a</i> $[C_{33}H_{45}N_4O_{10}S]^+$	689.2854	689.2859	0	
$[M'+D]^+$	<i>1a'</i> $[C_{33}H_{39}D_5N_4O_{10}S]^+$	694.3248	694.3250	0	
$[M+H\text{-photoreactive psoralen group}]^+$	<i>1b</i> $[C_{22}H_{39}N_4O_6S]^+$	487.2590	487.2507	17	
$[M'+D\text{-photoreactive psoralen group}]^+$	<i>1b'</i> $[C_{22}H_{35}D_4N_4O_6S]^+$	491.2903	491.2892	18	
$[(\text{psoralen group})C_{10}H_{20}NO_4 + H]^+$	<i>1c</i> $[C_{21}H_{26}NO_8]^+$	420.1914	420.1844	17	
$[(\text{psoralen group})C_{10}H_{19}DNO_4 + D]^+$	<i>1c'</i> $[C_{21}H_{23}D_3NO_8]^+$	423.1893	423.1951	14	
$[(\text{psoralen group})C_6H_{11}NO_2 + H]^+$	<i>1d</i> $[C_{17}H_{16}NO_5]^+$	314.1028	314.1022	2	
$[(\text{psoralen group})C_6H_{11}NO_2 + D]^+$	<i>1d'</i> $[C_{17}H_{15}DNO_5]^+$	315.1107	315.1136	18	
$[(\text{biotinyl group})C_2H_4N + H]^+$	<i>1e</i> $[C_{12}H_{20}N_3O_2S]^+$	270.1276	270.1408	18	
$[(D_2\text{-biotinyl group})C_2H_4N + D]^+$	<i>1e'</i> $[C_{12}H_{17}D_3N_3O_2S]^+$	273.1511	273.1491	7	
<i>Quasi</i> -MS ³ of the $[M+H\text{-photoreactive psoralen group}]^+$ ion at m/z 487.2507					
$[M+H\text{-photoreactive psoralen group}]^+$	<i>1b</i> $[C_{22}H_{39}N_4O_6S]^+$	487.2590	487.2587	1	
$[M'+D\text{-photoreactive psoralen group}]^+$	<i>1b'</i> $[C_{22}H_{35}D_4N_4O_6S]^+$	491.2903	491.2817	18	
$[(\text{biotinyl group})C_2H_4N + H]^+$	<i>1e</i> $[C_{12}H_{20}N_3O_2S]^+$	270.1276	270.1291	6	
$[(D_2\text{-biotinyl group})C_2H_4N + D]^+$	<i>1e'</i> $[C_{12}H_{17}D_3N_3O_2S]^+$	273.1511	273.1491	7	

[spacer : C ₁₂ H ₂₅ N ₂ O ₄] ⁺	<i>If</i>	[C ₁₂ H ₂₅ N ₂ O ₄] ⁺	261.1808	261.1818	4
[spacer : C ₁₂ H ₂₃ D ₃ N ₂ O ₄] ⁺	<i>If'</i>	[C ₁₂ H ₂₂ D ₃ N ₂ O ₄] ⁺	264.2049	264.2149	38
[biotinyl group] ⁺	<i>Ig</i>	[C ₁₀ H ₁₅ N ₂ O ₂ S] ⁺	227.0854	227.0859	2
[D ₂ -biotinyl group] ⁺	<i>Ig'</i>	[C ₁₀ H ₁₃ D ₂ N ₂ O ₂ S] ⁺	229.1011	229.1037	11
[spacer : C ₁₀ H ₂₀ NO ₄] ⁺	<i>Ih</i>	[C ₁₀ H ₂₀ NO ₄] ⁺	218.1386	218.1403	8
[spacer : C ₁₀ H ₁₈ D ₂ NO ₄] ⁺	<i>Ih'</i>	[C ₁₀ H ₁₈ D ₂ NO ₄] ⁺	220.1549	220.1599	23
[spacer : C ₈ H ₁₄ NO ₂] ⁺	<i>Ii</i>	[C ₈ H ₁₄ NO ₂] ⁺	156.1091	156.1082	6
[spacer : C ₈ H ₁₃ DNO ₂] ⁺	<i>Ii'</i>	[C ₈ H ₁₃ DNO ₂] ⁺	157.1183	157.1218	23
[spacer : C ₆ H ₁₀ NO] ⁺	<i>Ij</i>	[C ₆ H ₁₀ NO] ⁺	112.0762	112.0760	2
[spacer : C ₆ H ₉ DNO] ⁺	<i>Ij'</i>	[C ₆ H ₉ DNO] ⁺	113.0841	113.0880	34

Table A.2: Characteristic product ions observed in the CID-MS/MS of the $[M+H]^+$ ion at m/z 492.2278 from *p*-aminobenzoyl biocytin 2.

<i>p</i> -Aminobenzoyl-Biocytin 2 (Mr. 491.2202 Da)					
CID-MS/MS of the $[M+H]^+$ ion at m/z 492.2277					
Fragment ions		Characteristic ions	Calculated m/z	Observed m/z	Relative error ppm
$[M+H]^+$	<i>2a</i>	$[C_{23}H_{34}N_5O_5S]^+$	492.2281	492.2278	1
$[M'+D]^+$	<i>2a'</i>	$[C_{23}H_{26}D_8N_5O_5S]^+$	500.2907	500.2951	9
$[M+H-H_2O]^+$	<i>2b</i>	$[C_{23}H_{32}N_5O_4S]^+$	474.2175	474.2172	1
$[M'+D-D_2O]^+$	<i>2b'</i>	$[C_{23}H_{26}D_6N_5O_4S]^+$	480.2645	480.2559	18
[(biotinyl group) $C_5H_9N]^+$	<i>2c</i>	$[C_{15}H_{24}N_3O_2S]^+$	310.1589	310.1598	3
[(D ₂ -biotinyl group) $C_5H_9N]^+$	<i>2c'</i>	$[C_{15}H_{22}D_2N_3O_2S]^+$	312.1746	312.1686	19
[biotinyl group] $^+$	<i>2d</i>	$[C_{10}H_{15}N_2O_2S]^+$	227.0854	227.086	3
[D ₂ -biotinyl group] $^+$	<i>2d'</i>	$[C_{10}H_{13}D_2N_2O_2S]^+$	229.1011	229.1001	4
[<i>p</i> -aminobenzoyl] $^+$	<i>2e</i>	$[C_7H_6NO]^+$	120.0449	120.0447	2
[D ₂ - <i>p</i> -aminobenzoyl] $^+$	<i>2e'</i>	$[C_7H_4D_2NO]^+$	122.0606	122.0619	11
[2,3,4,5-tetrahydro-pyridine + H] $^+$	<i>2f</i>	$[C_5H_{10}N]^+$	84.0813	84.0809	5
[2,3,4,5-tetrahydro-pyridine + D] $^+$	<i>2f'</i>	$[C_5H_9DN]^+$	85.0981	85.1011	35

Table A.3: Characteristic product ions observed in the CID-MS/MS of the $[M+H]^+$ ion at m/z 534.2561 from the photoreactive Biotin 3.

Photoactivatable Biotin 3 (Mr. 533.2532 Da)					
CID-MS/MS of the $[M+H]^+$ ion at m/z 534.2630					
Fragment ions	Characteristic ions	Calculated m/z	Observed m/z	Relative error ppm	
$[M+H]^+$	<i>3a</i>	$[C_{23}H_{36}N_9O_4S]^+$	534.2611	534.2561	9
$[M'+D]^+$	<i>3a'</i>	$[C_{23}H_{31}D_5N_9O_4S]^+$	539.3002	539.2868	25
[(biotinyl group) $C_7H_{14}N_2$] $^+$	<i>3b</i>	$[C_{17}H_{29}N_4O_2S]^+$	353.2011	353.2059	14
[(D ₂ -biotinyl group) $C_7H_{13}DN_2$] $^+$	<i>3b'</i>	$[C_{17}H_{26}D_3N_4O_2S]^+$	356.2246	356.2093	43
[(biotinyl group) $C_5H_{12}N_2$] $^+$	<i>3c</i>	$[C_{15}H_{27}N_4O_2S]^+$	327.1855	327.1898	13
[(D ₂ -biotinyl group) $C_5H_{12}N_2$] $^+$	<i>3c'</i>	$[C_{15}H_{24}D_3N_4O_2S]^+$	330.2084	330.1982	31
[(biotinyl group) C_3H_7N] $^+$	<i>3d</i>	$[C_{13}H_{22}N_3O_2S]^+$	284.1433	284.1441	3
[(D ₂ -biotinyl group) C_3H_6DN] $^+$	<i>3d'</i>	$[C_{13}H_{19}D_3N_3O_2S]^+$	287.1667	287.1551	40
[biotinyl group] $^+$	<i>3e</i>	$[C_{10}H_{15}N_2O_2S]^+$	227.0854	227.0806	21
[D ₂ -biotinyl group] $^+$	<i>3e'</i>	$[C_{10}H_{13}D_2N_2O_2S]^+$	229.1011	229.1037	11
[1,5 diazacyclohexene] $^+$	<i>3f</i>	$[C_4H_8N_2]^+$	84.0887	84.0839	33
[1,5 -D- diazacyclohexene] $^+$	<i>3f'</i>	$[C_4H_7DN_2]^+$	85.0766	85.0780	16
[spacer: C_3H_8N] $^+$	<i>3g</i>	$[C_3H_8N]^+$	58.0651	58.0667	28
[spacer: $C_3H_6D_2N$] $^+$	<i>3g'</i>	$[C_3H_6D_2N]^+$	60.0813	60.0821	13

Table A.4: Characteristic product ions observed in the CID-MS/MS of the $[M+H]^+$ ion at m/z 733.3637 and the *quasi*-MS³ analysis of the $[M+H\text{-biotinyl group}]^+$ ion at m/z 507.2847 from the PEO-Biotin Dimer **4**.

PEO-Biotin-Dimer 4 (Mr. 732.3550 Da)					
CID-MS/MS of the $[M+H]^+$ ion at m/z 733.3634					
Fragment ions		Characteristic ions	Calculated m/z	Observed m/z	Relative error ppm
$[M+H]^+$	<i>4a</i>	$[C_{32}H_{57}N_6O_9S_2]^+$	733.3628	733.3637	1
$[M'+D]^+$	<i>4a'</i>	$[C_{32}H_{50}D_7N_6O_9S_2]^+$	740.4176	740.4083	13
$[M+H\text{-biotinyl group}]C_2H_5N]^+$	<i>4c</i>	$[C_{20}H_{38}N_3O_7S]^+$	464.2430	464.2416	3
$[M'+D\text{-}(D_2\text{-biotinyl group})C_2H_4DN]^+$	<i>4c'</i>	$[C_{20}H_{33}D_5N_3O_7S]^+$	469.2822	469.2781	9
$[biotinyl group(C_2H_5N)]^+$	<i>4e</i>	$[C_{12}H_{20}N_3O_2S]^+$	270.1276	270.1283	3
$[D_2\text{-biotinyl group}(C_2H_4DN)]^+$	<i>4e'</i>	$[C_{12}H_{17}D_3N_3O_2S]^+$	273.1511	273.1481	11
$[biotinyl group]^+$	<i>4g</i>	$[C_{10}H_{15}N_2O_2S]^+$	227.0854	227.0852	9
$[D_2\text{-biotinyl group}]^+$	<i>4g'</i>	$[C_{10}H_{13}D_2N_2O_2S]^+$	229.1011	229.1031	9
<i>Quasi</i> -MS ³ of the $[M+H\text{-biotinyl group}]^+$ ion at m/z 507.2832					
$[M+H\text{-biotinyl group}]^+$	<i>4b</i>	$[C_{22}H_{43}N_4O_7S]^+$	507.2852	507.2847	1
$[M'+D\text{-}(D_2\text{-biotinyl group})]^+$	<i>4b'</i>	$[C_{22}H_{37}D_6N_4O_7S]^+$	513.3322	513.3204	23
$[spacer : C_{12}H_{28}N_2O_5 + H]^+$	<i>4d</i>	$[C_{12}H_{29}N_2O_5]^+$	281.2070	281.2060	4
$[spacer : C_{12}H_{24}D_4N_2O_5 + D]^+$	<i>4d'</i>	$[C_{12}H_{24}D_5N_2O_5]^+$	286.2468	286.2399	24
$[biotinyl group(C_2H_5N)]^+$	<i>4e</i>	$[C_{12}H_{20}N_3O_2S]^+$	270.1276	270.1301	9
$[D_2\text{-biotinyl group}(C_2H_4DN)]^+$	<i>4e'</i>	$[C_{12}H_{17}D_3N_3O_2S]^+$	273.1511	273.1481	11
$[spacer : C_{10}H_{23}NO_5 + H]^+$	<i>4f</i>	$[C_{10}H_{24}NO_5]^+$	238.1654	238.1639	6
$[spacer : C_{10}H_{20}D_3NO_5 + D]^+$	<i>4f'</i>	$[C_{10}H_{20}D_4NO_5]^+$	242.1967	242.1929	16
$[biotinyl group]^+$	<i>4g</i>	$[C_{10}H_{15}N_2O_2S]^+$	227.0854	227.0850	2
$[D_2\text{-biotinyl group}]^+$	<i>4g'</i>	$[C_{10}H_{13}D_2N_2O_2S]^+$	229.1011	229.1031	9

Table A.5: Characteristic product ions observed in the CID-MS/MS of the $[M+H]^+$ ion at m/z 880.1818 and the quasi-MS³ analysis of the $[M+2H-Na]^+$ ion at m/z 858.2064 from the Sulfo- SBED 5.

Sulfo-SBED 5 (Mr. 879.1784 Da)					
CID-MS/MS of the $[M+H]^+$ ion at m/z 880.1853					
fragment ions		Characteristic ions	Calculated m/z	Observed m/z	Relative error ppm
$[M + H]^+$	<i>5a</i>	$[C_{32}H_{43}N_9NaO_{11}S_4]^+$	880.1862	880.1818	5
$[M' + D]^+$	<i>5a'</i>	$[C_{32}H_{37}D_6N_9NaO_{11}S_4]^+$	886.2332	886.2174	18
$[M' + H - N_2]^+$	<i>5c</i>	$[C_{32}H_{43}N_7NaO_{11}S_4]^+$	852.1956	852.1804	18
$[M' + D - N_2]^+$	<i>5c'</i>	$[C_{32}H_{36}D_7N_7NaO_{11}S_4]^+$	859.2349	859.2261	10
[M+H-(biotinyl group) - (photoactivatable aryl azide group)]⁺	<i>5e</i>	$[C_{16}H_{25}N_3NaO_9S_3]^+$	522.0645	522.0893	47
[M+D-(D₂-biotinyl group) - (D-photoactivatable aryl azide group)]⁺	<i>5e'</i>	$[C_{16}H_{22}D_3N_3NaO_9S_3]^+$	525.2212	525.2109	20
[M+H-(C₁₆H₁₄N₂O₈S₃)+Na]⁺	<i>5g</i>	$[C_{22}H_{29}N_7NaO_3S]^+$	494.1944	494.1780	33
[M+D-(C₁₆H₁₂D₂N₂O₈S₃)+Na]⁺	<i>5g'</i>	$[C_{22}H_{26}D_3N_7NaO_3S]^+$	497.1015	497.1144	26
[(biotinyl group)C₁₂H₁₅N₃O]⁺	<i>5i</i>	$[C_{22}H_{30}N_5O_3S]^+$	444.2063	444.2029	8
[(D₂biotinyl group)C₁₂H₁₂D₃N₃O]⁺	<i>5i'</i>	$[C_{22}H_{25}D_5N_5O_3S]^+$	449.2461	449.2382	18
[(biotinyl group)C₅H₆N₂O]⁺	<i>5k</i>	$[C_{16}H_{22}N_4O_3S]^+$	350.1412	350.1410	1
[(D₂-biotinyl group)C₅H₅DN₂O]⁺	<i>5k'</i>	$[C_{16}H_{19}D_3N_4O_3S]^+$	353.1647	353.1717	20
[(biotinyl group)⁺	<i>5m</i>	$[C_{10}H_{15}N_2O_2S]^+$	227.0854	227.0851	1
[D₂-biotinyl group]⁺	<i>5m'</i>	$[C_{10}H_{13}D_2N_2O_2S]^+$	229.1011	229.0948	27
[phenyl azide + H]⁺	<i>5n</i>	$[C_6H_6N_3]^+$	120.0449	120.0454	4
[phenyl azide + D]⁺	<i>5n'</i>	$[C_6H_5DN_3]^+$	121.064	121.0665	20
[2,3,4,5-tetrahydro-pyridine + H]⁺	<i>5o</i>	$[C_5H_{10}N]^+$	84.0807	84.0788	23
[2,3,4,5-tetrahydro-pyridine + D]⁺	<i>5o'</i>	$[C_5H_9DN]^+$	85.0891	84.0869	26
Quasi-MS³ of the $[M+2H - Na]^+$ ion at m/z 858.2060					
$[M + 2H - Na]^+$	<i>5b</i>	$[C_{32}H_{44}N_9O_{11}S_4]^+$	858.2068	858.2064	0

[M' + 2D - Na] ⁺	5b'	[C ₃₂ H ₃₇ D ₇ N ₉ O ₁₁ S ₄] ⁺	865.2591	865.2456	16
[M + H - (2,5dioxopyrrolidine-3- sulfonic acid)] ⁺	5d	[C ₂₈ H ₄₁ N ₈ O ₆ S ₃] ⁺	681.2305	681.2298	1
[M' + D - (D ₂ - 2,5dioxopyrrolidine-3- sulfonic acid)] ⁺	5d'	[C ₂₈ H ₃₄ D ₇ N ₈ O ₆ S ₃] ⁺	688.2815	688.297	23
[(biotinyl group) C ₆ H ₁₀ NO (photoactivatable aryl azide group)] ⁺	5f	[C ₂₃ H ₃₀ N ₇ O ₄ S] ⁺	500.2074	500.2061	3
[(D ₂ -biotinyl group) C ₆ H ₉ DNO (D- photoactivatable aryl azide group)] ⁺	5f'	[C ₂₃ H ₂₆ D ₄ N ₇ O ₄ S] ⁺	504.2393	504.2223	34
[(biotinyl group) C ₅ H ₁₀ N ₂ O (phenylazide group)+H] ⁺	5h	[C ₂₂ H ₃₀ N ₇ O ₃ S] ⁺	472.2131	472.2045	18
[(D ₂ -biotinyl group) C ₅ H ₉ DN ₂ O (phenyl azide group)+D] ⁺	5h'	[C ₂₂ H ₂₆ D ₄ N ₇ O ₃ S] ⁺	476.2444	476.2414	7
[(biotinyl group)C ₁₂ H ₁₅ N ₃ O] ⁺	5i	[C ₂₂ H ₃₀ N ₅ O ₃ S] ⁺	444.2063	444.2082	4
[(D ₂ biotinyl group)C ₁₂ H ₁₂ D ₃ N ₃ O] ⁺	5i'	[C ₂₂ H ₂₅ D ₅ N ₅ O ₃ S] ⁺	449.2461	449.2436	6
[(biotinyl group)C ₁₂ H ₁₂ N ₂ O] ⁺	5j	[C ₂₂ H ₂₇ N ₄ O ₃ S] ⁺	427.1762	427.1759	1
[(D ₂ -biotinyl group)C ₁₂ H ₁₁ DN ₂ O] ⁺	5j'	[C ₂₂ H ₂₄ D ₃ N ₄ O ₃ S] ⁺	430.2039	430.1953	20
[(biotinyl group)C ₅ H ₉ N] ⁺	5l	[C ₁₅ H ₂₄ N ₃ O ₂ S] ⁺	310.1589	310.1586	1
[(D ₂ -biotinyl group)C ₅ H ₇ N] ⁺	5l'	[C ₁₅ H ₂₂ D ₂ N ₃ O ₂ S] ⁺	312.1746	312.1721	8
[(biotinyl group) ⁺	5m	[C ₁₀ H ₁₅ N ₂ O ₂ S] ⁺	227.0854	227.0852	1
[(D ₂ -biotinyl group) ⁺	5m'	[C ₁₀ H ₁₃ D ₂ N ₂ O ₂ S] ⁺	229.1011	229.0948	27

APPENDIX B
MALDI-MS AND MALDI-CID-MS/MS DATA FOR THE ANALYSIS OF THE
NATIVE AND PERMETHYLATED CORE OLIGOSACCHARIDE SJ 48R
(CHEMOTYPE II)

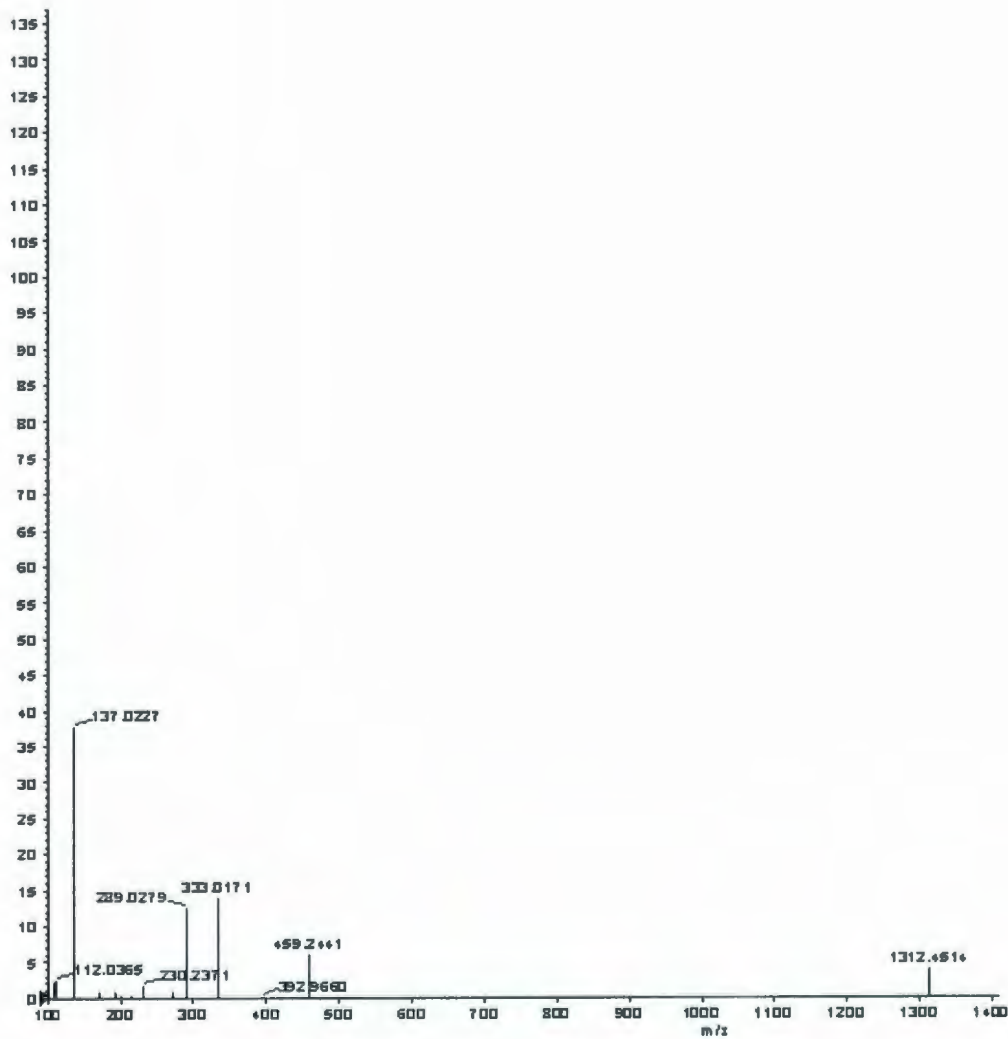


Figure B.1: MALDI-MS (+) of the homogeneous mixture of the native core oligosaccharide.

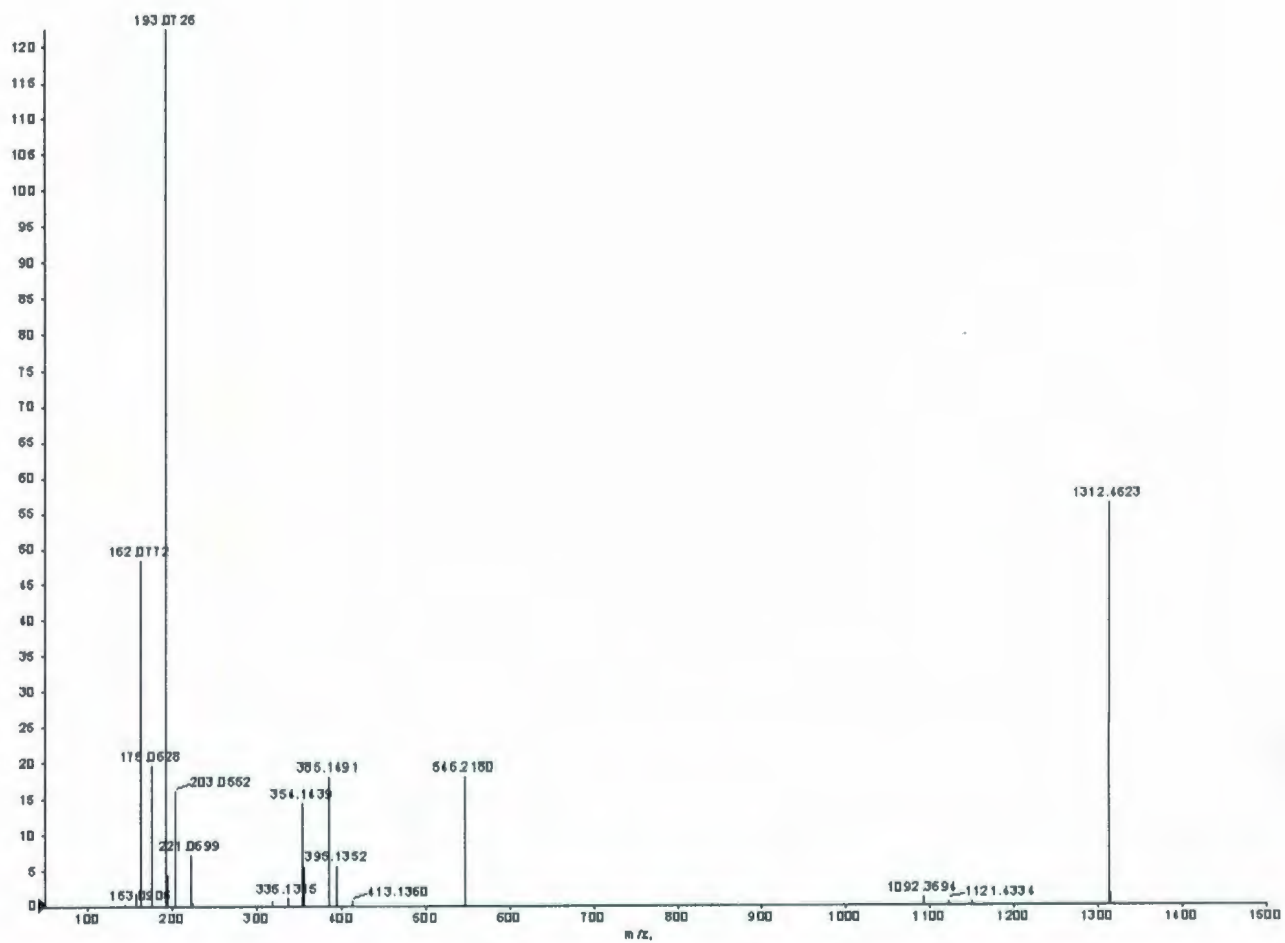


Figure B.2: MALDI-CID-MS/MS (+) of the selected precursor ion at m/z 1312.4514 from the homogeneous mixture of the native core oligosaccharide.

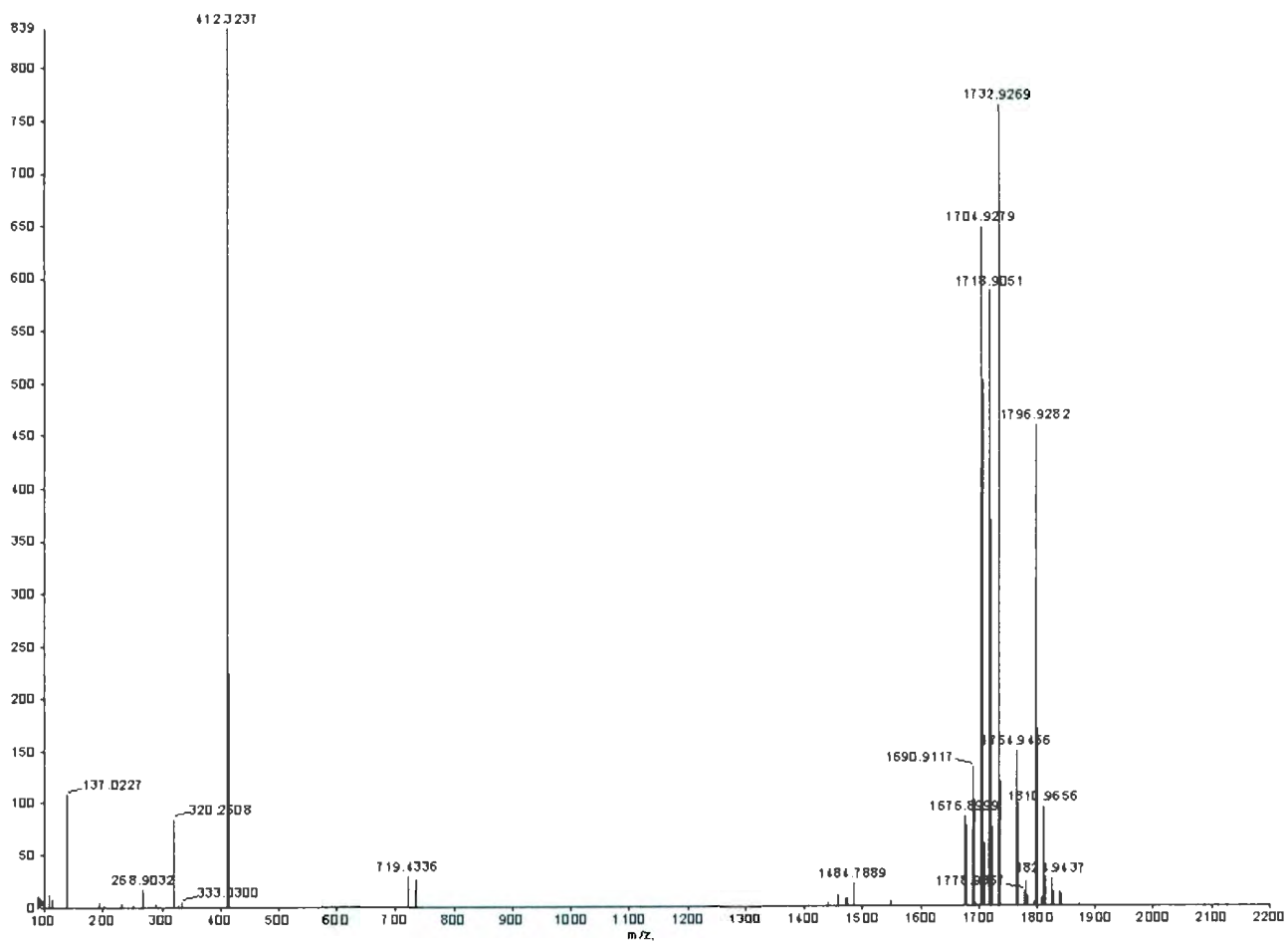


Figure B.3: MALDI-MS (+) of the homogeneous mixture of the permethylated core oligosaccharide.

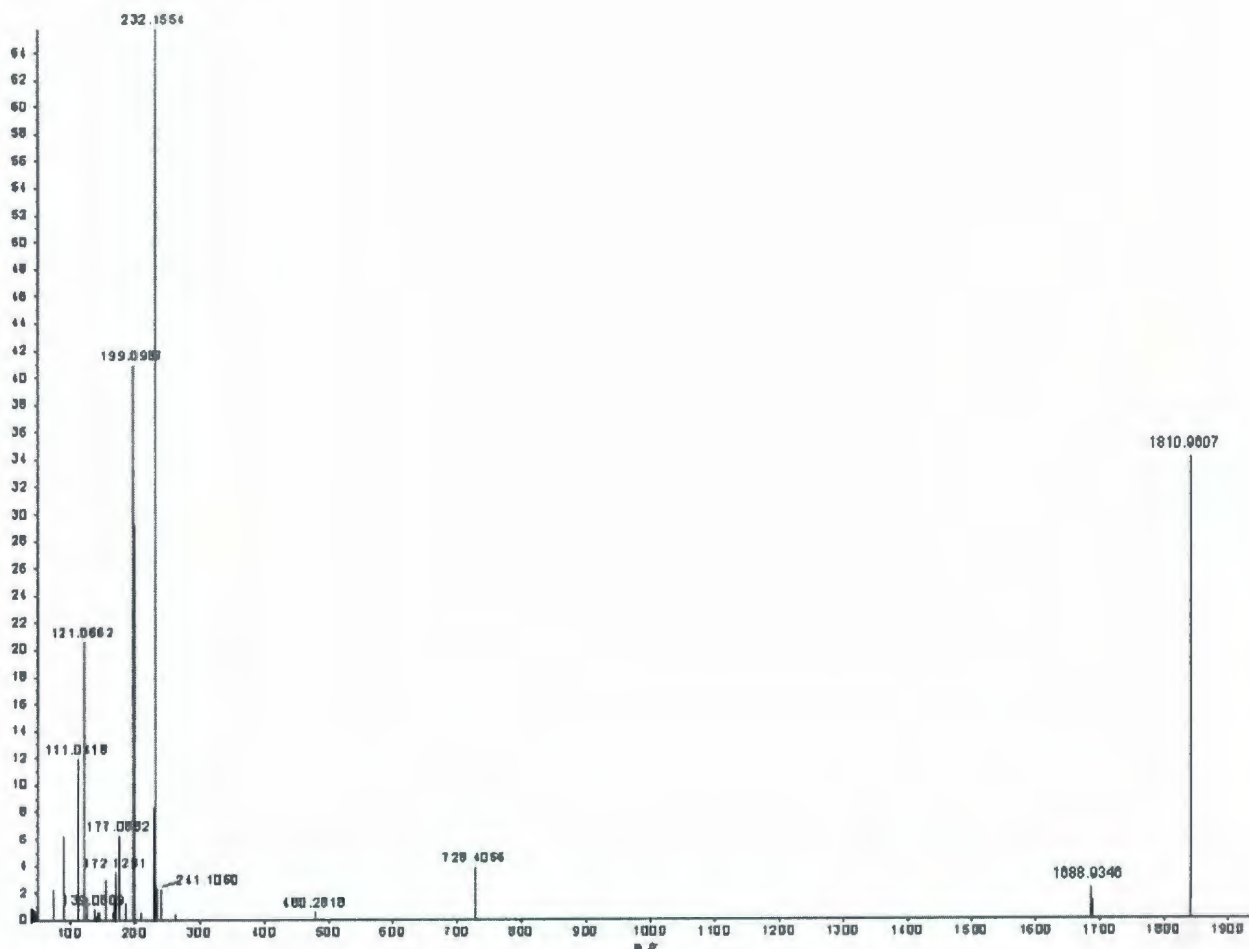


Figure B.4: MALDI-CID-MS/MS of the selected precursor ion at m/z 1810.9656 from the permethylated core oligosaccharide.

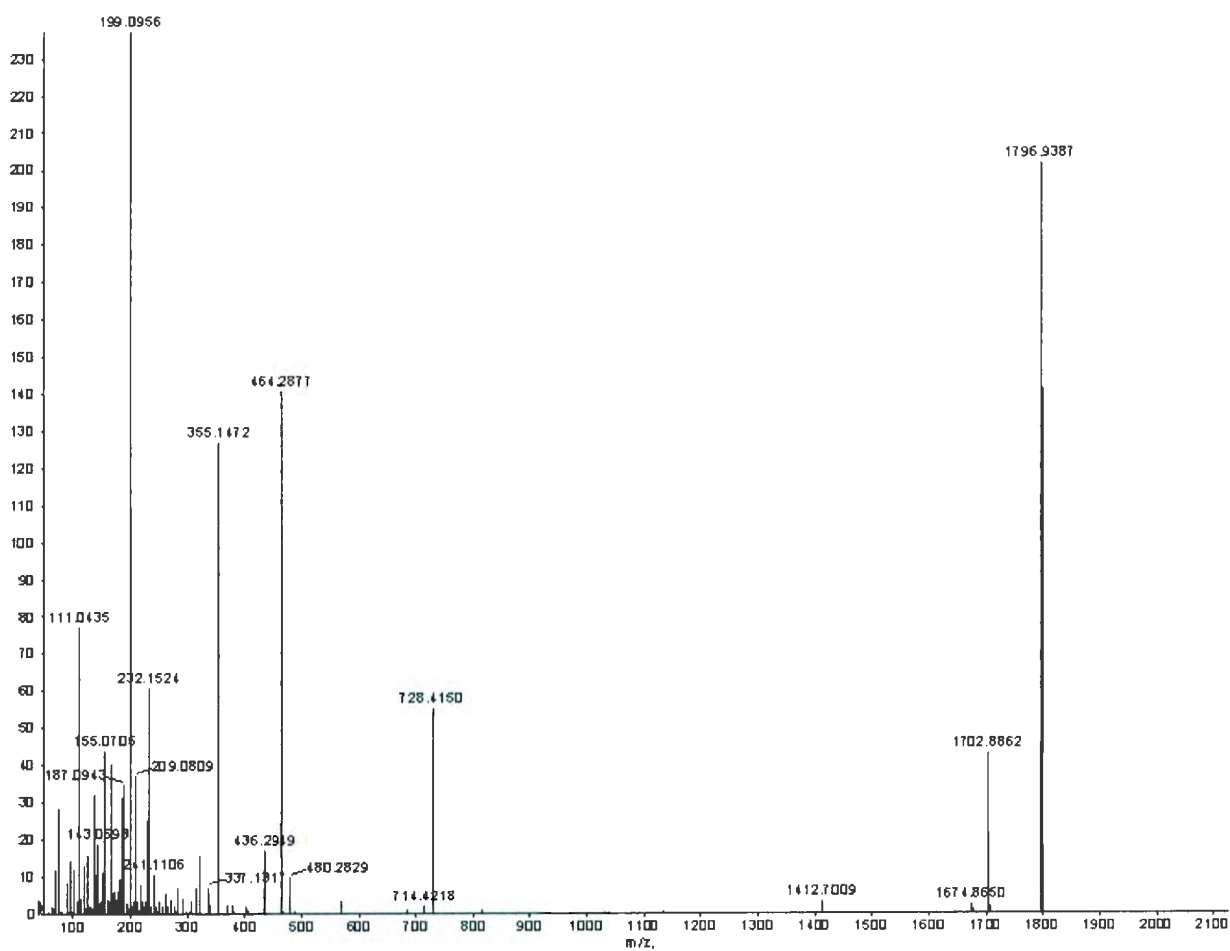


Figure B.5: MALDI-CID-MS/MS of the selected precursor ion at m/z 1796.9282 from the permethylated core oligosaccharide.

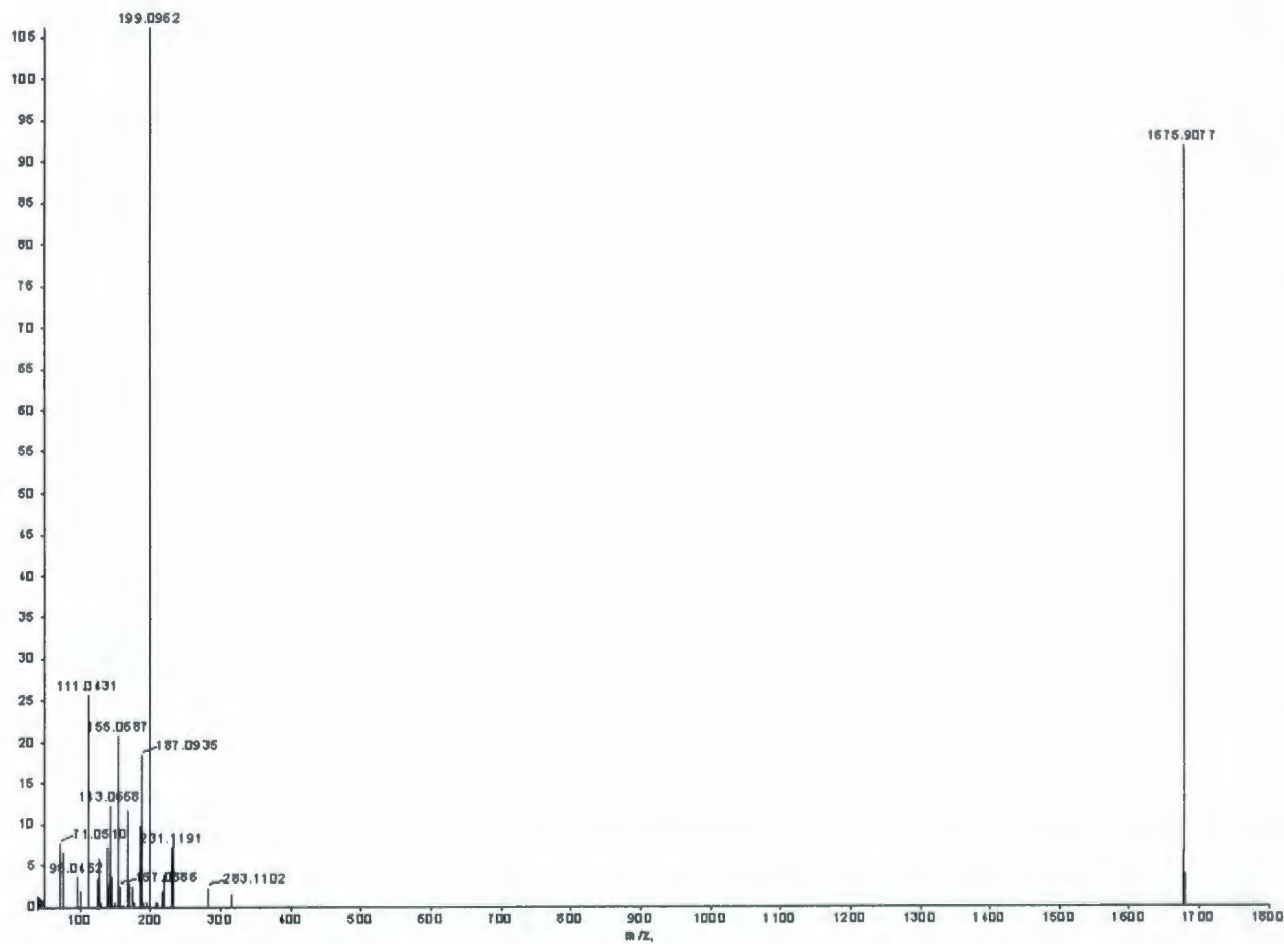


Figure B.6: MALDI-CID-MS/MS of the selected precursor ion at m/z 1676.8969 from the permethylated core oligosaccharide.

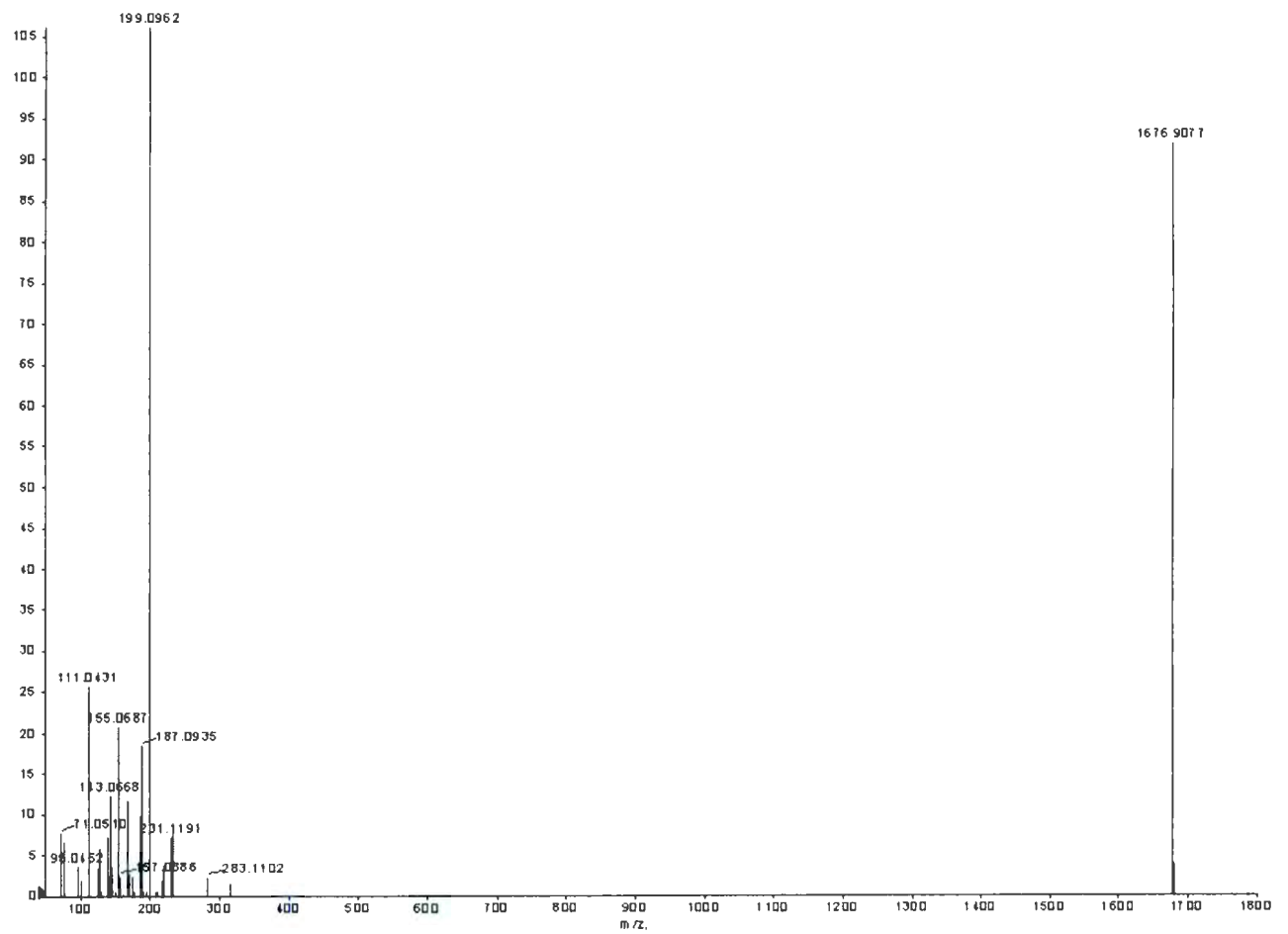


Figure B.6: MALDI-CID-MS/MS of the selected precursor ion at m/z 1676.8969 from the permethylated core oligosaccharide.



